

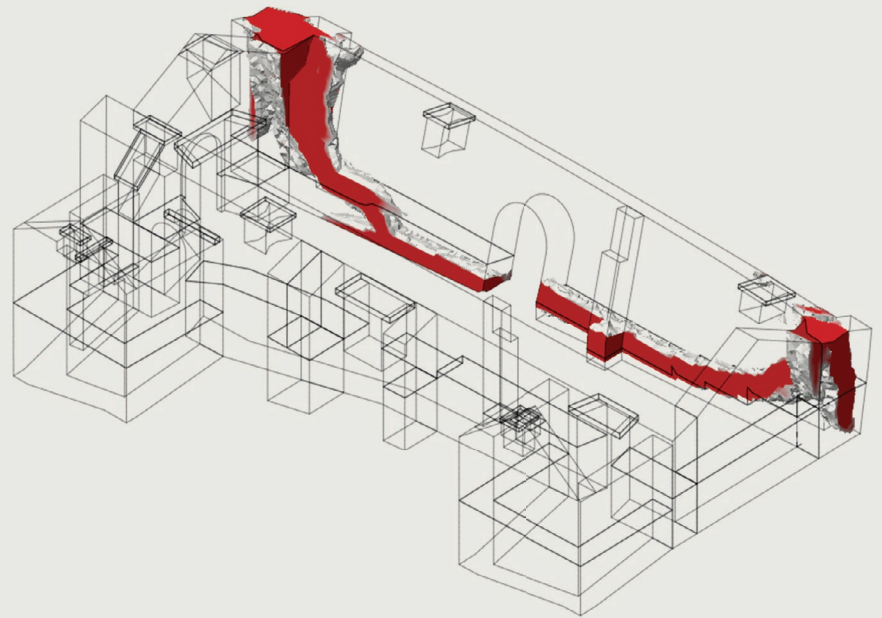
# Seismic Retrofitting Project

## Recommendations for Advanced Modeling of Historic Earthen Sites

### Research Report

Paulo B. Lourenço and João M. Pereira

In collaboration with Giorgos Karanikoloudis,  
Federica Greco, and Claudia Cancino



# Seismic Retrofitting Project

## Recommendations for Advanced Modeling of Historic Earthen Sites

Paulo B. Lourenço and João M. Pereira

In collaboration with Giorgos Karanikoloudis, Federica Greco,  
and Claudia Cancino

THE GETTY CONSERVATION INSTITUTE  
LOS ANGELES  
TECMINHO – UNIVERSITY OF MINHO  
GUIMARÃES, PORTUGAL

© 2018 J. Paul Getty Trust and TecMinho – University of Minho

The Getty Conservation Institute  
1200 Getty Center Drive, Suite 700  
Los Angeles, CA 90049-1684  
United States  
Telephone (+1) 310 440-7325  
Fax (+1) 310 440-7702  
E-mail: [gciweb@getty.edu](mailto:gciweb@getty.edu)  
[www.getty.edu/conservation](http://www.getty.edu/conservation)

TecMinho – University of Minho  
Campus de Azurém  
Alameda da Universidade  
P-4800-058 Guimarães  
Portugal  
Telephone (+351) 253 510-590  
Fax (+351) 253 510-591  
E-mail: [tecm@tecminho.uminho.pt](mailto:tecm@tecminho.uminho.pt)  
[www.tecminho.uminho.pt](http://www.tecminho.uminho.pt)

The Getty Conservation Institute (GCI) works internationally to advance conservation practice in the visual arts—broadly interpreted to include objects, collections, architecture, and sites. The Institute serves the conservation community through scientific research, education and training, field projects, and the dissemination of information. In all its endeavors, the GCI creates and delivers knowledge that contributes to the conservation of the world's cultural heritage.

Founded in 1990, TecMinho is a private non-profit association supported by the University of Minho and the Association of Municipalities of Vale do Ave, Portugal. Its mission is to connect the University of Minho to society, especially in the areas of science and technology, and to contribute to regional development by improving the competitiveness of organizations and increasing the skills of individuals.

ISBN: 978-1-937433-53-6 (online resource)

ISBN: 978-1-937433-54-3 (print)

Cover: © J. Paul Getty Trust, 2017. Model: Giorgos Karanikoloudis.



**The Getty Conservation Institute**



Universidade do Minho



# Contents

|   |     |
|---|-----|
| Project Participants                              | v   |
| SRP Peer Review Group                             | vii |
| <b>CHAPTER 1</b>                                  |     |
| <b>Introduction</b>                               |     |
| The Seismic Retrofitting Project                  | 9   |
| Content   | 10  |
| <b>CHAPTER 2</b>                                  |     |
| <b>Structural Analysis Methods</b>                |     |
| Static Analysis                                   | 13  |
| <i>Linear Elastic</i>                             | 13  |
| <i>Limit Analysis</i>                             | 14  |
| <i>Nonlinear Analysis</i>                         | 15  |
| <i>Pushover Analysis</i>                          | 17  |
| <i>Comparison of Static Analysis Methods</i>      | 19  |
| Dynamic Analysis                                  | 22  |
| <i>Response Spectrum Analysis</i>                 | 22  |
| <i>Time History Analysis</i>                      | 23  |
| <b>CHAPTER 3</b>                                  |     |
| <b>User Guidance on the Finite Element Method</b> |     |
| Planning the Analysis                             | 27  |
| Model Geometry                                    | 28  |
| <i>Element Type</i>                               | 28  |
| <i>2D vs. 2.5D vs. 3D</i>                         | 30  |
| <i>Meshing</i>                                    | 32  |
| Materials   | 33  |
| <i>Supports and Loads</i>                         | 34  |
| <i>Model Calibration/Verification</i>             | 34  |
| <i>Interpretation of Results</i>                  | 35  |

**CHAPTER 4****Constitutive Models**

|  |    |
|--|----|
| Nonlinear Behavior                         | 37 |
| Micro and Macro Models                     | 37 |
| Constitutive Models in Commercial Software | 41 |
| <i>DIANA</i>                               | 41 |
| <i>ABAQUS</i>                              | 42 |
| <i>Comparison for Commercial Software</i>  | 45 |

**CHAPTER 5****Recommended Properties for Numerical Modeling**

|                               |    |
|-------------------------------|----|
| Masonry Structures in General | 49 |
| Earthen Structures            | 51 |

**CHAPTER 6****Application Example: Adobe House**

|  |    |
|--|----|
| General Description of the Models                        | 53 |
| Experimental Results for Calibration of Numerical Models | 54 |
| Numerical Analysis                                       | 55 |
| <i>Definition of the Finite Element Model</i>            | 55 |
| <i>Nonlinear Static Analysis</i>                         | 57 |
| Conclusions of the Comparison                            | 59 |

**CHAPTER 7****Application Example: Kuñotambo, Peru**

|  |    |
|--|----|
| General Description of the Building        | 61 |
| Definition of the Finite Element Model     | 62 |
| Material Model and Mechanical Properties   | 65 |
| Numerical Results and Observed Conclusions | 65 |

**CHAPTER 8****Conclusions**

69

**References**

71

# Project Participants

## **Seismic Retrofitting Project—Modeling Phase**

### **PROJECT DIRECTORS**

Paulo B. Lourenço,  
Professor, University of Minho, Portugal

Claudia Cancino  
Senior Project Specialist, Getty Conservation Institute, Los Angeles

### **PARTICIPANTS**

Alberto Barontini,  
Research Assistant, University of Minho, Portugal

Maria Pia Ciocci,  
Research Assistant, University of Minho, Portugal

Nicole Declet  
Intern (2017–18), Getty Conservation Institute, Los Angeles

Giorgos Karanikoloudis  
Research Assistant, University of Minho, Portugal

Federica Greco  
Former Research Assistant (2015–2016), University of Minho, Portugal  
Former Intern (2016–17), Getty Conservation Institute, Los Angeles

Susan Macdonald  
Head, Building and Sites, Getty Conservation Institute, Los Angeles

João M. Pereira,  
Postdoctoral Research Associate, University of Minho, Portugal

Kelly Wong  
Former Project Specialist (2015–2017), Getty Conservation Institute, Los Angeles



# SRP Peer Review Group

Organized by the Getty Conservation Institute (GCI) as part of the Seismic Retrofitting Project (SRP), the following professionals participated in peer review meetings in Lima on July 18–21, 2011 and in Cusco on January 23–27, 2017. The SRP peer review group consists of experienced professionals in seismic retrofitting, analytical modeling of historic masonry structures, and conservation of earthen architecture. The meetings, which included formal talks and site visits, were designed to provide maximum opportunity for informal discussion among a select group of experts.

The objective of the first meeting was to review the SRP Construction Assessment of selected building prototypes. The meeting also included a review of the SRP Proposal for the Testing and Modeling Phase, which was developed in collaboration with the GCI by the Escuela de Ciencias e Ingeniería of the Pontificia Universidad Católica del Perú (PUCP, SRP partner) and the Department of Architecture and Civil Engineering at the University of Bath (SRP partner from 2011 to 2014), respectively. The objective of the second meeting was to review the results of the completed testing developed by PUCP and the modeling results of the un-retrofitted and retrofitted SRP building prototypes, designed and developed by TecMinho, University of Minho (GCI consultant from 2015 to 2018).

In advance of both meetings, peer reviewers received extensive documentation of the work carried out by the SRP team. Peer reviewers' comments were highly valuable for the SRP team and enriched the methodology and results of the project. This publication serves as a testament to their voice and influence.

Eng. Rafael Aguilar \*\*

Associate Professor, Pontificia Universidad Católica del Perú

Arch. André Aninat Jolly \*\*

Head, Sustainable Conservation Project Workshop, Fundación Altiplano Msv, Chile

Eng. Carlos Casabonne \*\*

Senior Principal, Gallegos, Casabonne, Arango, Ingenieros Civiles SAC

Arch. Mariana Correia \*\*

President, ESG/Escola Superior Gallaecia, Portugal, and former President PROTERRA Iberian-American Network

Eng. Matthew DeJong \*\*\*

Senior Lecturer, University of Cambridge

Eng. Carmen Kuroiwa \*

Gerente de Investigación y Normalización, Servicio Nacional de Capacitación para la Industria de la Construcción (SENCICO)

Arch. Philippe Garnier \*\*\*

Director, Human Settlements, CRAterre-ENSAG



Arch. Eng. Stephen Kelly \*\*\*  
Secretary-General, International Scientific Committee on the Analysis and Restoration of Structures of Architectural Heritage (ISCARSAH)

Eng. Terrence Paret \*\*  
Senior Principal, Wiss, Janney, Elstner Associates, Inc.

Eng. Pere Roca \*\*  
Professor, Technical University of Catalonia

Eng. Nicola Tarque \*\*  
Associate Professor, Pontificia Universidad Católica del Perú

Eng. Julio Vargas Neumann \*\*\*  
Member, International Scientific Committee on the Conservation of Earthen Architectural Heritage (ISCEAH) and World Heritage Earthen Architecture Programme (WHEAP)

Eng. Humberto Varum \*  
Professor, University of Porto, Member of ISCEAH

Eng. Fred Webster \*  
Former Member, Getty Seismic Adobe Project (GSAP)

\* = Attended first meeting (July 2011)

\*\* = Attended second meeting (January 2017)

\*\*\* = Attended both meetings

# Introduction

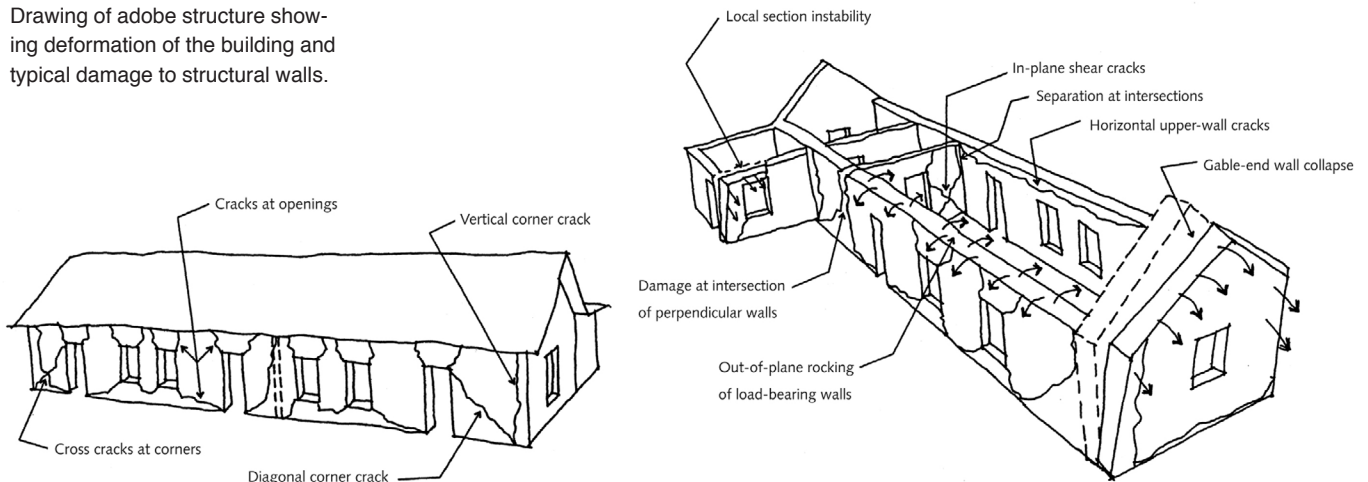
Sun-dried mud brick, or adobe as it is commonly known in Latin America and other regions of the world, is one of the oldest and most widely used building materials in the world. Adobe is still used in many developing countries because soil is easily available and self-construction is simple and economical. Furthermore, adobe dwellings have suitable thermal and acoustic characteristics. However, they are extremely vulnerable to earthquakes. Walls are the main structural elements of earthen buildings, and their seismic vulnerability is a result of their high mass, which produces high inertial forces, and their very low tensile strength, which yields a brittle type of failure and can result in sudden collapse (Torrealva 2012).

Failure modes in adobe constructions under seismic loading depend on the mechanical properties of units and mortar and on the overall geometric configuration of the building (Varum et al. 2014). Given the magnitude and direction of the inertial forces, the corresponding structural damage is composed of in-plane failure in parts of the building (rocking, sliding, diagonal tension, and toe crushing), as well as out-of-plane failure, under flexural hinge lines, formed usually at the base or at intermediate heights (Lourenço et al. 2011; Tolles et al. 1996) (fig. 1.1).

## The Seismic Retrofitting Project

During the 1990s, the Getty Conservation Institute (GCI) carried out a major research and laboratory testing program, the Getty Seismic Adobe Project (GSAP), which investigated the performance of historic adobe structures during earthquakes and developed cost-effective retrofit methods that substantially preserve the authenticity of these buildings.

**FIGURE 1.1.**  
Drawing of adobe structure showing deformation of the building and typical damage to structural walls.



Results of this research have been disseminated in a series of publications in both English and Spanish (Tolles, Kimbro, and Ginell 2002).

In 2006, the GCI's Earthen Architecture Initiative convened two meetings: the Getty Seismic Adobe Project Colloquium and New Concepts in Seismic Strengthening of Historic Adobe Structures. Held at the Getty Center, the meetings focused on implementation of the GSAP. Papers presented at the first meeting, the GSAP colloquium, as well as the main conclusions of the colloquium's roundtable discussions, were published as part of the proceedings (Hardy, Cancino, and Ostergren 2009). The participants in the colloquium concluded that the GSAP methodology was excellent and effective. However, the methodology's reliance on high-tech materials and professional expertise was a deterrent to it being more widely implemented.

On August 15, 2007, an earthquake of 8.0 Moment Magnitude (Mw) and a maximum local Modified Mercalli Intensity (MMI) of VII–VIII occurred with an epicenter off the coast of Pisco, Peru, resulting in 519 deaths and 1,366 injuries. A total of 650,000 people were affected and 80,000 dwellings damaged. From October 28 to November 2, 2007, a rapid assessment to better understand the failure of fifteen historic earthen sites was performed by a multidisciplinary team of national and international experts convened by the GCI. The assessment, which was organized in response to a request from the former Instituto Nacional de Cultura del Perú (INC, Peruvian National Institute of Culture; now the Ministerio de Cultura del Perú, or Peruvian Ministry of Culture), was also published (Cancino 2011).

Following the GSAP conclusions and the findings from the Pisco earthquake assessment, the GCI initiated in 2009 the Seismic Retrofitting Project (SRP), with the objective of adapting GSAP techniques to better match the equipment, materials, and technical skills available in many countries with earthen sites. Using four Peruvian historic earthen buildings representing typologies across Latin America, the GCI—in collaboration with the Ministerio de Cultura del Perú, the Escuela de Ciencias e Ingeniería of the Pontificia Universidad Católica del Perú (PUCP), and the University of Minho—is designing, testing, and implementing seismic retrofitting techniques and maintenance programs with locally available materials that will improve the structural performance and safety of earthen buildings while minimizing loss of historic fabric. The Department of Architecture and Civil Engineering at the University of Bath and the Department of Civil, Environmental and Geomatic Engineering at University College London have also been SRP partners from 2010 to 2012 and from 2013 to 2014, respectively.

From 2015 until 2017, the University of Minho used modeling as a method to understand structural behavior of the SRP building prototypes and validate the retrofitting techniques later design for them. The way modeling has been used is quite innovative, has advanced the field of structural analysis of structures made of earth, and is worth publishing.

## **Content**

This publication is the first in a series within the SRP, under the auspices of the GCI. Its publication is intended to help professionals and researchers in the field of structural engineering with the assessment of historic earthen structures using advanced numerical modeling techniques. The other reports in the series are “Modeling of Prototype Buildings” (report #2) and “Simplified Calculations for the Structural Analysis of Earthen Historic Sites” (report #3).

In addition to this introduction, this publication is composed of seven chapters. Chapter 2 presents the main structural analysis methods available, both static and dynamic, to assist the reader with different techniques used to assess structures under different loading conditions. Chapter 3 provides a user guide on the finite element method (FEM). FEM is the most used technique to assess the structural behavior of buildings, and chapter 3 gives an overall perspective and guidance on how to use this numerical tool, starting from planning the analysis through interpreting the results.

Chapter 4 deals with the nonlinear behavior of the materials, focusing on masonry in general, which provides relevant data to model earthen masonry sites. Hereafter, masonry is used to represent any kind of unit assemblage (e.g., clay bricks, stone blocks, or adobe). Additionally, the behavior of rammed earth is similar to that of adobe masonry, and the described models are also applicable, as they are all based in the assumption of low tensile strength. Different modeling techniques or homogenization techniques are presented, including the different constitutive models available in commercial software, compared using a simple example.

Chapter 5 gathers available information on the mechanical properties of adobe masonry. Due to the nature of the materials, the scatter in terms of mechanical properties is considerable. This chapter provides the reader with a summary of the available reported and standardized mechanical properties for adobe masonry.

Finally, chapters 6 and 7 present application examples of the use of numerical modeling techniques to assess adobe structures. Chapter 6 gives an example of an adobe house experimentally tested in the shaking table at PUCP. This example shows how advanced numerical modeling techniques are able to replicate the structural behavior of these elements. Chapter 7 gives an example of a real adobe structure (the church of Santiago Apóstol de Kuñotambo, Peru) to highlight some of the critical points and difficulties when modeling historic earthen buildings. More extensive examples of applications are given in report #2 of this series (“Modeling of Prototype Buildings”). Chapter 8 compiles the main conclusions and recommendations on modeling of historic earthen structures.



# Structural Analysis Methods

Structural analysis is the determination of the effects of loads on physical structures and their components. Structural analysis uses the fields of applied mechanics, material sciences, and mathematics to determine the response of a structure when subjected to a specific load in terms of deformations, internal forces, support reactions, stresses, and so forth.

In past decades, there has been considerable development in numerical methods of structural analysis. It is now possible, assisted by a computer, to analyze structures with a high level of accuracy. New numerical methods and new analysis capabilities have been, to some extent, incorporated in the practice of structural engineering, even if not always in the best possible form (Lourenço 1998).

This chapter gives an overview on the available structural analysis methods, showing their potential and limitations as well as comparisons between the different methods. A distinction is made between static and dynamic methods as their considerations and assumptions are rather different.

## Static Analysis

### Linear Elastic

The theory of elasticity introduced by Robert Hooke established that all materials and structures deflect when they are loaded. This theory defined the relation between forces and deflections as stiffness. Linear elastic analysis assumes that the material obeys Hooke's law (eq. 1):

$$E = \sigma / \varepsilon \quad (1)$$

Here,  $E$  is Young's modulus, or elasticity modulus,  $\sigma$  is the stress, and  $\varepsilon$  is the strain.

Generally, this is the case in most civil engineering structures for low stress levels, as the ones experienced in a structure submitted to everyday loading conditions. However, it must be stated that materials have a maximum stress that they can sustain under a specific loading condition. Linear elastic structural analysis does not take this into account, meaning that Hooke's law is applied to determine the response of the structure independent of the stress level attained.

Linear elasticity is quite problematic in the case of masonry structures under tension, as the material cracks at very low stress levels. One possibility when using such an approach to assess masonry structures is to define an "allowable maximum stress," which permits the user to identify within the model the areas where a concentration of stresses would be high enough to result in cracks. There are even some techniques that allow the user to take into consideration crack-induced damage in a structure using this method. The user can define a different stiffness for a specific set of elements (areas) where cracks

already exist in the structure or in areas where a previous elastic analysis predicts high tensile stresses. The user may choose to simply lower the stiffness, meaning that some “damage” in the selected area is taken into account, or the user can assume a zero stiffness, meaning that the selected area is not able to transfer any stress (simulating a fully developed crack).

The main advantage in using this structural analysis method is the low required time to run these simulations. However, with the advances in computers, the more time-consuming techniques are now becoming much faster to run. In addition, the process of an ad hoc definition of damage location will often require multiple iterations, with a number of calculations, and is hardly objective.

The use of linear elastic analysis, especially in the case of masonry, is debatable and should be avoided (Lourenço 2001). There are three different aspects that make linear elastic analysis unsuitable for masonry and earthen structures: First, masonry possesses very low tensile strength, and it usually is not possible to make provisions to cover all zones where tensile stresses may appear. Second, the question “what is the maximum tensile stress admissible?” cannot be answered with a linear elastic analysis, as the maximum admissible value depends on the distribution of stresses itself. If the area of the structure related to the crack propagation is rather large, the relevant stored energy might be too high and the structural behavior ends up quite brittle. If the relevant stored energy is low, the behavior can be rather ductile. Additionally, the linear elastic peak stresses in a structure are often meaningless quantities. Due to the application of concentrated loads and strong geometric discontinuities, for example, openings in walls, the elastic peak stress is, theoretically, infinite and the value obtained in the finite element analysis depends only on the mesh discretization, such as the element size. Third, the act of preparing a finite element model usually is time consuming. Given the effort and costs involved in the preparation of the model, the additional time requirements to carry out a nonlinear static analysis are often marginal and its benefits for understanding the behavior of the structure are high (Lourenço 2001).

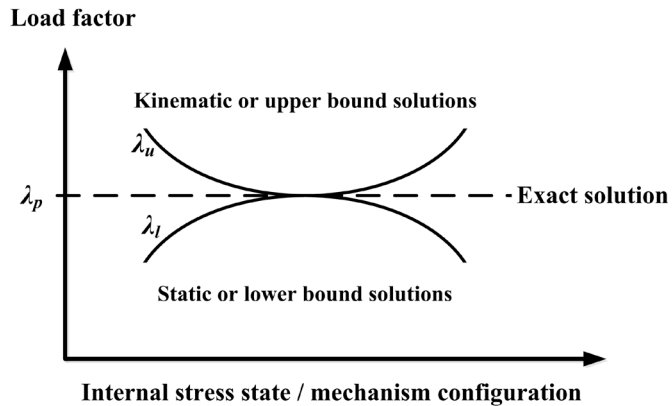
### **Limit Analysis**

Limit analysis is a structural analysis method to estimate the collapse load of a given structural model. This method is based on a set of limit theorems, which are based on the conservation of energy.

Johansen (1930) used the upper bound techniques of limit analysis and developed the yield-line theory for reinforced concrete slab design. The application of stress fields to reinforced concrete beam design, based on the concept of the lower bound theorem of limit analysis, was first proposed by Drucker (1961). This approach has been extended and expanded to the design of concrete structures by Muttoni, Schwartz, and Thurlimann (1997). Similarly, upper and lower bound concepts of limit analysis were used by Heyman (1969) to explain the modern view of the traditional design and assessment of masonry arches.

At the limit state, the structure is about to collapse. In this case, both a statically and kinematically admissible collapsing mechanism exists at the limit state (Roca, Cervera, and Gariup 2010). Gilbert (2007) provides a graphic depiction of the relationship between theorems in figure 2.1. Here,  $\lambda$  is the load factor, a scalar with no units that multiplies the set of loads applied to the structure. For the limit state analysis of masonry structures, Heyman (1969) essentially provides the lower bound theorem, while Kooharian (1952) establishes the upper bound theorem.

**FIGURE 2.1.**  
Diagram depicting the relationship between upper and lower bound theorems in limit state analysis (Gilbert 2007).



Limit analysis can be assumed as adequate for the analysis of historical masonry structures if a zero tensile stress is assumed and a ductile response is expected (Lourenço 2001). Limit analysis is based either on the lower bound (static) method or on the upper bound (kinematic). Thrust-line analysis is an example of the static method and hinge analysis for arches is an example of the kinematic method. The effects of previous applications of loading may generally be ignored and a monotonic increase of the intensity of actions may be assumed.

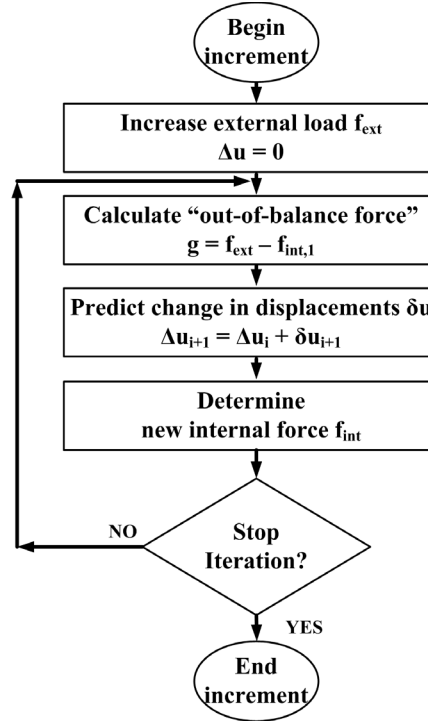
With respect to thrust-line analysis, it must be stressed that its application to larger structures is rather cumbersome and the issue of structural safety is difficult to solve adequately. This method is of interest as a pedagogical tool for engineering students because it demonstrates clearly the flow of forces in a no-tension material such as masonry, even if its application to real structures is often not straightforward (Lourenço 2001). On the contrary, collapse mechanism analysis is a useful tool for engineering purposes. The inherent difficulty in its use is the selection of the adequate collapse mechanism for a given load combination. For traditional masonry constructions, such as the buildings in historic centers, the method can be readily applicable to analysis and strengthening (Lourenço 2002). For more complex and unique monumental structures, this method is still of interest to calculate strengthening, once the relevant collapse mechanisms are identified and the structural behavior is understood resorting to a nonlinear analysis (Nielsen 1998).

### Nonlinear Analysis

In nonlinear analysis, the relation between force and displacement is no longer linear. The relation becomes nonlinear and the current displacements often depend on the displacements at earlier stages. In such analysis, the objective is to calculate a displacement vector that balances the internal and external forces, taking into account different nonlinear effects. Thus, the problem becomes discrete in space (finite elements) but also in time (increments), meaning that to achieve the equilibrium at the end of each increment, an iterative solution algorithm is used in most cases: an incremental-iterative solution procedure (TNO DIANA 2009). In nonlinear analysis, the internal force vector usually depends nonlinearly on the displacements, due to nonlinear mechanical behavior of the materials (physical or material nonlinear analysis). However, the external force vector can also be dependent on the displacements, as the magnitude or direction of the loading depends on the displacement (geometric nonlinear analysis). It is also possible to have both types of nonlinearity in the same analysis.



FIGURE 2.2.  
Chart showing the general  
incremental-iteration process  
(TNO DIANA 2009).



The solution of the nonlinear problem can be implicit or explicit. The implicit approach is useful in problems in which time dependency of the solution is not an important factor (often referred to as statics), whereas the explicit approach is most helpful in solving high deformation time-dependent problems such as crash or blast (or dynamics). In any case, the explicit approach can be used also for static problems, for example by using large damping.

The general procedure for the (implicit) incremental-iterative process can be seen in figure 2.2. The total displacement increment ( $\Delta u$ ) is adapted iteratively by iterative increments ( $\delta u$ ) until equilibrium is reached, up to a prescribed tolerance. The incremental displacement at iteration  $i + 1$  is calculated as follows:

$$\Delta u_{i+1} = \Delta u_i + \delta u_{i+1} \quad (2)$$

There are several different iterative procedures; however, the only difference between them is the way  $\delta u$  is determined. The iterative increments are calculated using a "stiffness matrix" ( $K_i$ ), which represents the relation between the force vector and displacement vector:

$$\delta u_i = K_i^{-1} g_i \quad (3)$$

Here,  $g_i$  is the out-of-balance force vector at the start of iteration  $i$ .

Usually, commercial software allows the user to choose from different possible iteration methods. As an example, DIANA software allows the user to choose from three iterative procedures: (a) Newton-Raphson method, (b) quasi-Newton method, and (c) linear and constant stiffness method. Besides these iterative procedures, there are variations of the iteration algorithm, such as the arc-length method, which adapts the increment size.

Within the Newton-Raphson method are two distinct subclasses: regular Newton-Raphson and modified Newton-Raphson. Both methods use equation 3 to determine the iterative increment of the displacement vector. The difference between both subclasses is the moment at which the stiffness matrix is evaluated. In the regular Newton-Raphson, the

stiffness relation is evaluated every iteration (fig. 2.3a), meaning that the calculation of equation 3 is based on the last known situation, even if it is not an equilibrium state. The modified Newton-Raphson evaluates only the stiffness at the start of the increment (fig. 2.3b), meaning that the calculation is always based on a converged equilibrium state (TNO DIANA 2009). These differences usually result in the regular Newton-Raphson needing fewer iterations, but every iteration is relatively time consuming, while the opposite occurs in the case of the modified Newton-Raphson.

The quasi-Newton method, or secant method, uses the information of previous solution vectors and out-of-balance force vectors during the increment to achieve a better approximation (fig. 2.3c). Unlike the previous methods, the secant does not evaluate a completely new stiffness matrix every iteration. In this case, the stiffness of the structure is determined from the known positions at the equilibrium path. The secant method can be used efficiently because the inverse of the new stiffness matrix can be derived directly from the previous secant stiffness and the update vectors using the Sherman-Morrison formula (TNO DIANA 2009).

The linear stiffness method uses a linear stiffness matrix during the analysis (fig. 2.3d). This method has the lowest convergence rate, but it costs the least time per iteration since the stiffness matrix needs to be evaluated only once. The constant stiffness method used the stiffness matrix evaluated in the previous increment.

FIGURES 2.3A–D.

Iteration methods: (a) regular Newton-Raphson method; (b) modified Newton-Raphson method; (c) secant method, or quasi-Newton method; (d) linear stiffness method (TNO DIANA 2009).

### Pushover Analysis

Pushover is a nonlinear analysis method for seismic assessment, where a structure is subjected to gravity loading and a monotonic lateral load pattern representing inertial forces related to the mass of the structure, which continuously increases through elastic and inelastic behavior until an ultimate condition is reached (fig. 2.4). This lateral load pattern represents the range of base shear induced by earthquake loading, and its configuration

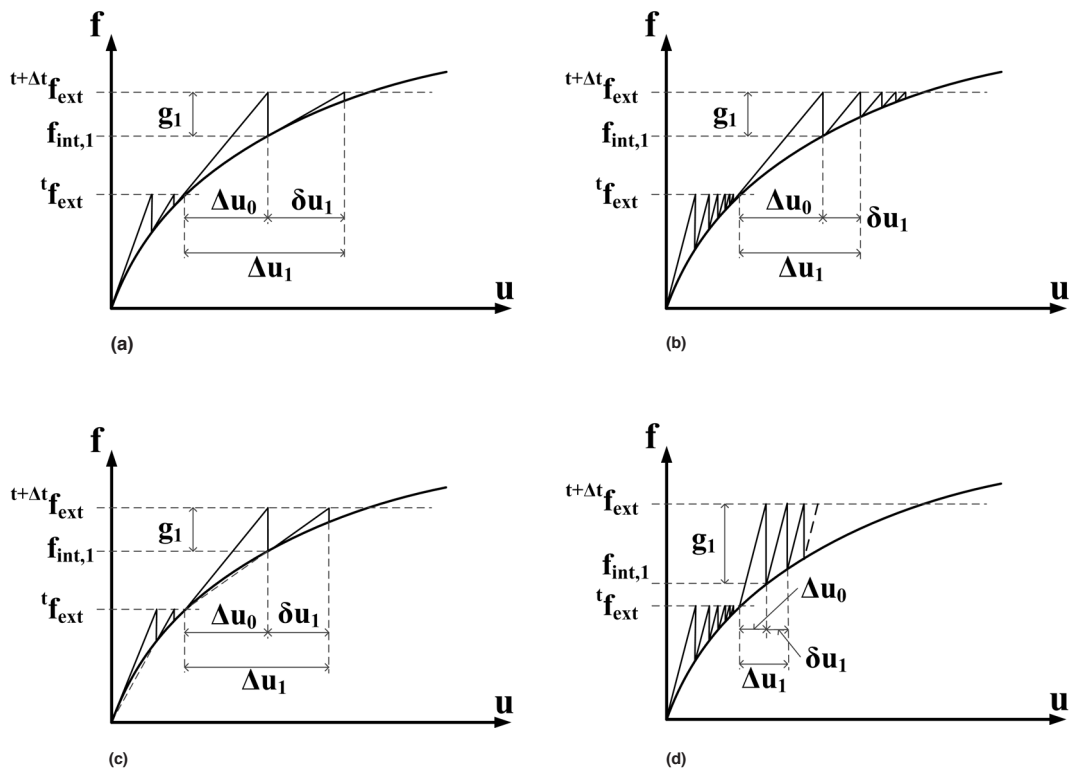
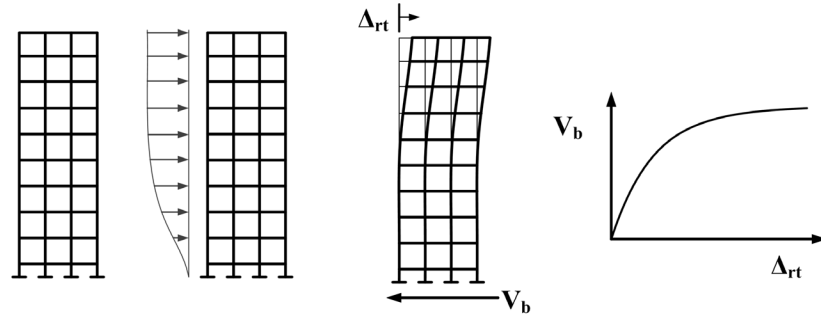


FIGURE 2.4.

Diagram and graph showing typical pushover analysis procedure and outcome.



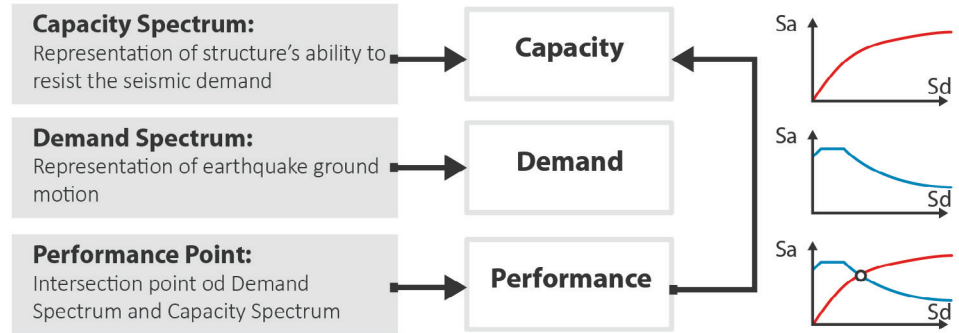
varies according to the type of pushover analysis used, typically uniform, inverted triangular or mode proportional.

Output generates a static-pushover curve which plots a strength-based parameter against deflection in a representative point, typically the roof level or the level with the largest displacement (see fig. 2.4). Results provide insight into the ductile capacity of the structural system and indicate the mechanism, load level, and deflection at which failure occurs. Some normative documents, such as ASCE 41-06 (2007), define different performance criteria based on the static-pushover curve.

To perform a pushover analysis for the assessment of seismic safety, the user must define a load pattern that approximates the distribution of inertia forces. There are several possibilities when choosing the load pattern acting on the structure. In invariant lateral force distributions, the load distribution is constant throughout the analysis. Here, the most frequently used distributions are the ones proportional to the mass of the structure (Betti and Vignoli 2011; Roca et al. 2013; Ivancic et al. 2014) and proportional to the first modal shape (Lourenço et al. 2012). The latter must be used carefully in historic structures, as the first modes are often complex and have low participation mass. However, frequently used, these types of pushover analysis have some limitations, namely the inability to detect changes in the nonlinear dynamic characteristics due to the evolution of damage in the structure (Krawinkler 1995). More advanced pushover analyses have been formulated, such as the modal pushover analysis and the adaptive pushover analysis (FEMA 440 2004; Aydinöglu 2003; Papanikolaou and Elnashai 2005).

The lateral distribution pattern of the equivalent seismic load has an influence on the results of the analysis. Several studies have been developed to compare the different lateral load distribution patterns. It has been shown that mass proportional load distribution usually induces more extensive damage, while the first mode proportional mass distribution induces more damage on the higher parts of the structure (Galasco, Lagomarsino, and Penna 2006). The estimation of the maximum shear capacity of the structure is usually lower when using the first mode proportional load pattern (Saloustros et al. 2015; Simões et al. 2014; Endo, Pelà, and Roca 2016). When comparing the results of pushover analysis with nonlinear dynamic analysis, it seems that mass proportional distributions are able to predict a maximum shear capacity closer to the one predicted using nonlinear dynamic analysis (Endo et al. 2015; Endo, Pelà, and Roca 2016). However, some cases have been reported as having the first mode proportional distribution closer to nonlinear dynamic analysis in the case of masonry buildings without box behavior (Lourenço et al. 2011). In terms of displacement capacity, it appears that the pushover analysis, independent of the load distribution pattern, underestimates the displacement capacity of the structure when compared with nonlinear dynamic analysis (Pelà, Aprile, and Benedetti 2013; Endo et al. 2015; Endo, Pelà, and Roca 2016).

**FIGURE 2.5.**  
Chart and graphs showing the seismic assessment procedure.

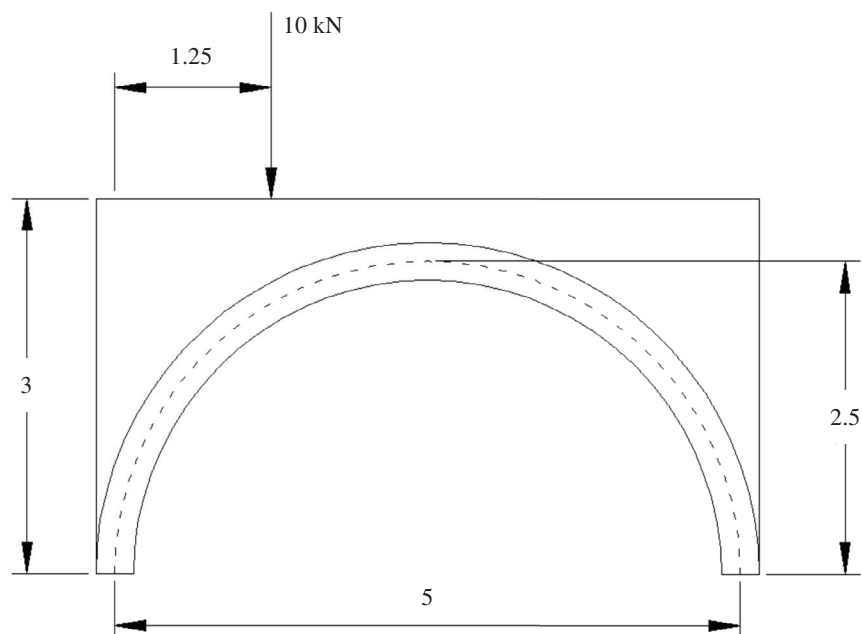


Pushover analysis is one of the most robust analyses for seismic assessment. The European normative in fact suggests the application of the N2 method proposed by Fajfar (2000), based on the combination of pushover analysis with the capacity spectrum approach (correlating the displacement capacity of the structure to the displacement demand of the expected earthquake) (fig. 2.5). When compared with more advanced analysis types, such as nonlinear dynamic analysis, pushover analysis has been revealed to be a suitable and practical approach for seismic assessment (Lourenço 2001; Lourenço et al. 2011; Endo et al. 2015; Endo, Pelà, and Roca 2016). From all the available load distribution patterns, mass proportional appears to be the most reliable pushover method for masonry structures (Saloustros et al. 2015; Endo, Pelà, and Roca 2016).

### Comparison of Static Analysis Methods

The following exercise illustrates the different static analysis methods described previously; see Lourenço (2001) for details. These methods are applied to a semicircular arch (fig. 2.6). The arch has a span of 5.0 m, a rise of 2.5 m, a thickness of 0.3 m, and a width of 1.0 m. A nonstructural backfill up to a height of 3.0 m is considered in the analyses. The loads considered include the weight of the arch (volumetric weight  $\gamma = 20 \text{ kN/m}^3$ ) and fill ( $\gamma = 15 \text{ kN/m}^3$ ) as dead load, and a point load of 10 kN at a quarter span as live load.

**FIGURE 2.6.**  
Geometry of the arch adopted for static analysis (Lourenço 2001).

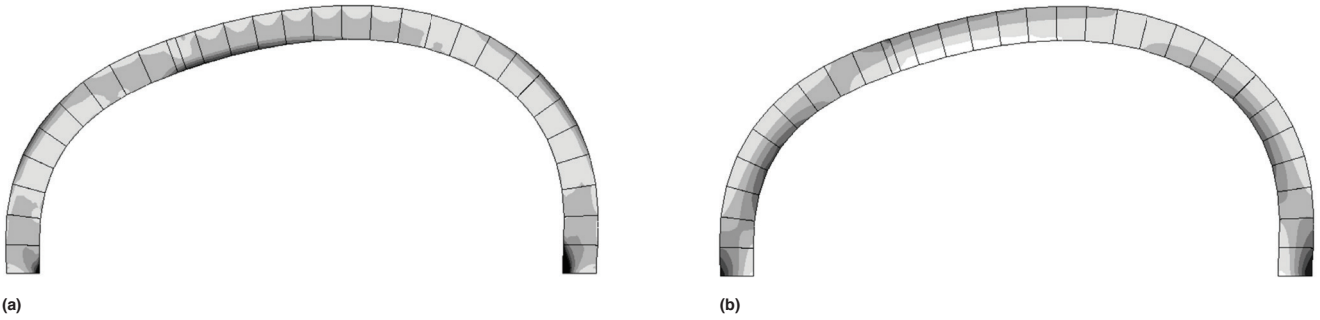


The following structural analyses were carried out: (a) linear elastic finite element analysis; (b) kinematic limit analysis (or hinge analysis); (c) static limit analysis (or thrust-line analysis), with calculation of the so-called geometric safety factor; (d) nonlinear physical finite element analysis; and (e) nonlinear combined physical/geometrical finite element analysis. In all cases, the dead load is applied first, followed by the monotonic application of the live load until failure.

For the linear elastic analysis, eight-node plane stress elements (for the units), combined with six-node line interface elements (for the interface), were adopted (see chapter 3 for a discussion on element types and chapter 5 for a discussion on modeling strategies for masonry and earthen buildings). The following elastic properties were assumed: (a) units, Young's modulus of 10,000 MPa and Poisson ratio of 0.2; and (b) interface, normal stiffness of 2400 N/mm<sup>3</sup> and transverse stiffness of 1000 N/mm<sup>3</sup> (see chapter 5 for recommended material properties for historic structures). The results of the linear elastic analysis are shown in figures 2.7a and 2.7b in terms of maximum and minimum principal stresses. In order to establish the safety of the structure being considered, it is usual to define some allowable maximum stress in case of linear elastic analysis. If the allowable maximum stress is zero, then no load can be applied to the arches for this type of analysis. Therefore, a low value should be considered as usually exhibited by masonry. Here, a maximum allowable tensile stress,  $f_{ta}$ , of 0.2 MPa and unlimited compressive stress were assumed. For the adopted mesh discretization (as the peak values depend on the mesh discretization), the obtained safety factor was 0.3.

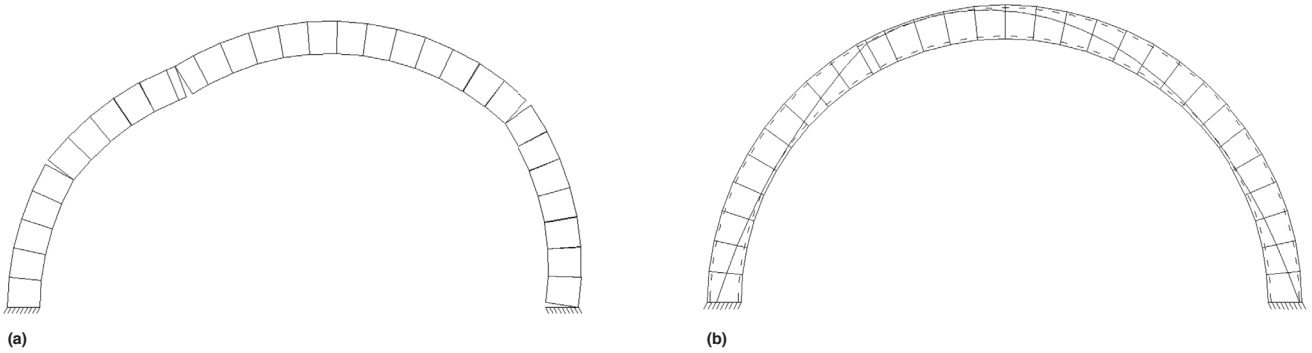
For the limit analysis, a nonlinear programming implementation of the limit analysis was adopted (Orduña and Lourenço 2001). Commercial software is available for this purpose, such as RING by LimitState Ltd. For this type of analysis, it is necessary to know the ultimate strength properties of the materials, being that the elastic properties of the materials are not relevant. It was assumed that failure can occur only in the joints of the model and that the properties were as follows: (a) zero tensile strength and unlimited compressive strength; (b) friction angle of 37 degrees or friction coefficient of 0.75; and (c) zero dilatancy. Figures 2.8a and 2.8b show the obtained collapse mechanism and thrust line. The safety factor of the structure can be evaluated when using this type of analysis. The kinematic safety factor is 1.8. The geometric safety factor (Heyman 1969), which represents the ratio between the actual thickness of the arch and the (minimum) thickness of an internal arch with the original span and is able to resist the original applied load, is 1.2.

The finite element mesh used for the linear elastic analysis was also adopted for the nonlinear analyses. In this case, both the elastic and inelastic properties of the materials are required. The elastic properties used for the linear elastic analyses and the inelastic properties used for the limit analyses were again used for this nonlinear analysis, now together. Both physical nonlinear behavior and combined physical/geometrical nonlinear behavior were considered. Figures 2.9a and 2.9b show the results of the physical nonlinear analysis, in terms of minimum principal stresses and deformed meshes, at peak load. The results for the combined physical/geometrical nonlinear analyses were quite similar to the results shown in figures 2.9a and 2.9b. A second nonlinear analysis was carried out, adopting some limited, yet non-zero, strength. For this purpose, a tensile strength,  $f_t$ , of 0.2 MPa, a cohesion of 0.3 MPa, and a fracture energy of 0.1 N/mm were assumed in the joints. Note that this tensile strength will degrade to zero and is not an assumed constant value as the admissible tensile strength,  $f_{ta}$ , above. Again, both physical and combined physical/geometrical nonlinear behavior were analyzed. Safety of the structure can also be evaluated when using nonlinear analysis. For zero tensile strength and physical nonlinear analysis, the ultimate load factor (i.e., the scalar multiplying the point load) is 1.8, as for kinematic limit analysis.



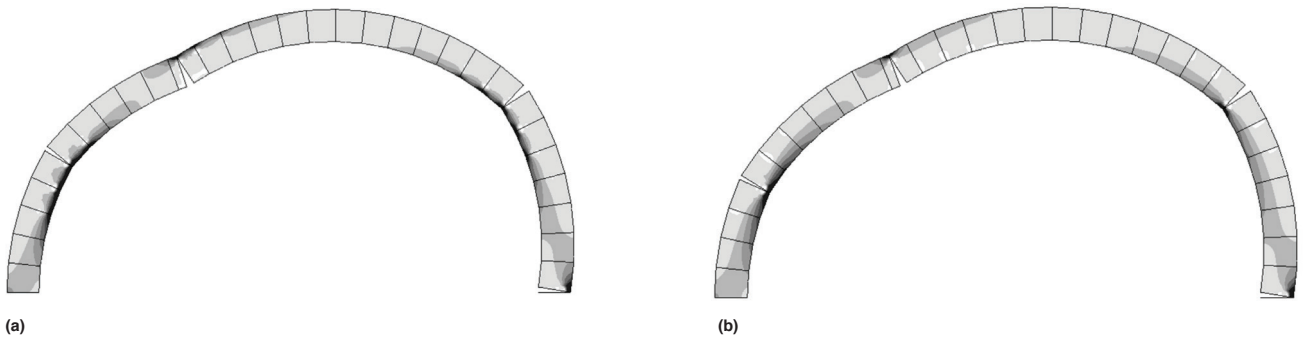
FIGURES 2.7A, 2.7B.

Diagrams showing results of linear elastic finite element analysis in a masonry semicircular arch subjected to a point load (Lourenço 2001): (a) maximum value of the principal stresses (peak value:  $0.64 \text{ N/mm}_2$ ); (b) minimum value of the principal stresses (peak value:  $-1.0 \text{ N/mm}_2$ ).



FIGURES 2.8A, 2.8B.

Diagrams showing results of limit analysis in a masonry semicircular arch subjected to a point load (Lourenço 2001): (a) failure mechanism (kinematic load factor 1.8); (b) thrust line and internal minimum thickness arch (indicated by dotted lines) (geometric load factor 1.2).



FIGURES 2.9A, 2.9B.

Drawings showing failure mechanism and minimum principal stresses at ultimate load for nonlinear physical analysis for a masonry semicircular arch (Lourenço 2001): (a) zero tensile strength (peak value:  $-5.4 \text{ N/mm}_2$ ); (b) non-zero (low and degrading) tensile strength (peak value:  $-5.4 \text{ N/mm}_2$ ).

Figure 2.10 shows the load-displacement diagrams for the nonlinear analyses calculations and the ultimate load factor for the kinematic limit analysis, whereas table 2.1 shows the obtained maximum load factors in the different analyses.

The linear elastic analysis gives information about the deformational behavior and stress distribution of the structure. The limit analysis provides information about the failure mechanism of the structure. The nonlinear analysis gives full information. For the simple arch presented here, physical nonlinear analysis and kinematic limit analysis provide the same failure mechanism and ultimate load factor (if a zero tensile strength is assumed). Also, if geometrical nonlinear behavior is included in the analysis, the ultimate load factor is reduced by about 10% for this structure.

The consideration of a non-zero, yet low and degrading, tensile strength increased the ultimate load factor considerably (about 40%). Therefore, when using a non-zero tensile strength, special care might be necessary in real case applications: (a) tensile strength is

FIGURE 2.10.

Load-displacement graph showing the different nonlinear analyses and limit analysis safety factors for a masonry semicircular arch ( $f_t$  is the tensile strength of masonry, which degrades) (Lourenço 2001).

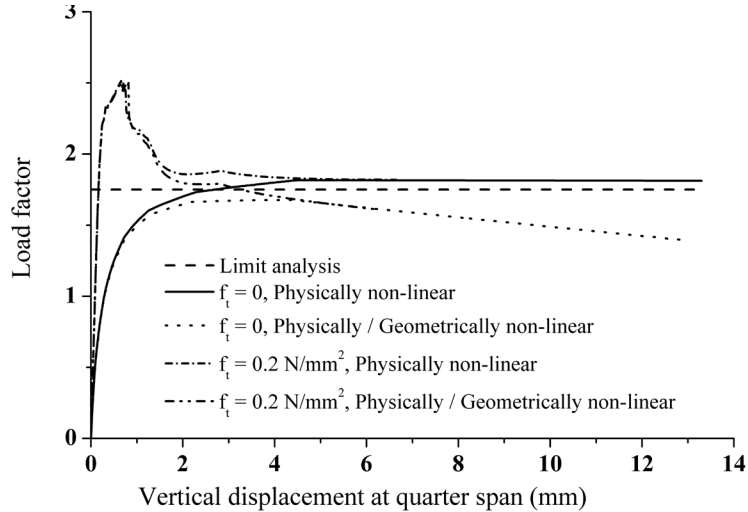


TABLE 2.1.

Maximum load factors for the different analyses considered (Lourenço 2001).

| Approach/Analysis Type                              | Max. Load Factor |
|---|------------------|
| Allowable stresses ( $f_{ta} = 0.2$ MPa)            | 0.3              |
| Kinematic limit analysis                            | 1.8              |
| $f_t = 0$ , physical nonlinear                      | 1.8              |
| $f_t = 0$ , physical and geometrical nonlinear      | 1.7              |
| $f_t = 0.2$ MPa, physical nonlinear                 | 2.5              |
| $f_t = 0.2$ MPa, physical and geometrical nonlinear | 2.5              |

difficult to assess, and (b) tensile strength might be severely reduced at critical locations. Also, the post-peak response obtained in a nonlinear analysis is an important issue when addressing structural safety. Brittle responses provide little warning and should require larger safety to provide similar risk levels. In the present case, the residual capacity of a non-zero tensile strength structure is similar to the zero tensile strength capacity, and this residual load factor seems to be the one to adopt for engineering purposes.

In conclusion, the different nonlinear methods and the limit analysis method provide rather similar results in terms of capacity of the structure (a maximum load factor of about 1.8). Conversely, linear elastic analysis cannot be used and provides an unrealistic low value, which corresponds to the onset of the first crack (in this case about 1/6 of the maximum load). Masonry arches (and most historic structures) crack easily, but the structure is not necessarily unsafe. Therefore, linear elastic analysis should not be used. The geometric safety factor (equal to 1.2) cannot be related to the ultimate load factor, meaning that it should not be used to define safety levels, at least according to the modern code-based approach.

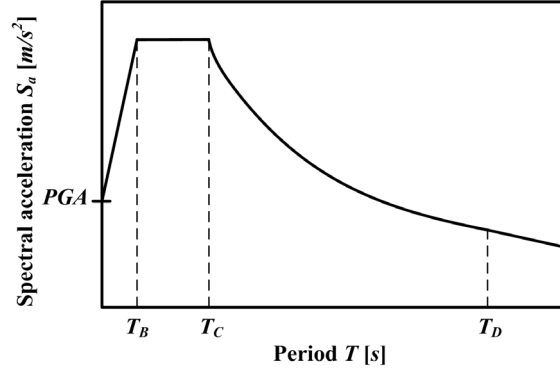
## Dynamic Analysis

### Response Spectrum Analysis

Response spectrum analysis is a linear dynamic analysis method that measures the contribution from each natural mode of vibration to indicate the likely maximum seismic response of an essentially elastic structure. The results of a response spectrum analysis

FIGURE 2.11.

Example of a spectral acceleration diagram of an earthquake. PGA is peak ground acceleration, or the maximum ground acceleration that occurs during an earthquake.



are given in terms of individual and combined modal forces (Gupta 1992). A response spectrum analysis requires the specification of an excitation spectrum (fig. 2.11), also known as a period-acceleration spectrum. The excitation spectrum is specified by a base excitation, nodal, or element load, and a diagram with period-dependent load multiplication coefficients.

Response spectrum analysis is based on the mode superposition principle. The modal response may be combined using different approaches, such as (a) absolute sum (ABS); (b) square root of the sum of the squares (SRSS); or (c) complete quadratic combination (CQC). The ABS method is simply a summation of the absolute values of the modal results (eq. 4). The SRSS method is a technique that does not take into account modal damping or cross coupling (eq. 5). The CQC method accounts for modal damping; however, if damping is zero, CQC gives the same result as SRSS (eq. 6). These three methods for modal combination are the most commonly used.

$$\text{ABS method: } F_{max} = \sum_{i=1}^N |F_{i,max}| \quad (4)$$

$$\text{SRSS method: } F_{max} = \sqrt{\sum_{i=1}^N F_{i,max}^2} \quad (5)$$

$$\text{CQC method: } F_{max} = \sqrt{\sum_{i=1}^N \sum_{j=1}^N \rho_{ij} |F_{i,max} F_{j,max}|} \quad (6)$$

Here,  $\rho_{ij}$  is a correlation coefficient, which varies between zero and unity,  $F_{i,max}$  is the maximum modal response for mode  $i$ , and  $N$  is the number of modes.

Response spectrum analysis is useful for assessment of structures because it relates structural type selection to dynamic performance. It also can be used to understand the main vibration modes in each direction, as well as to define a proper distribution of the forces for a pushover analysis. However, in the case of masonry buildings, which are characterized by having highly nonlinear behavior, a linear elastic analysis is not the most suitable technique.

### Time History Analysis

Time history analysis provides evaluation of dynamic structural response under loading, which varies according to the specified time function (ground motion accelerograms). These analyses can be linear or nonlinear, depending on the considerations made on the material's mechanical properties. These types of analysis are usually taken as the most representative when assessing the seismic behavior of structures. However, there are a few drawbacks: (a) these analyses are very time consuming; (b) they may be dependent on the



selection of the applied ground motion accelerograms; and (c) they involve complexity in terms of execution and interpretation of the results.

Although its use is allowed in building codes for seismic assessment of structures (Bommer and Ruggeri 2002), time history analysis seems to be mostly used for academic and research purposes, being occasionally used in high-impact structures (complex or safety-critical facilities). To properly take into account the variability of the action, seismic building codes require several analyses to be performed with different ground motion accelerations. The process of selection and production of the ground motion accelerograms and the number of analyses required by the seismic building codes make this analysis unfeasible for a design office.

As stated, one key parameter for such computations is the input motion, or the ground accelerogram. The method to develop these accelerograms is not always clearly defined in the seismic building codes (e.g., EC8 2004). Possible alternatives include (Bommer and Acevedo 2004): (a) using artificial spectrum-compatible accelerograms; (b) using synthetic accelerograms generated from seismological source models; and (c) using real accelerograms recorded during earthquakes.

The first type of accelerograms (artificial spectrum-compatible) are obtained by generating a power spectral density function from the code response spectrum (fig. 2.12) and deriving signals compatible to that spectrum (Bommer and Acevedo 2004; Iervolino, Maddaloni, and Cosenza 2008). Even though it is possible to obtain acceleration time-series that are compatible with the elastic design spectrum, the generated accelerograms often have an excessive number of cycles of strong motion and consequently have unrealistically high energy content (Bommer and Acevedo 2004). The difficulty of the artificial time history generation methods lies in trying to match a single ground motion to a design response spectrum that is not intended to represent the motion from an individual earthquake (Naeim and Kelly 1999). The design response spectrum is generally a result of a statistical analysis that considers the influence of several seismic sources simultaneously; hence, the response at different periods may be driven by earthquakes in different sources,

**FIGURE 2.12.** Example of an artificial spectrum-compatible generated accelerogram (SeismoArtif 2016 software, SeismoSoft).



and the spectrum is the envelope of spectra corresponding to scenarios in each of the sources (Reiter 1990; Bommer, Scott, and Sarma 2000).

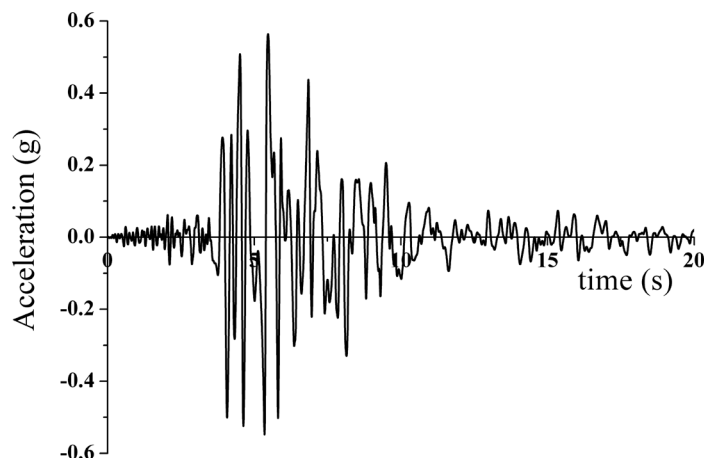
The second type of accelerogram are synthetic accelerograms and can be generated from seismological source models, accounting for path and site effects. In general, there are difficulties in defining appropriate input parameters such as source, path, and site characteristics. To generate synthetic accelerograms, there is a need for the definition of a specific earthquake scenario in terms of magnitude and rupture mechanism in addition to geological conditions and location of the site. Generally, most of these parameters are not available, particularly when using seismic building codes (Bommer, Acevedo, and Douglas 2003). Software for ground motion generation has been developed (e.g., Zeng, Anderson, and Yu 1994; Beresnev and Atkinson 1998; Boore 2003), but the application, in terms of defining the many parameters required to characterize the earthquake source, will generally require the engineer to engage the services of a specialist consultant in engineering seismology.

The third type of accelerograms, real ground motion accelerograms, contain a wealth of information about the nature of the ground shaking. Due to the increase of available strong ground motion records, using and scaling real recorded accelerograms has become more common (fig. 2.13). Despite the continued growth of the global strong motion data-bank, there are many combinations of earthquake parameters that can make obtaining suitable records difficult in some circumstances (Bommer, Acevedo, and Douglas 2003).

In seismic codes, the guidelines for preparation of ground motion input for dynamic analysis are generally poor (Bommer and Ruggeri 2002). The code-based prescriptions for records often require compatibility with a smooth design acceleration spectrum. For example, Eurocode 8 (EC8 2004) allows employment of all three kinds of accelerograms listed above as an input for seismic structural analysis. The EC8 prescriptions request matching the average spectral ordinates of the chosen record set to the target code-based spectral shape. The accelerogram set must consist of at least seven recordings to consider the mean of the response. Otherwise, if the size of the set is from three to six, the maximum response to the records within the sets needs to be considered.

Nonlinear time history analysis of masonry structures is complex and time consuming. Masonry structures are characterized by low values of tensile strength, meaning that there will be important cracking in the structure, with cracks opening, closing, and reopening. This mechanical behavior present in masonry introduces in the numerical calculations some numerical noise, due to the fast transition from linear elastic behavior to a fully cracked

FIGURE 2.13.  
Example of a real recorded  
accelerogram.



state involving almost zero stiffness (Mendes and Lourenço 2010). This fast and constant change in the displacement field tends to originate the propagation of high-frequency spurious vibrations (Cervera, Oliver, and Faria 1995). Therefore, it is important to use an appropriate time integration method. The Hilber-Hughes-Taylor integration method (the HHT method, or the  $\alpha$  method) allows the introduction of numerical dissipation without degrading accuracy (TNO DIANA 2009). This method requires the definition of an  $\alpha$  parameter that varies between  $-1/3$  and  $0$ . For  $\alpha = 0$ , the method reduces to the Newmark method. For values of  $\alpha$  between  $-1/3$  and  $0$ , the scheme is second-order accurate and unconditionally stable. Decreasing  $\alpha$  means increasing the numerical damping. This damping is low for low-frequency modes and high for high-frequency modes (TNO DIANA 2009).

One other important aspect when performing a time history analysis is the definition of the time step for each increment of the analysis. Commercial software offers different possibilities to address this aspect. The most common approach is to explicitly define a constant time step throughout the analysis. To properly define an adequate time step, there are some recommendations. TNO DIANA (2009) suggests that the time step  $\Delta t$  should be determined according to equation 7:

$$\Delta t = \frac{1}{20} T_i \quad (7)$$

Here,  $T_i$  is the lowest period with relevance for the structural behavior.

One other possibility when addressing time integration analysis is to use explicit calculations as opposed to implicit. Explicit methods calculate the state of a system at a later time from the state of the system at the current time, while implicit methods find a solution by solving an equation involving both the current state of the system and the later one. Whereas an implicit calculation must iterate to determine the solution to a nonlinear problem, an explicit calculation determines the solution without iterating by explicitly advancing the kinematic state from the previous increment. Explicit analysis will be performed with smaller time steps when compared with implicit analysis, meaning that the required number of increments to complete the analysis will be higher in the explicit analysis. Explicit analysis may be more efficient if the same analysis using an implicit method requires many iterations, but there is the risk that the obtained result is incorrect if inadequately used. Some commercial software allows both possibilities (e.g., ABAQUS/Standard and ABAQUS/Explicit). Still, for earthquake engineering, due to the fast change in accelerations and the random nature of the input, explicit methods are rarely used.

# User Guidance on the Finite Element Method

The finite element method (FEM) has become possibly the most powerful analysis tool for solving engineering problems. FEM is a computational numerical technique most commonly used to solve complex engineering problems by dividing them into smaller, manageable blocks or problems. It should be kept in mind that a finite element analysis (FEA) does not produce a formula (closed-form expression) as a solution and does not solve a class of problems (only a specific problem), and that the solution is approximate (entailing some error).

To analyze a structure using FEM, the structure is idealized as a numerical conceptual model where the structure is broken down into a finite number of regions or parts (elements). These elements are connected to one another at specific points (nodes). This assembly of elements and nodes is called *mesh*.

To shorten the computational time required to provide the solution to the problem, to maximize the confidence in this solution, and to minimize errors in the analysis process, the modeler (or analyst) must (a) understand the physics of the problem and the behavior of the finite elements; (b) select the proper element type(s), element number, and element arrangement; (c) understand the effects of the used simplifications and assumptions; and (d) critically evaluate the results and, if possible and/or needed, make modifications in the model to improve its accuracy.

## Planning the Analysis

Before starting any analysis, it is important to think and plan the approach to be used for the problem at hand. It is important to have a clear understanding of (a) what the objectives are; (b) what criteria will be used to evaluate the objectives; (c) what the required output is considering the required objectives; (d) how much of the structure needs to be modeled; (e) what the boundary conditions and loads are; and (f) other relevant applicable aspects.

Decision making at critical moments throughout the modeling process requires training, experience, and expert opinion. The decisions made will influence the accuracy and the required computational time of the solution. The critical steps at which these decisions need to be made are as follows:

- Choice of type of analysis
- Definition of material properties and constitutive models
- Definition of geometry details and level of detail (or simplifications)
- Selection of element type(s) and modeling approach
- Selection and application of supports, constraints, and loads

## Model Geometry

As discussed in chapter 2, the analysis of historic masonry monuments is a very complex task. In general terms, there are two major steps required when facing these kind of engineering problems: (a) idealization of the geometry and (b) idealization of the materials. These two steps have much influence on the response of the structure. In the specific case of historic structures, the common findings are as follows:

- Geometry data are incomplete.
- Information about the internal composition of the structural elements is also incomplete.
- Significant changes in composition of structural elements occurred, associated with long construction periods.
- Construction sequence is unknown, also affecting the actual load distribution in the structure.
- Existing damage in the structure is unknown.

This lack of information or uncertainty must be accepted and may be considered when idealizing the geometry of the model, for example by performing sensitivity analysis affecting the most relevant influencing factors. It is evident that the analysis of historic masonry structures contains many simplifications. Therefore, the idealization of the geometry should be kept as simple as possible, while being adequate for solving the problem under consideration.

## Element Type

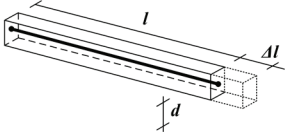
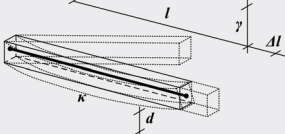
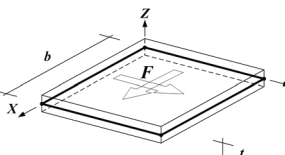
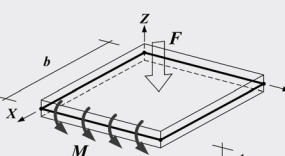
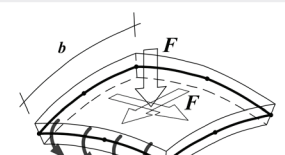
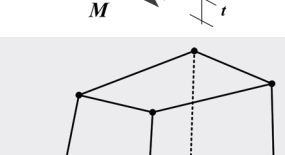
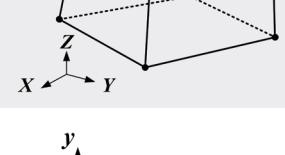
In general, when using FEM software, there are several different types of elements available to idealize the problem. Some types are more relevant for general applications, while others have a more limited application. Table 3.1 summarizes the available element types in most FEM software.

In the specific case of historic masonry structures, the geometry can usually be idealized in different ways, namely using linear elements (truss or beam elements), plane “two-dimensional” elements (shell elements, often denoted by 2.5D), or fully three-dimensional elements (solid elements). Truss or beam elements are usually used to idealize linear structural components, such as truss elements for steel tie rods or stitching bars or beam elements for lintels, arches, beams, and columns. Typical applications of shell elements are roofs, walls, and slabs but also vaults or domes, being flat or curved components. Solid elements are general-purpose elements. It is not straightforward to define the conditions under which a given idealization of the geometry is the most appropriate one. The geometry of historic masonry structures is rather complex as there often is no distinction between decorative and structural elements. Therefore, it is not clear which approach is the best, and, in several cases, the final adopted strategy involves a combination of some or all of the above-mentioned element types. It is also beneficial that, at an early phase of the analysis, different models are tried and compared, aimed at verifying the results of the element type selection and defining the most adequate model.

One other important aspect of model discretization is the element order. Element order refers to the polynomial representation of the element’s shape functions, being usually linear or quadratic. This is a mathematical function that, within the element, interpolates the solution between the discrete values (i.e., displacements or rotations) obtained at the mesh nodes. Because FEA obtains a solution for degrees of freedom (DOF) values only

TABLE 3.1.

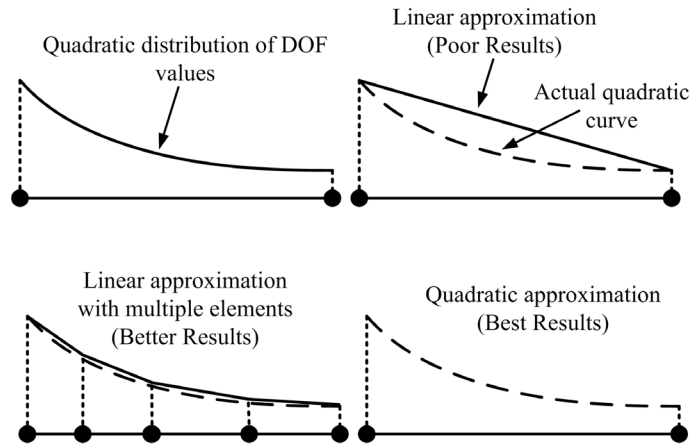
Summary of typically available FEM element types (TNO DIANA 2009).

| Element Type                     | Brief Description   | Generic Scheme  |
|----------------------------------|---|---|
| <b>Truss element</b>             | Truss elements are linear elements in which the deformation can only be the axial elongation ( $D/l$ or $e$ ).  |    |
| <b>Beam element</b>              | Beam elements are linear elements in which the deformation can be axial elongation ( $D/l$ ), shear deformation ( $g$ ), curvature ( $k$ ), and torsion ( $f$ ).  |    |
| <b>Plane stress element</b>      | Plane stress elements are two-dimensional elements in which the deformation can only be translations ( $u_x$ and $u_y$ ) in the plane of the element.   |    |
| <b>Plate bending element</b>     | Plate bending elements are two-dimensional elements in which the deformation can only be rotations in the direction of the plane of the element ( $\phi_x$ and $\phi_y$ ) and translation in the direction perpendicular to the plane of the element ( $u_z$ ). |    |
| <b>Shell element</b>             | Shell elements are two-dimensional elements in which the deformation can only be the translations in the three general directions ( $u_x$ , $u_y$ , and $u_z$ ) and the rotations in the directions of the plane of the element ( $\phi_x$ and $\phi_y$ ).      |   |
| <b>Solid element</b>             | Solid elements are three-dimensional general-purpose elements in which the deformation can be the translations in the three general directions ( $u_x$ , $u_y$ , and $u_z$ ).   |  |
| <b>Contact/interface element</b> | Contact or interface elements are special elements that are able to describe a specific behavior between two other elements, providing a relation between the stresses (tractions) on the surfaces and their relative displacements.                            |  |

at the nodes, a shape function is required to map the nodal degrees of freedom values to points within the element. The choice of the element order directly affects the accuracy of the solution (Rajadurai et al. 2014) (fig. 3.1).

When an element type is chosen, the modeler is implicitly choosing and accepting the element shape function assumed for that element type. Therefore, the element order information should be checked before choosing an element type. As depicted in figure 3.1, one alternative is to use linear elements in a finer mesh. Quadratic elements seem more

**FIGURE 3.1.**  
Comparison of element orders  
(Rajadurai et al. 2014).



appealing but, when complex nonlinear analysis is used, involving material deterioration (i.e., loss of strength), the robustness of the finite element type in these conditions can be more relevant than the order of the approximation. Linear elements are more constrained and are less prone to spurious movements than quadratic elements, in the presence of very low stiffness due to extensive inelastic behavior.

### 2D vs. 2.5D vs. 3D

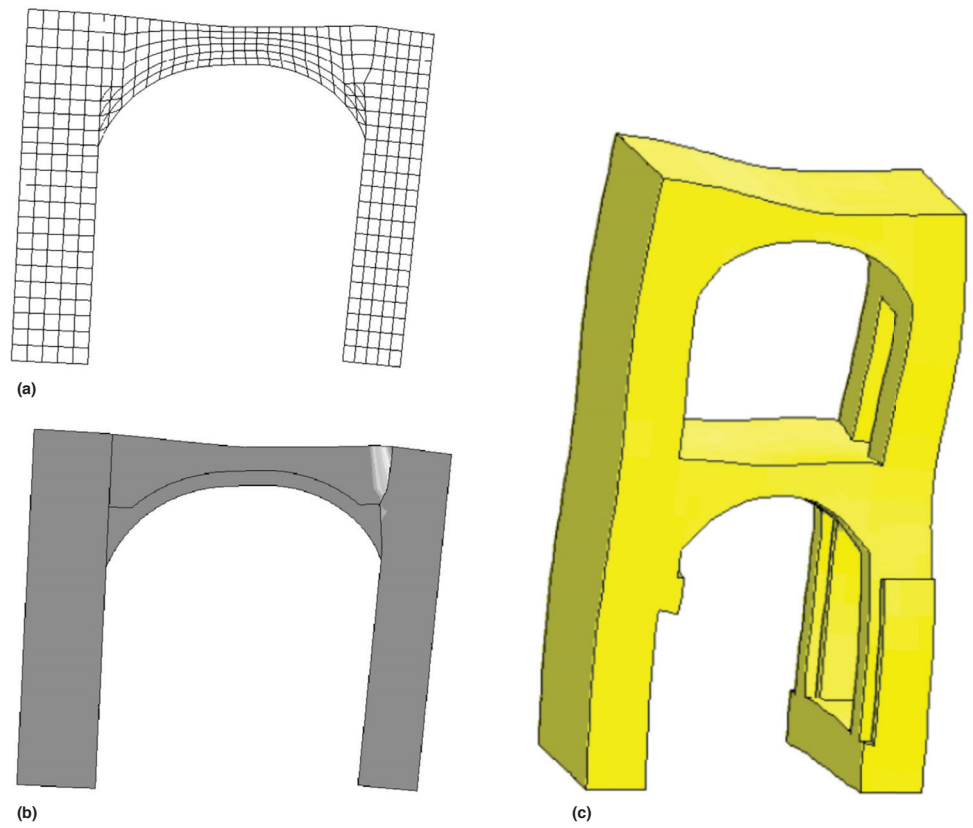
It seems that fully three-dimensional elements (3D) are the most appropriate type of element for historic structures; however, these are usually time consuming (considering the time used to prepare the model, perform the actual calculations, and analyze the results). Shell models (2.5D), on the other hand, exhibit a variation of stresses along the thickness of the element, requiring attention and often the increase of integration points along its thickness. Moreover, shell models consider only the middle plan of the element, while the rigid stiffness of the connection between two orthogonal elements is not considered. The connection stiffness is particularly important for the global response in the case of historic masonry structures, as the walls are generally very thick when compared to their length or height. Similarly, if shells are used for vaults or domes, the stiffness of the connections can be partly misrepresented. Finally, there are cases in which only a part of the structure can be analyzed and the full building does not need to be represented. Proper boundary conditions that allow the user to take into consideration the rest of the structure, for example using springs or interface elements, may need to be introduced. Finally, plane stress models (2D) are often inapplicable to historic structures, given the intrinsic three-dimensional effects present. In a few cases, they can be used to analyze parts of the building (e.g., an arch, a barrel vault, or a long wall).

Comparisons are made using different modeling approaches. Figures 3.2a–c show models of the cloister of a Cistercian monastery in Salzedas, Portugal. The two-dimensional model (fig. 3.2a) was adopted for performing a nonlinear analysis that allowed an understanding of the damage to the structure (fig. 3.2b) and to assess its safety. The three-dimensional model (fig. 3.2c) is shown only for academic purposes and includes analysis with soil-structure interaction. The difference in displacements and stresses at specific control points at the barrel vault was less than 10% (Lourenço 2001).

Figures 3.3a and 3.3b show models of the refectory of the monastery of Jerónimos, Portugal. Two modeling approaches were used: (a) three-dimensional elements (fig. 3.3a) and (b) shell elements (fig. 3.3b). It is worth noting that the three-dimensional model yields

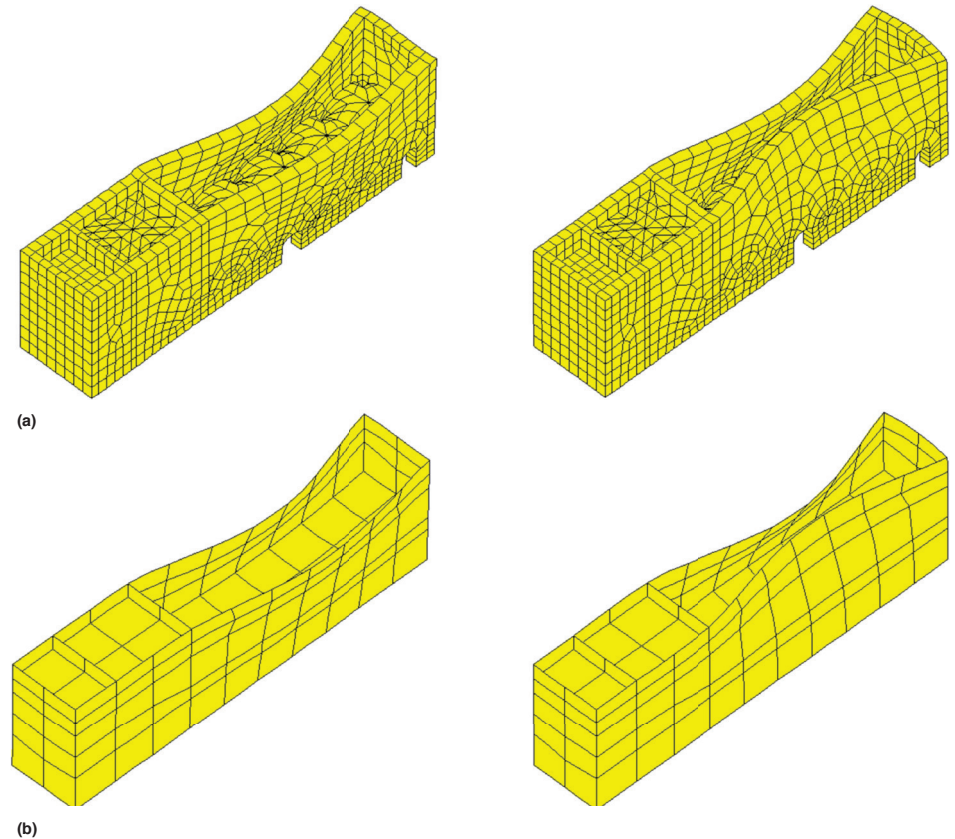
FIGURES 3.2A–C.

Models of the cloister of an eighteenth-century Cistercian monastery in Salzedas, Portugal, showing (a) deformed shape of two-dimensional model at failure; (b) damage pattern of two-dimensional model at failure; (c) deformed shape of three-dimensional model (Lourenço 2001).



FIGURES 3.3A, 3.3B.

Models of the refectory of the monastery of Jerónimos, Portugal, showing the shape of the first two vibration modes: (a) three-dimensional elements; (b) shell elements (Lourenço and Mourão 2001).





similar results to those of the simplified shell model for the first two vibration modes. Nevertheless, there was a need to correct the thickness of the walls in the shell model to consider the additional stiffness provided by the connection of the thick walls. Also, the location of the horizontal elements representing the slabs needs to be carefully selected (Lourenço and Mourão 2001). The model with 3D elements is certainly more appropriate to study the refectory, but the simplified shell model was adopted for a global analysis under seismic loading of the full compound of the monastery (in-plan size greater than  $300 \times 50 \text{ m}^2$ ).

One possible source of errors in the analysis of historic masonry structures is the use of fully three-dimensional elements and very coarse meshes, particularly across the thickness, meaning that in some cases there is only one lower-order element through the thickness of the structural element (Lourenço 2001). This discretization may provide large errors in bending and the accuracy of the results may be compromised. In fact, some authors suggest that an acceptable finite element mesh with solid elements should consist of five finite elements through the thickness (Bjorkman and Piotter 2008).

Finally, careful analysis of the building is recommended before starting to model it and to understand where each type of element can be introduced to the best of its use and the acceptable complexity level. Quite often the best modeling solution comprises different types of elements.

### **Meshing**

An FEM model is broken down into individual finite elements according to a systematic procedure known as meshing the model. The shape and size of the elements have an important impact on the solution. A mesh that is too coarse can produce inaccurate solutions, while a mesh that is too fine will result in excessive computation time, particularly if nonlinear static or dynamic analysis is carried out. Still, according to the FEM theory, as the mesh gets finer, it gets closer to the true solution (see the section “Model Calibration/Verification” below, which is related to how representative the model is of the structure, not with the mathematics involved and the accuracy of the model). The modeler may then perform a mesh convergence exercise that includes the following steps: (1) mesh once and solve; (2) mesh finer and solve again; (3) check if the difference between the previous results in control points or sections are within a certain percentage; and (4) repeat the second step and compare the global number of DOF until the difference between meshes is within an acceptable percentage. It should be noted that this exercise may be performed in terms of representative displacements, as they converge faster than stresses. At the scale of monumental masonry structures, an element dimension of approximately 10 to 30 cm may result in an appropriate level of mesh refinement (Atamturktur 2006). It is not uncommon that 500,000 to 1 million degrees of freedom are found in large historic structures, which makes nonlinear analysis lengthy and demanding.

One solution is to use coarser meshes in regions with a low gradient of strains/stresses and to use finer discretization in regions where a high gradient of strains/stresses is expected. FEM software allows transitions from coarser to finer meshes within the same model. The regions to expect a high gradient of strains/stresses include cutouts, openings, cracks, and supports; entrant corners or sharply curved edges; vicinity of concentrated loads; and abrupt changes in thickness, material properties, or cross-sectional areas (fig. 3.4).

When discretizing two- and three-dimensional problems, one must avoid finite elements of high aspect ratios (the aspect ratio of a two- or three-dimensional element is the ratio between its largest and smallest dimensions). As a rough guideline, elements with aspect ratios exceeding 3 require caution and those exceeding 10 should not be used (DNV GL

**FIGURE 3.4.**  
Examples of situations with a high gradient of strains/stresses where a locally refined discretization (in red) is recommended.

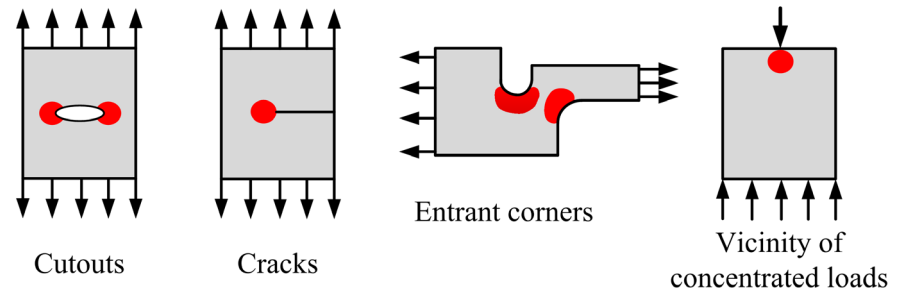
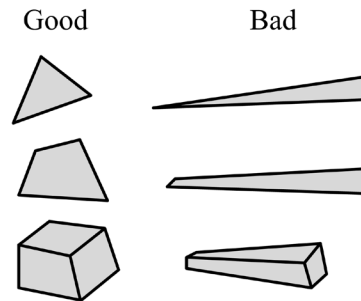


**FIGURE 3.5.**  
Examples of elements with good and bad aspect ratios.



2015) (fig. 3.5). Bad-shaped elements will not necessarily produce incorrect results, but they are likely to introduce problems during the analysis, particularly in the nonlinear field. Most FEA software gives warning prompts when the aspect ratio or the corner angle limits in elements are exceeded.

The modeler should keep it simple. Initial finite element models may have to be substantially revised to accommodate design changes or subsequent modeling decisions. There is little point in using complicated models that will not be able to accommodate refinements. During the refinement process, the modeler develops a better understanding of the underlying physics, possibly reinforced by experiments or observation, and a clearer picture of the performance of the building being studied.

## Materials

Material properties must be decided upon, depending on the boundary conditions and loading conditions of the building. A decision to keep the material linear elastic or the allowance for material change due to loading processes and/or time must be made before selecting the material properties. The behavior of masonry is nonlinear. The behavior in tension at low stress level is inelastic due to cracking. The behavior in compression at higher stress levels is also inelastic due to irreversible damage. Because of the mortar joints, the material is also anisotropic and heterogeneous. Moreover, historic masonry elements usually have multiple layers, with the presence of an inner core and external leaves in walls (and columns, in many cases) and infill material in vaults.

Masonry is a material exhibiting distinct directional properties, owing to the mortar joints, which act as planes of weakness. In general, the approach toward its numerical representation may focus on the micro modeling of the individual components, units and mortar, or the macro modeling of masonry as a composite (Rots 1991). In the specific case

of modeling full-scale masonry buildings, the usual approach is to consider the representation of masonry as a homogeneous composite material. Micro-modeling approaches are more suitable for smaller models, such as individual structural components. Chapter 4 presents a detailed revision of the material behavior and the available constitutive models, including a discussion of micro and macro modeling.

## Supports and Loads

Boundary conditions, or supports, have great influence on the computed results. For a true representation of the actual system in the finite element model, boundary conditions must be represented as closely as possible to the actual conditions of the structure. In the case where only a portion of the structure is modeled, it is difficult to assign correct boundary conditions, as that portion of the structure modeled is supported elastically. The estimation of boundary conditions is difficult in historic buildings. The choices may be partly imposed by the modeler's intuition and by the capacity of the finite element modeling software.

Because boundary conditions are applied to the DOF at the nodes rather than to the element, the prescription of boundary conditions is related to the selection of the element types. For example, if a wall is modeled with fully three-dimensional elements and all nodes at the base are pinned, this provides a clamping restraint. If a wall is modeled with shell elements, a hinged foundation is easier to apply. In most commercially available finite element modeling software, physical constraints are applied by zero displacements or rotations at the user-defined nodes. For situations of partial restraints, an elastic foundation, which is usually simulated by a series of springs or interface elements, can be used.

It is of great importance to start with physically reasonable boundary conditions in the initial finite element model. If empirical data are available, the initial model can be calibrated with successive iterations so that the finite element modeling solutions correlate to the experimentally obtained data or observed building performance.

Loads can be applied to nodes, such as thermal, inertial, concentrated, or distributed forces in the form of nodal displacement or nodal force. Loads can also be applied in surfaces or volumes. The arrangement of loading conditions depends on the analysis type. In static analysis, defining the gravitational acceleration is usually necessary, together with existing external loads. In modal analysis, the results are independent of any load input. In the case of transient analysis, a user-defined time-dependent loading must be adopted.

One common issue when dealing with full building modeling is the consideration of live loads or special concentrated loads in modal analysis or pushover analysis. For such analysis, these loads can be considered by converting them into inertial loads. One simple example is the consideration of live loads in a floor, which can be converted into mass and added to the mass of the floor elements by adjusting the density of the material.

## Model Calibration/Verification

After obtaining an analysis result, one key aspect is not to assume immediately that the results are correct. Questions need to be asked by the analyst or modeler whether the obtained displacements, stresses, or strains make sense. The following five simple actions can be used to aid the modeler in ensuring that the model is correct and to improve the analysis results:

1. Check global structural reactions against global applied loads. This step is particularly important to make sure there were no mistakes in the load input.
2. Use deformed shapes and animations to check load and support definitions. Here, the analyst or modeler should use linear static analysis (typically, gravity loading can be used for this purpose). Combined load behavior is often difficult to predict, and separating each load into its own load case allows loads to be checked individually.
3. Use stress or strain contour plots to check mesh connectivity. Sometimes the modeling process provides parts of the structure improperly connected to the rest of the structure, or some elements are missing. The presence of very high stress/strain peaks may indicate a meshing error. Again, linear elastic analysis and gravity loading seem adequate for this purpose.
4. Alternatively or complementary to the previous step, perform modal analysis to check the mesh connectivity. In the case of full-scale monumental structures, gravity loading might not identify all meshing errors.
5. Whenever possible, compare the results to tests, theory, expedite hand calculations, experimental in situ testing data, or the building condition. It is important to maintain a critical view of the obtained results. Examples of expedite hand calculations are the stress level at the base of a wall or column, or the frequencies of a building. An example of measurements that can be carried out in a building are the frequencies and mode shapes (using dynamic identification), and an example of building condition is crack surveying and mapping of the real building and comparing this with the model-predicted cracks in the building under dead load and/or a known past event such as soil settlements from an earthquake.

## Interpretation of Results

After the verification of the model, and having developed an acceptable level of confidence in the model, interpretation of the results is critical, requiring extensive processing time and an inquisitive mind. Because monumental masonry structures represent complex engineering problems, it is not advised to consider the obtained results as final and correct. Engineering experience and common sense play an important role in the interpretation of the obtained results regarding this kind of structure. As stated above, hand calculations and simplified models can be carried out using alternative expedite software. Moreover, verification is strongly recommended using the existing condition of the building and in situ testing, as discussed above.

Again, given the uncertainties involved in the process, a key aspect when dealing with this kind of structure is to perform a sensitivity analysis. This allows the modeler to determine the effects of model input parameters and modeling decisions on the response, providing further insight into the problem and allowing the definition of critical aspects.



# Constitutive Models

In this chapter, the constitutive models available for masonry will be addressed. Different approaches for modeling masonry are presented, such as smeared cracking and damage plasticity as well as micro and macro approaches. The available models implemented in selected commercial finite element method (FEM) software are also presented and compared.

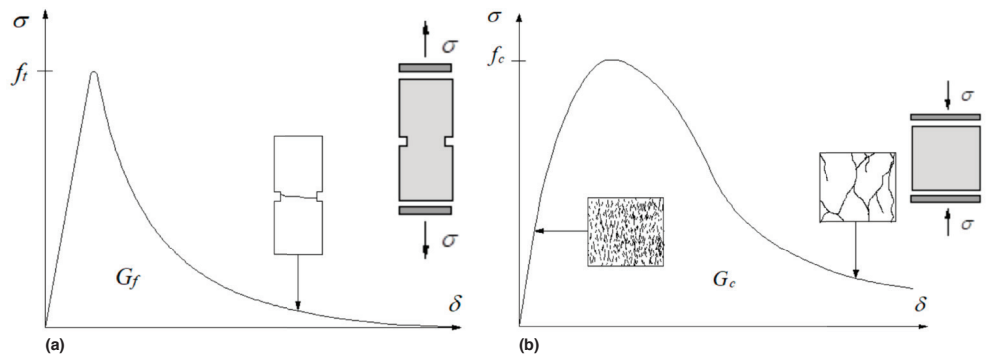
## Nonlinear Behavior

Masonry has a nonlinear behavior and manifests a nonductile post-peak softening behavior, which consists in a gradual strength decrease of the material under a continuous increase of deformation. This characteristic is typical of quasi-brittle materials. Figures 4.1a and 4.1b show characteristic stress-displacement diagrams in uniaxial tensile and compressive behavior (Lourenço 1996).

Here,  $f_t$  and  $G_f$  are the tensile strength and fracture energy, and  $f_c$  and  $G_c$  refer to the compressive strength and fracture energy. The strength is the maximum value of the stress-displacement curve. The procedure to calculate the fracture energy has been indicated, for example, by Jansen and Shah (1997). The relation between the fracture energy and the strength is the ductility index (eq. 8) (see chapter 5 for the recommended values for these parameters).

$$d = G / f \tag{8}$$

**FIGURES 4.1A, 4.1B.**  
Diagrams showing characteristic stress displacement of quasi-brittle materials under uniaxial loading: (a) tensile behavior; (b) compressive behavior (Lourenço 1996).



## Micro and Macro Models

In the 1960s, the numerical simulation of concrete fracture was initiated as a first application of nonlinear constitutive models. Ngo and Scordelis (1967) and Rashid (1968) introduced discrete cracking and smeared crack models, respectively. In general, the discrete model

is aimed at the simulation of the initiation and propagation of dominant cracks. The smeared crack model started with the idea that in concrete many small cracks are initiated, which only at a later stage of the loading process link up to form one or more dominant cracks. Because each individual crack is not numerically solved, the smeared crack model is able to capture the deterioration process through a constitutive model, in which cracks over the continuum are distributed evenly.

The discrete crack approach to fracture is intuitive, because a crack is introduced as a geometric entity. Figure 4.2 shows a mesh in which nodes are physically separated to represent a crack in the bottom center. Initially, this approach was implemented by letting the crack grow when the force at the node ahead of the crack tip exceeded a tensile strength criterion. At this stage, the node splits into two nodes and the tip of the crack is assumed to propagate to the next node. Again, once the force at this new node exceeds the tensile strength criterion, it splits and the procedure is repeated, as shown in the crack vertical propagation in figure 4.2.

In its original form, this discrete crack approach has certain disadvantages. Because the crack is forced to propagate along the element's boundaries, it becomes mesh dependent. Although some techniques, such as automatic re-meshing, have been introduced and implemented in computer codes (Ingraffea and Saouma 1985), a computational complication takes place, namely because the continuous change in topology is inherent in discrete crack approaches. Methods such as meshless methods were also developed to overcome these limitations (Belytschko, Lu, and Gu 1994) but showed difficulties with robust three-dimensional implementations and the large computational demand (Borst et al. 2004). A finite element method accommodating the propagation of discrete cracks through elements was proposed by Moes, Dolbow, and Belytschko (1999), which exploits the partition-of-unity property of finite element shape functions (Babuska and Melenk 1997). Originally, the discrete crack model was introduced using elastic fracture mechanics and, because of that, special functions were required to simulate the near-tip singularity (Moes, Dolbow, and Belytschko 1999). Many new developments occurred in the past decades, but these remain of application to specific tailored research problems.

In the smeared crack approach, the nucleation of one crack in the volume that is attributed to an integration point is translated into a deterioration of the current stiffness and strength at that integration point (Borst et al. 2004). When the combination of stresses satisfies a given criterion (usually the major principal stresses reaching the tensile strength), a crack is initiated. This implies that at the integration point where the stress and strain variables are monitored, the isotropic stress-strain relation is replaced by an orthotropic elastic-type relation, with the direction normal and tangential to the crack being the orthotropic axes (Rashid 1968).

FIGURE 4.2.  
Diagram showing early discrete crack modeling (Ngo and Scordelis 1967).

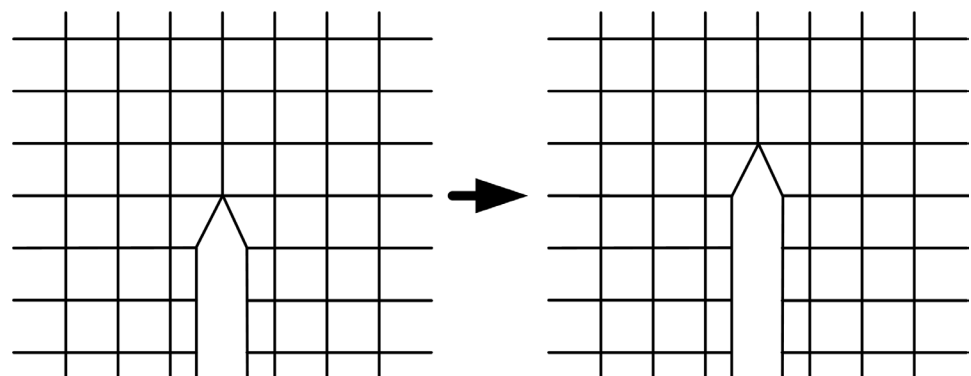
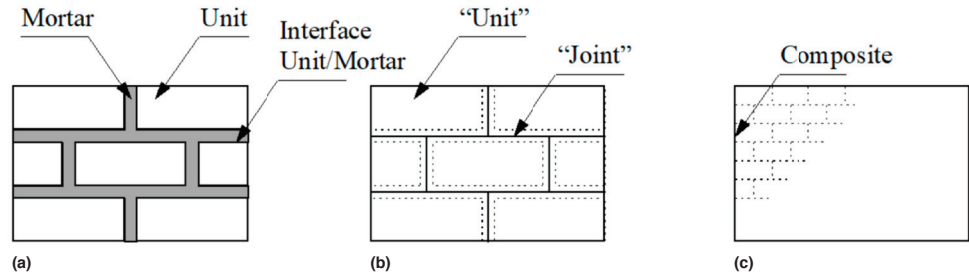


**FIGURE 4.3A–C**  
Diagrams of modeling strategies for masonry structures: (a) detailed micro model; (b) simplified micro model; (c) macro model (Lourenço 1996).



There are several possibilities to solve the problem of modeling masonry. The available alternatives depend on how detailed the modeling is and whether the model is able to describe accurately different types of failure (Lourenço 1996; Lopez, Oller, and Onate 1998). Usually the alternatives are classified as detailed micro model, simplified micro model, and macro model (fig. 4.3).

In the first alternative (detailed micro model), both bricks and mortar are considered as continuum elements with specified failure criteria. The interface between bricks and mortar is considered with interface elements, which represent the discontinuities. This approach completely reproduces the geometry of the wall; taking into account the level of detail, it is assumed that it can represent most failure mechanisms in masonry.

In the second alternative (simplified micro model), the bricks are considered as continuum elements with specified failure criteria, but the mortar joints and interface elements are redefined as individual elements to represent the contact area. This approach maintains the general geometry of the wall; however, because the individual elements that represent joints and interface are not represented, some types of failure mechanisms cannot be reproduced in this type of failure (e.g., due to the transversal expansion of mortar over bricks, when compressed until failure).

The last alternative (macro model) considers the masonry as a homogeneous element. Because of its characteristics, this approach should be able to reproduce the general structural behavior of a masonry panel, but it is not able to reproduce all types of failure mechanisms.

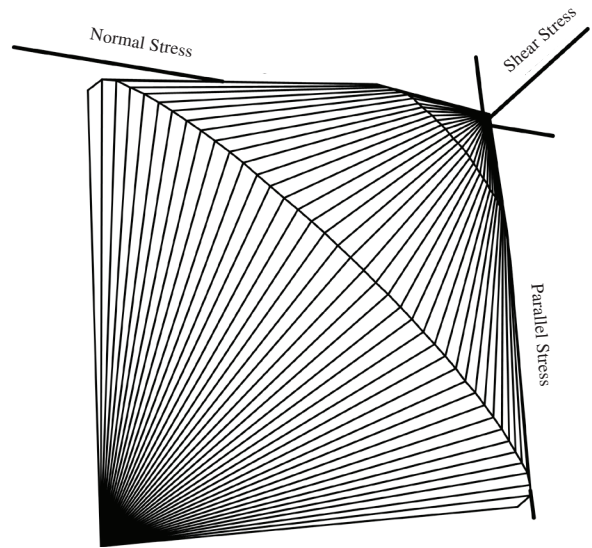
Generally, the more detailed the model, the harder it is to implement. This is particularly important when deciding which model to use for a specific application. Micro models are more suitable for the study of single walls or special localized problems (e.g., openings, wall intersections, arches, and domes). On the other hand, macro models are faster and easier to represent the structural behavior of a whole building. One other important aspect to take into consideration when choosing the type of model to use is that, in general, micro models require more detailed information on the material properties.

One of the first developed models able to represent the nonlinear behavior of masonry was proposed by Page (1978). This model considers masonry as a two-phase material (brick and mortar). Bricks are represented with plane stress quadrilateral finite elements. The mortar joints are represented by linkage elements. These elements can deform only in normal and shear directions. Later, Page, Kleeman, and Dhanasekar (1985) also proposed a macro model to represent masonry. A large experimental campaign on half-scale brick masonry was performed (Page 1981, 1983). The information obtained from the experimental tests allowed the development of stress-strain relationships able to reproduce the inelastic behavior of masonry and different forms of failure of masonry, taking into account the orientation of the joints (fig. 4.4).

Lourenço (1996) proposed two models to describe the nonlinear behavior of masonry: (a) a composite interface model, which is a micro model, and (b) an anisotropic continuum



FIGURE 4.4.  
Image showing 3D failure surface of masonry (Page, Kleeman, and Dhanasekar 1985).



model, which is a macro model. The composite interface model is defined through joints that concentrate the inelastic behavior of the masonry. The plasticity model of the joints is able to reproduce three different types of failure mechanism: (a) tension cutoff; (b) Coulomb friction; and (c) elliptical cap (fig. 4.5). Good agreement was found with experimental tests. The anisotropic continuum model, also from Lourenço (1996), is defined by considering an orthotropic continuum model for masonry, taking into account a Rankine-type yield criterion for tensile failure (cracking) and a Hill-type yield criterion for compressive failure (crushing) (fig. 4.6). Again, good agreement was found with experimental tests. Both models require a relatively large number of parameters to be used.

There are many other proposals for micro and macro approaches of masonry for the analysis of simple and complex structures. These proposals include different types of modeling strategies and are oriented to different types of masonry. Sayed-Ahmed and Shrive (1996) developed a nonlinear model for hollow masonry using isoparametric shell elements. This model considers the nonlinear behavior of masonry in compression due to progressive cracking as well as geometric nonlinearities. Zhuge, Thambiratnam, and Corderoy (1998) developed a model for unreinforced masonry under in-plane dynamic loads. Park et al. (2011) developed a model to take into consideration the effect of the wall-slab interaction in the seismic design of masonry structures. This model represents a

FIGURE 4.5.  
Diagram showing 3D failure surface for composite interface model (Lourenço 1996).

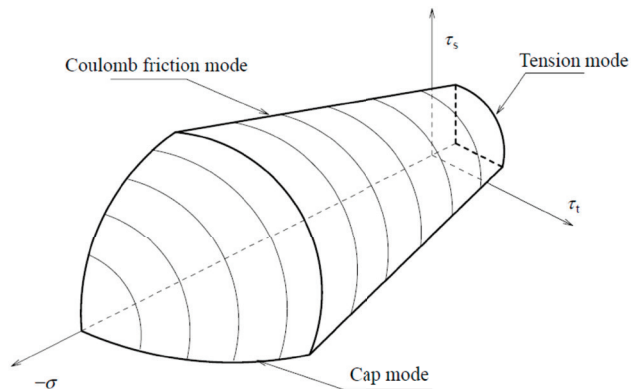
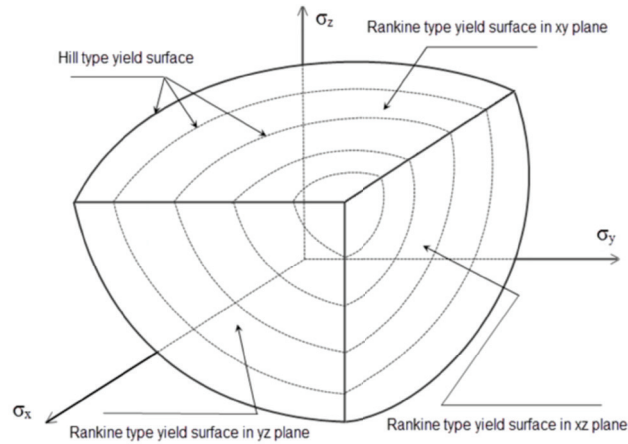


**FIGURE 4.6.**  
Diagram showing 3D failure surface for anisotropic continuum model (Lourenço 1996).



complete wall and is composed of three beams connected in an I-shaped form (top and bottom horizontal beams and one vertical beam). The connections between the beams and the adjacent structure are modeled with springs. There are many other models to represent the nonlinear behavior of different types of masonry elements under different conditions. Some examples can be found in Pietruszczak and Niu (1992); Anthoine (1995); Crisafulli (1997); Lopez, Oller, and Onate (1998); Zucchini and Lourenço (2002); Chen, Moon, and Yi (2008); and Milani and Lourenço (2009).

## Constitutive Models in Commercial Software

In this section, some of the available commercial FEM software, widely disseminated and appropriate for use in advanced computer simulations, is presented in terms of constitutive models for masonry structures. The presented commercial FEM codes are DIANA, by TNO DIANA (now DIANA FEA BV), and ABAQUS, by Dassault Systèmes. It is important to mention that existing masonry structures often have multileaf walls that are difficult to detect without in situ testing. These unknown construction details are important while modeling a historic structure, and overcomplex constitutive models should not be used. In particular, isotropic models are recommended in most engineering applications.

### DIANA

DIANA (DIplacement method ANALyser) is an extensive multipurpose finite element software package that is dedicated but not exclusive to a wide range of problems arising in civil engineering, including structural, geotechnical, tunneling, earthquake disciplines, and oil and gas engineering. With regard to the assessment of masonry structures considering nonlinear behavior of masonry, this software has different possibilities for the constitutive models of masonry materials (considering only macro-modeling approaches), namely the following:

- Total strain-based crack (TSC) model can describe both the tensile and the compressive behavior of a given material with one stress-strain relationship.
- Engineering masonry model, developed for cyclic loading, is a smeared failure model and can be applied with plane stress and curved shell elements.

The TSC model is one of the most commonly used for masonry-related simulations and is explained in more detail in this section. This constitutive model, available in DIANA, is based on total strain and is developed along the lines of the modified compression field theory originally proposed by Vecchio and Collins (1986). This model follows a smeared approach for the fracture energy.

During the loading phase, the material is subjected to both tensile and compressive stresses, which can result in cracking and crushing of the material. It is assumed that damage recovery is not possible. The loading-unloading-reloading condition is monitored with some internal constraints that are determined for both tension and compression to model the stiffness degradation in tension and compression separately. As shown, the model is not adequate for seismic loading in presence of compressive damage, as secant unloading to the origin is present (fig. 4.7).

The TSC model available in DIANA can describe both the tensile and the compressive behavior of a given material with one stress-strain relationship. This stress-strain relationship in tensile behavior can be idealized in several different approaches, including constant, linear, exponential, and brittle (figs. 4.8a–d). Similarly, the compressive behavior can also be idealized in different approaches, such as elastic, constant, and parabolic (figs. 4.9a–c).

Within the TSC models, two distinct approaches are available and can be distinguished as (a) TSFC (total strain fixed crack) model and (b) TSRC (total strain rotating crack) model. In both formulations, the crack is initiated when the maximum principal stress equals the tensile strength of the material, and its initial orientation is normal to the maximum principal strain. The main difference between these two formulations is related to the crack orientation during the inelastic process. In the TSFC model, the coordinate system is fixed upon cracking according to the principal strain directions and remains invariant during the total analysis process. Each integration point admits a maximum of two orthogonal cracks. The TSRC model allows a gradual correction of the initial crack direction, as the crack plane can rotate during the analysis. The crack direction rotates with the principal strain axes, ensuring that the crack remains normal to the direction of the maximum principal strain. In the fixed formulation, a shear retention parameter is required for the definition of the model shear behavior, while in the rotating model the shear softening occurs implicitly as a result of the principal stress and strain conditions. Several studies showed that the TSRC model should be used in shear-dominated applications (Rots 1988) and that fixed crack models should not be used for existing (unreinforced) masonry structures.

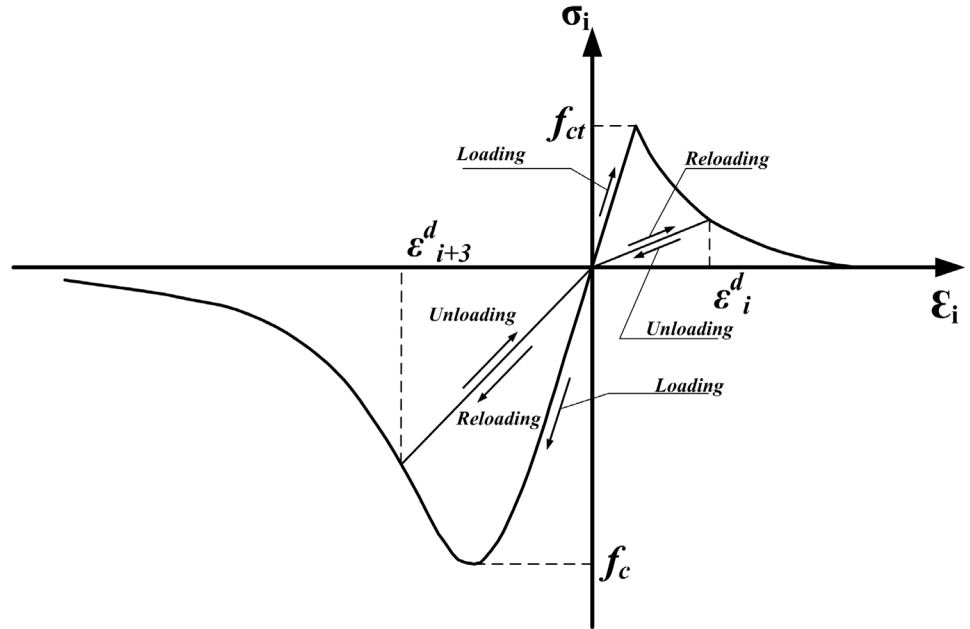
To use this constitutive model in DIANA, the modeler usually must supply the following parameters: (a) density ( $\rho$ ); (b) Young's modulus ( $E$ ); (c) compressive strength ( $f_c$ ); (d) compressive fracture energy ( $G_c$ ); (e) tensile strength ( $f_t$ ); and (f) mode-I fracture energy ( $G_f$ ). Note that the fracture energy is divided by some factor related to the element volume ( $h$ ) to ensure mesh-independent results. This factor is normally termed *characteristic length* or *crack bandwidth*.

## ABAQUS

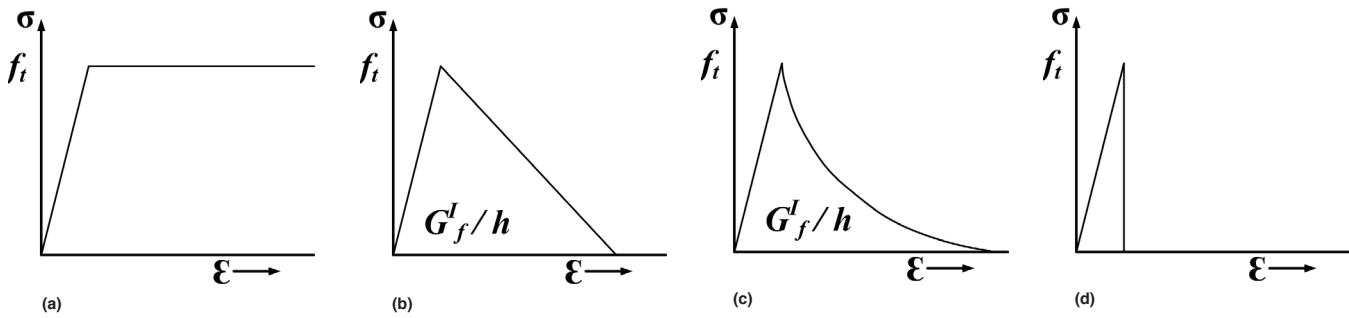
ABAQUS offers solutions for both routine and sophisticated engineering problems covering a vast spectrum of industrial applications. It also offers the possibility of performing analysis with implicit and explicit solvers.

Three different constitutive models are offered in ABAQUS for the analysis of quasi-brittle materials: (a) the smeared crack model in ABAQUS/Standard; (b) the brittle cracking model in ABAQUS/Explicit; and (c) the concrete damage plasticity model (CDP) in both ABAQUS/Standard and ABAQUS/Explicit. Each model can be applied to all types of finite elements: beams, trusses, shells, and solids.

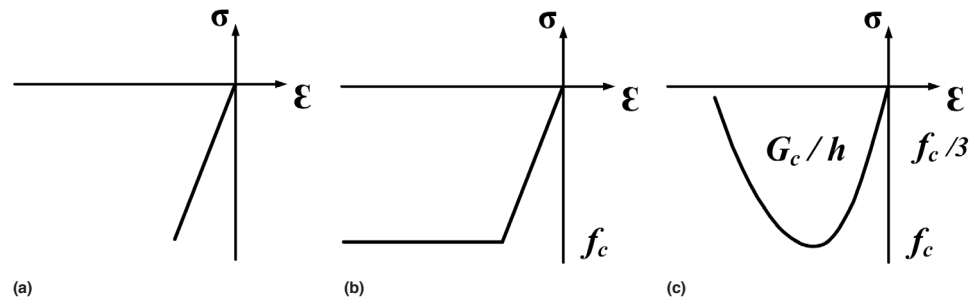
FIGURE 4.7.  
Diagram showing loading-unloading-reloading condition for total strain models.



FIGURES 4.8A–D.  
Examples of the available tensile behavior in DIANA (TNO DIANA 2009): (a) constant; (b) linear; (c) exponential; (d) brittle.



FIGURES 4.9A–C.  
Examples of the available compressive behavior in DIANA (TNO DIANA 2009): (a) elastic; (b) constant; (c) parabolic.



The smeared crack model is intended for applications in which the material is subjected to essentially monotonic straining and a material point exhibits either tensile cracking or compressive crushing. Plastic straining in compression is controlled by a “compression” yield surface. Cracking is assumed to be the most important aspect of the behavior, and the representation of cracking and post-cracking anisotropic behavior dominates the modeling.

The brittle cracking model is intended for applications in which the material behavior is dominated by tensile cracking and compressive failure is not important. The model includes

consideration of the anisotropy induced by cracking. In compression, the model assumes elastic behavior. A simple brittle failure criterion is available to allow the removal of elements from a mesh.

The CDP model is based on the assumption of scalar isotropic damage and is designed for applications in which the material is subjected to arbitrary loading conditions, including cyclic loading. The model takes into consideration the degradation of the elastic stiffness induced by plastic straining in both tension and compression. It also accounts for stiffness recovery effects under cyclic loading. As this is the model with wider application, it will be explained in more detail.

The CDP model used in ABAQUS software is a modification of the Drucker-Prager model by Lubliner et al. (1989) and Lee and Fenves (1998). In particular, the shape of the failure surface in the deviatoric plane (fig. 4.10) does not need to be a circle and is governed by parameter  $K_c$ . This parameter can be interpreted as a ratio of the distances between the hydrostatic axis and, respectively, the compression meridian and the tension meridian in the deviatoric plane. This ratio is always higher than 0.5, and when it assumes the value 1, the deviatoric cross section of the failure surface becomes a circle (Kmieciak and Kaminski 2011). The CDP model requires four additional parameters to be defined: the dilatation angle, the flow potential eccentricity, the ratio of initial equibiaxial compressive yield stress to initial uniaxial compressive yield stress, and the viscosity parameter. For these parameters, the ABAQUS user's manual (ABAQUS 2010) suggests values as indicated in table 4.1. Additional information regarding this model can be found in Kmieciak and Kaminski (2011) and Jankowiak and Lodygowski (2005).

FIGURE 4.10.  
Diagram of the failure surface in a CDP model, represented in the deviatoric plane  $S_1$ ,  $S_2$ , and  $S_3$  (Kmieciak and Kaminski 2011).

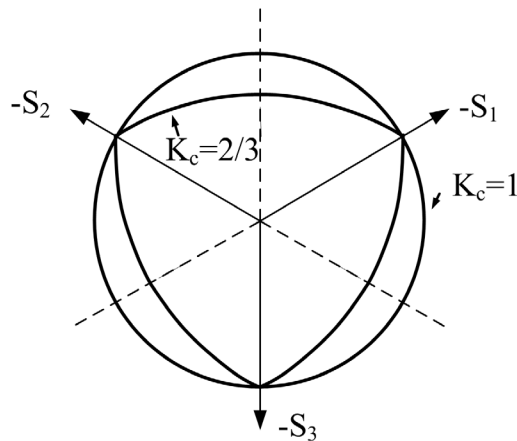


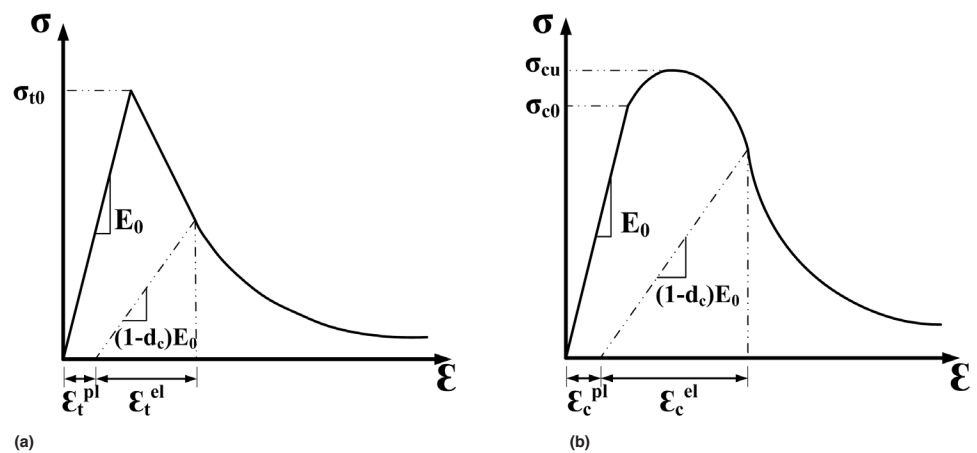
TABLE 4.1.  
Default parameters suggested by the ABAQUS user's manual (ABAQUS 2010).

| Parameter                     | Value |
|-------------------------------|-------|
| Dilatation angle ( $\psi$ )   | 40°   |
| Eccentricity ( $\epsilon$ )   | 0.1   |
| $f_{bd}/f_{c0}$               | 1.16  |
| $K_c$                         | 0.667 |
| Viscosity parameter ( $\mu$ ) | 0.0   |

The CDP model assumes that the failure for tensile cracking and compressive crushing of the material is characterized by damage plasticity. The model uses the concept of isotropic damage evolution in combination with isotropic tensile and compressive plasticity to represent the inelastic and fracture behavior of the material. The model also allows the definition of strain hardening in compression and strain softening in tension. The usually adopted stress-strain curves in tension and compression can be seen in figures 4.11a and 4.11b.

The process for using this constitutive model in ABAQUS requires inputting in the same parameters as DIANA. As previously mentioned, it is important that the fracture energy is divided by some factor related to the element volume ( $h$ ) to ensure mesh-independent results. This factor is normally termed characteristic length or crack bandwidth. It should be adopted for tension and compression, even if ABAQUS only considers this factor automatically for tension.

FIGURES 4.11A, 4.11B.  
Diagrams showing stress-strain relations: (a) in tension; (b) in compression (Lubliner et al. 1989).

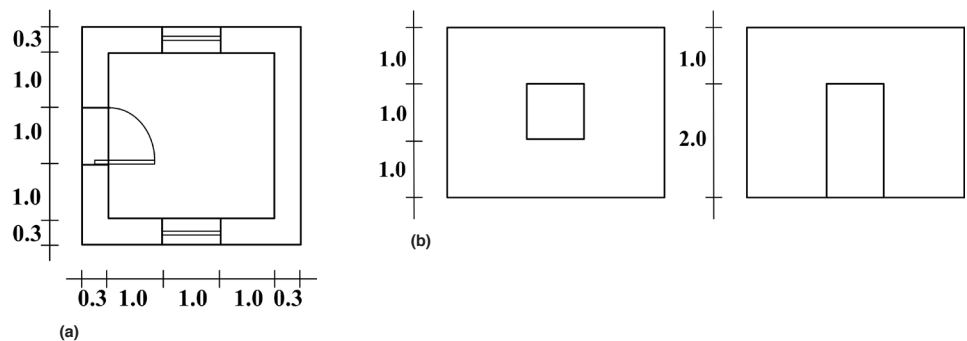


### Comparison for Commercial Software

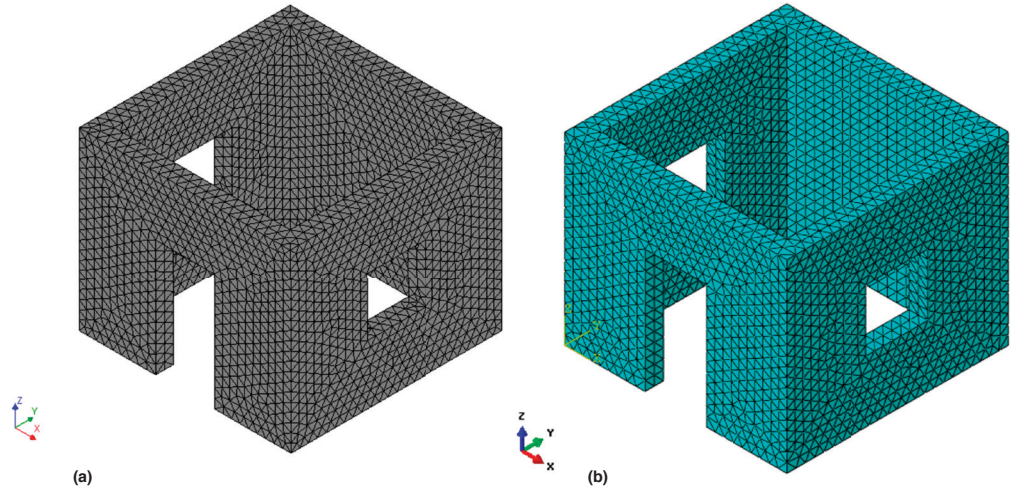
A simple model of a structure was developed and analyzed in DIANA and ABAQUS to compare results. The dimensions of the numerical model are shown in figures 4.12a and 4.12b. In DIANA and ABAQUS, a three-dimensional solid elements approach was followed.

At the bottom of the walls, all translations are blocked (pinned), but this represents a clamped foundation. The model was subjected to a lateral load (in the Y-direction) proportional to its mass, meaning that an acceleration was applied to the model in the Y-direction.

FIGURES 4.12A, 4.12B.  
Schematics of numerical model dimensions: (a) plan view; (b) elevation in meters.



FIGURES 4.13A, 4.13B.  
Images showing finite element meshes of the numerical model, using (a) DIANA; (b) ABAQUS.



To mesh the numerical model, the available automatic algorithms were used in both DIANA and ABAQUS, using tetrahedron-type solid elements and keeping a maximum element size of 150 mm. The resulting meshes can be seen in figures 4.13a and 4.13b and were composed of 23,838 elements in DIANA and 28,272 elements in ABAQUS.

In DIANA, the TSC model (rotating cracks) was used. An exponential stress-strain relationship was adopted in tensile behavior (see fig. 4.8c) and a parabolic stress-strain relationship was adopted in compressive behavior (see fig. 4.9c). The mechanical properties assigned to the constitutive model are presented in table 4.2. It is important to mention that the crack bandwidth is considered differently in ABAQUS (element size for linear elements) and DIANA (cubic root of the volume for 3D elements). This yields a difference of about two for the adopted mesh, and the fracture energy in DIANA was doubled for consistency.

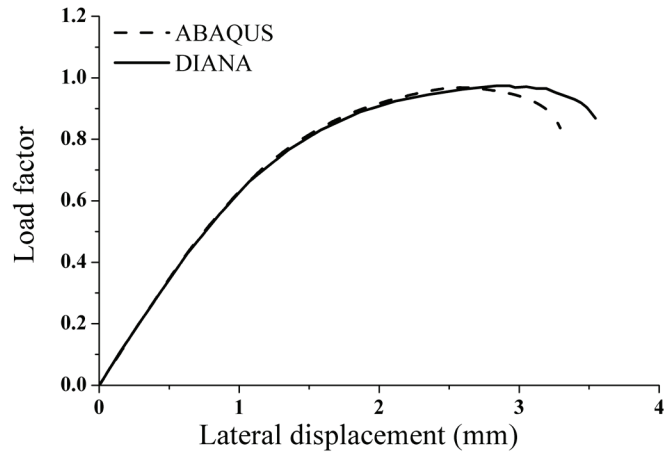
TABLE 4.2.  
Mechanical properties adopted.

| Mechanical Property            | Adopted Value          |
|--------------------------------|------------------------|
| $\rho$ (density)               | 1900 kg/m <sup>3</sup> |
| $E$ (Young's modulus)          | 500 MPa                |
| $f_c$ (compressive strength)   | 1.00 MPa               |
| $G_c$ (fracture energy)        | 1.60 N/mm              |
| $f_t$ (tensile strength)       | 0.10 MPa               |
| $G_t$ (fracture energy mode-I) | 0.05 N/mm              |

In ABAQUS, the CDP model was used. An exponential stress-strain relationship was adopted in tensile behavior and a parabolic stress-strain relationship was adopted in compressive behavior. The mechanical properties assigned to the constitutive model are the same as in DIANA. From the compressive stress-strain, the compressive strength-inelastic strain curve was extracted and introduced in the constitutive model. The ABAQUS/Standard (implicit) routine was used to perform the analysis.

Both analyses were performed until softening behavior could be found in the capacity curves, and the results in terms of capacity curve are shown in figure 4.14. Here, the dis-

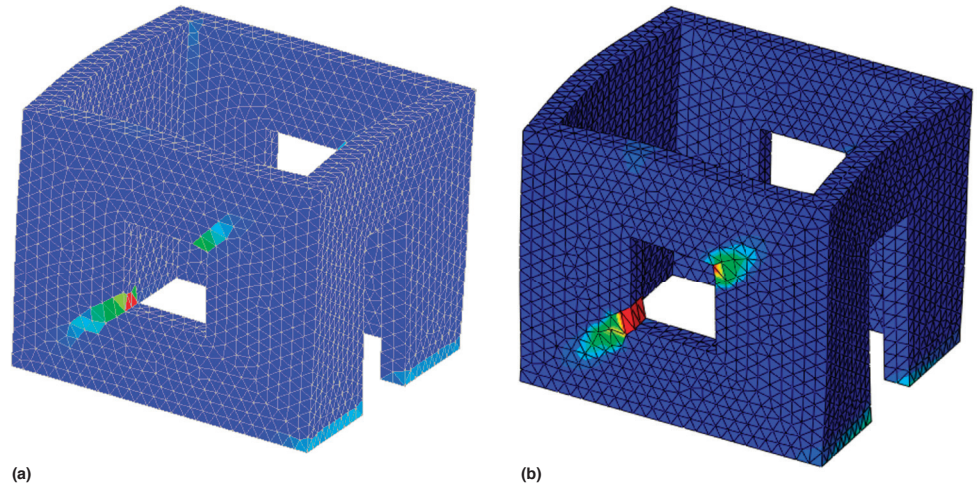
FIGURE 4.14.  
Graph showing analysis results in terms of capacity curves.



placement was captured as the average of the displacements of the four external top corners of the model. The load factor corresponds to the ratio between the base reaction forces in the Y-direction and the self-weight of the model in the Z-direction. In figure 4.14, it is possible to see that both models showed the same capacity (0.3% difference). The displacement at maximum capacity is slightly higher in the TSRC model (10% higher). The initial stiffness of the model is the same for both models. Besides the capacity curve, the failure modes were compared. In both models, shear cracks developed in the lateral walls, starting at the corners of the windows and propagating to the corners of the walls (fig. 4.15). Here, as an indicator of the locations of the cracks, the maximum principal strains are plotted.

As can be seen from the presented results, both models were able to reproduce the same failure mode, with shear cracking in the lateral walls. Both models estimate the same capacity in terms of lateral load, demonstrating the reliability of these tools. Even considering that this example is a rather simple one, some differences are to be expected.

FIGURES 4.15A, 4.15B.  
Maximum principal strains as an indicator of cracking: (a) DIANA; (b) ABAQUS. Red indicates the maximum value (wide crack) and blue indicates no crack.







## Recommended Properties for Numerical Modeling

Because masonry exhibits manifestly nonlinear behavior, an adequate material constitutive model needs to be selected to achieve reliable simulations. Constitutive models, either using a micro- or macro-modeling approach, require the input of several mechanical properties. The nature of masonry materials (being composed of units and mortar) allows several different combinations of constituent materials and unit arrangements. This results in some scatter of reference values available in the literature, even if the reasonable changes in the material properties will not affect the results to a large extent. This chapter gathers available sources of information regarding the mechanical properties of masonry structures.

### Masonry Structures in General

As stated in chapter 3, masonry is a heterogeneous material, being composed of units and mortar. The mechanical properties of masonry are greatly dependent on the physical and mechanical properties of its components. Eurocode 6 (EC6 2005) establishes the following relation to determine the compressive strength of masonry as a composite (eq. 9):

$$f_c = K f_{bc}^{0.7} f_{mc}^{0.3} \quad (9)$$

Here,  $K$  is a constant that depends on the combination of unit and mortar (e.g., for dimensioned stone units,  $K$  is 0.45),  $f_{bc}$  is the compressive strength of a masonry unit, and  $f_{mc}$  is the compressive strength of masonry mortar.

Some normative documents (e.g., NZSEE 2006) suggest reference values for the mechanical properties of both mortar and brick, being defined in different classes according to visual inspections and hand tests (table 5.1). The Italian Technical Building Norm (NTC 2008) prescribes a range of values for the mechanical properties of different types of masonry (table 5.2). These values can be adjusted taking into consideration factors such

TABLE 5.1.  
Strength parameters for mortar and brick according to NZSEE (2006).

|        |       | Compressive Strength (mortar) | Compressive Strength (brick) | Tensile Strength (brick) | Young's Modulus | Poisson Ratio |
|--------|-------|-------------------------------|------------------------------|--------------------------|-----------------|---------------|
|        |       | $f_{mc}$ (MPa)                | $f_{bc}$ (MPa)               | $f_{bt}$ (MPa)           | $E$ (MPa)       | $\nu$         |
| Mortar | Stiff | 8.0                           |                              |                          | 12000           | 0.11          |
|        | Firm  | 4.0                           |                              |                          | 9000            | 0.07          |
|        | Soft  | 1.0                           |                              |                          | 7000            | 0.05          |
| Bricks | Hard  |                               | 20.0–30.0                    | 2.0–3.0                  | 18000           | 0.2           |
|        | Stiff |                               | 10.0–20.0                    | 1.0–2.0                  | 13000           | 0.2           |
|        | Soft  |                               | 1.0–5.0                      | 0.1–0.5                  | 4000            | 0.35          |

TABLE 5.2.

Reference values of mechanical parameters (maximum and minimum) for different types of masonry (NTC 2008).

| Masonry Typology   | $f_c$<br>(MPa) | $\tau$<br>(MPa) | $E$<br>(MPa) | $G$<br>(MPa) | $\rho$<br>kg/m <sup>3</sup> |
|--|----------------|-----------------|--------------|--------------|-----------------------------|
|  | min-max        | min-max         | min-max      | min-max      |                             |
| Rubble stone masonry (pebbles, erratic and irregular stone)                  | 1.0–1.8        | 0.020–0.032     | 690–1050     | 230–350      | 1900                        |
| Irregular stone masonry with external leaves of limited thickness and infill | 2.0–3.0        | 0.035–0.051     | 1020–1440    | 340–480      | 2000                        |
| Regular stone masonry with good bond   | 2.6–3.8        | 0.056–0.074     | 1500–1980    | 500–600      | 2100                        |
| Soft stone masonry (tuff, calcarenite, etc.)                                 | 1.4–2.4        | 0.028–0.042     | 900–1260     | 300–420      | 1600                        |
| Dressed rectangular stone masonry  | 6.0–8.0        | 0.090–0.120     | 2400–3200    | 780–940      | 2200                        |
| Solid brick masonry with lime mortar   | 2.4–4.0        | 0.060–0.092     | 1200–1800    | 400–600      | 1800                        |
| Perforated brick (< 40%) masonry with cement mortar                          | 5.0–8.0        | 0.240–0.320     | 3600–5400    | 875–1400     | 1500                        |
| Perforated brick (< 45%) masonry   | 4.0–6.0        | 0.300–0.400     | 3600–5400    | 1080–1620    | 1200                        |
| Perforated brick (< 45%) masonry with unfilled perpendicular joints          | 3.0–4.0        | 0.100–0.130     | 2700–3600    | 810–1080     | 1100                        |
| Concrete and lightweight concrete block masonry (voids: 45%–65%)             | 1.5–2.0        | 0.095–0.125     | 1200–1600    | 300–400      | 1200                        |
| Concrete block (< 45%) masonry   | 3.0–4.4        | 0.180–0.240     | 2400–3520    | 600–880      | 1400                        |

$f_c$  = average compressive strength of masonry  
 $\tau$  = average shear strength of masonry  
 $E$  = average value of the Young's modulus  
 $G$  = average value of the shear modulus  
 $\rho$  = average density

as the quality of the mortar, the thickness of the joints, the presence of regular masonry courses, transverse elements (through stones, headers, or other elements), or an excessively thick inner core. The American Standard (ASCE 41-06 2006) defines default lower bound masonry properties according to the masonry condition (table 5.3).

Young's modulus  $E$  is usually associated with compressive strength  $f_c$  by  $E = af_c$ , with a wide range of variation in  $a$ , which, according to Tomazevic (1999), is from 200 to 1000. In ASCE 41-06 (2006), the recommended relationship for existing masonry is  $E = 550f_c$  (Angelillo, Lourenço, and Milani 2014; Lumantarna, Biggs, and Ingham 2014), whereas in EC6 (2005) the recommended relationship is  $E = 1000f_c$ .

A level of uncertainty is present in the relation between tensile and compressive strength of masonry (Angelillo, Lourenço, and Milani 2014). The flexural strength of masonry, as stated in Eurocode 6 (EC6 2005), ranges from  $f_{xk1} = 0.05$  to 0.20 MPa for a plane failure parallel to bed joints and  $f_{xk2} = 0.10$  to 0.40 MPa for a plane failure

TABLE 5.3.

Default lower bound masonry properties (ASCE 41-06 2006).

| Property   | Masonry Condition |          |          |
|--|-------------------|----------|----------|
|  | Good              | Fair     | Poor     |
| Compressive strength (MPa)   | 6.21              | 4.14     | 2.07     |
| Young's modulus  | $550f_c$          | $550f_c$ | $550f_c$ |
| Flexural tensile strength (MPa)  | 0.14              | 0.07     | 0.00     |
| Shear strength (MPa)   |                   |          |          |
| Masonry with a running bond lay-up   | 0.19              | 0.14     | 0.09     |
| Fully grouted masonry with a lay-up other than running bond                  | 0.19              | 0.14     | 0.09     |
| Partially grouted or ungrouted masonry with a lay-up other than running bond | 0.08              | 0.06     | 0.03     |

perpendicular to bed joints, whereas in ASCE 41-06 (2006) the expected tensile strength varies from 0.00 to 0.14 MPa.

As far as the softening behavior of masonry is considered, the tensile and compressive fracture energy values, necessary for the presented constitutive models, can be derived according to the tensile and compressive strength and each ductility index (see eq. 8, chap. 4). For the compressive fracture energy, MC2010 (2010) suggests a value of  $d = 1.6$  mm for compressive strength lower than 12 MPa. The recommendation (Lourenço 2009b) is to increase this value for lower-strength materials (typically more ductile):

$$d = 2.8 - 0.1f_c \text{ [mm]} \quad (10)$$

For the tensile fracture energy, no relation can be found between strength and fracture energy and a value of 0.02 N/mm is recommended (Lourenço 2009a, 2009b).

## Earthen Structures

In the specific case of historic earthen structures, the information available in the literature is scarce. The mechanical properties of adobe masonry have a wide range of variation, depending mostly on the soil characteristics and workmanship. The compressive strength is mostly dependent on the properties of the adobe blocks and the thickness of mortar joints (Paulay and Priestley 1992). Yet, the high level of heterogeneity and large scatter of adobe masonry mechanical properties are evident even on a given site (table 5.4); thus, many specimens are often needed for obtaining results of high statistical accuracy. Given also the level of fragility and limited number of adobe specimens extracted from historic sites, the task of performing advanced testing on adobe masonry is difficult.

TABLE 5.4.

Mechanical properties of adobe masonry obtained from the literature. (Carina Fonseca, University College London, 2013. Revised TecMinho, 2018.)

| Reference  | Country  | Compressive Strength $f_c$ (MPa)         | Shear Strength $f_v$ (MPa)              | Modulus of Elasticity $E$ (MPa) | Shear Modulus $G$ (MPa) |
|--|----------|--|---|---------------------------------|-------------------------|
| Testing Results PUCP (tests performed on piers)  | Peru     | Ica: 0.46<br>Lima: 0.44                  | Ica: 0.014–0.050<br>Lima: 0.010–0.043   | Ica: 98<br>Lima: 48–75          | –                       |
| Testing Results PUCP (tests performed on units)  | Peru     | Ica: 0.59<br>Lima: 1.51<br>Kuño T.: 0.71 | –                                       | –                               | –                       |
| NTE E. 080 (2017)—Peruvian building code (piers) | Peru     | 0.20<br>(required minimum)               | 0.025<br>(ultimate strength)            | –                               | –                       |
| NTE E. 080 (2017)—Peruvian building code (units) | Peru     | 1.20<br>(ultimate strength)              | –                                       | –                               | –                       |
| Vargas et al. (1986)                             | Peru     | –  | 0.047–0.098<br>(from different sources) | –                               | –                       |
| Ottazzi et al. (1989)                            | Peru     | 1.64                                     | 0.070                                   | 181                             | –                       |
| Yamin et al. (2004)                              | Colombia | 1.22                                     | 0.314                                   | 117                             | 30                      |
| Quagliarini, Lenci, and Iorio (2010)             | Italy    | 1.00                                     | 0.140<br>0.270                          | 33                              | –                       |
| Tarque (2008)                                    | Peru     | 0.84                                     | 0.070                                   | 174                             | 78                      |
| Liberatore et al. (2006)                         | Italy    | –  | 0.021                                   | –                               | –                       |
| Varum et al. (2006)                              | Portugal | 1.13                                     | 0.109                                   | 183                             | 33                      |

The typical ancient masonry stones have a compressive strength ranging from 5 MPa (for schist) up to 150 MPa (for granite), and the typical clay bricks in ancient masonry have a compressive strength ranging from 5 to 20 MPa, whereas the adobe has only a compressive strength ranging from 0.5 to 3 MPa. This applies to the masonry units and not the masonry itself, which has a compressive strength lower than the unit strength. Table 5.4 shows some of the developed experimental work on the mechanical characterization of historic earthen masonry material. As stated previously, the scatter in the obtained results is evident, even if a value of compressive strength  $f_c$  in the range of 0.5 MPa seems on the safe side. Consideration of Young's modulus  $E = 200f_c$ , which is the minimum in Tomazevic (1999) per the section "Masonry Structures in General" above, provides a value of 100 MPa.

For the tensile strength, the minimum value of Eurocode 6 (EC6 2005) can be adopted:  $f_t = 0.05$  MPa. Finally, for the tensile and compressive fracture energies, the values of 0.02 and 1.4 N/mm, respectively, can be used per the section "Masonry Structures in General." Table 5.5 provides a proposal for mechanical data to be used for earthen historic masonry in the absence of more information.

TABLE 5.5.

Proposed values for historic adobe masonry structures.

| Mechanical Property            | Proposed Value |
|--------------------------------|----------------|
| $E$ (Young's modulus)          | 100 MPa        |
| Poisson ratio                  | 0.2            |
| $f_c$ (compressive strength)   | 0.5 MPa        |
| $G_c$ (fracture energy)        | 1.4 N/mm       |
| $f_t$ (tensile strength)       | 0.05 MPa       |
| $G_t$ (fracture energy mode-I) | 0.02 N/mm      |

# Application Example: Adobe House

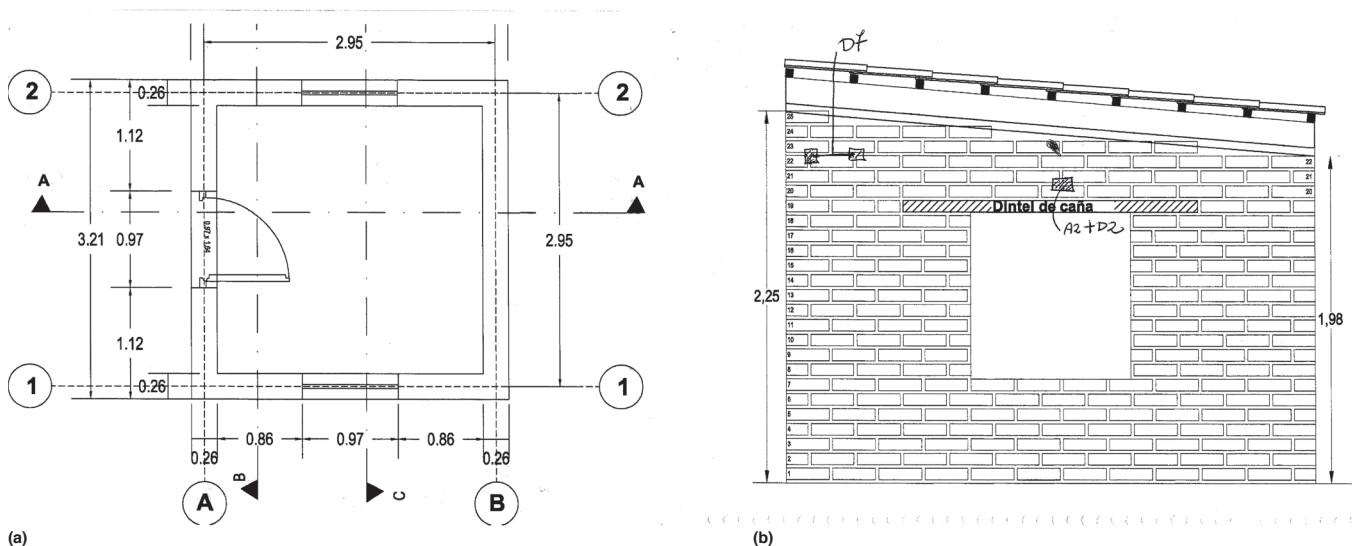
This chapter presents a numerical analysis of experimental tests performed by the Pontificia Universidad Católica del Perú (PUCP) on adobe models for the SismoAdobe conference in 2005 and published in Blondet et al. (2006). The numerical models presented are based on the experimental results from PUCP (also briefly presented here). This chapter focuses on reproducing the experimental results through nonlinear pushover analyses to validate the proposed constitutive model and modeling approach. Additional information can be found in Pereira and Lourenço (2016).

## General Description of the Models

The adobe models consisted of four walls 3.21 m long, of variable height, with a thickness of 0.26 m. The longitudinal walls (parallel to the direction of shaking) included a central window opening. The front transverse wall had a door opening, and the taller back wall did not have any openings. P lan view and elevation of the models are shown in figures 6.1a and 6.1b.

All models were built using traditional techniques, representative of seismically vulnerable adobe construction in Peru. The adobe blocks were fabricated using soil, coarse sand, and straw in proportions of 5:1:1. The blocks measured  $65 \times 250 \times 250 \text{ mm}^3$  and were laid with earth mortar made with soil, coarse sand, and straw in proportions of 3:1:1. Each specimen was built over a reinforced concrete foundation ring beam, which also served to anchor the specimen to the shaking table and as a support during transport from the construction yard to the laboratory.

FIGURES 6.1A, 6.1B.  
Views of the adobe models used in the numerical analysis: (a) plan view; (b) elevation (PUCP).



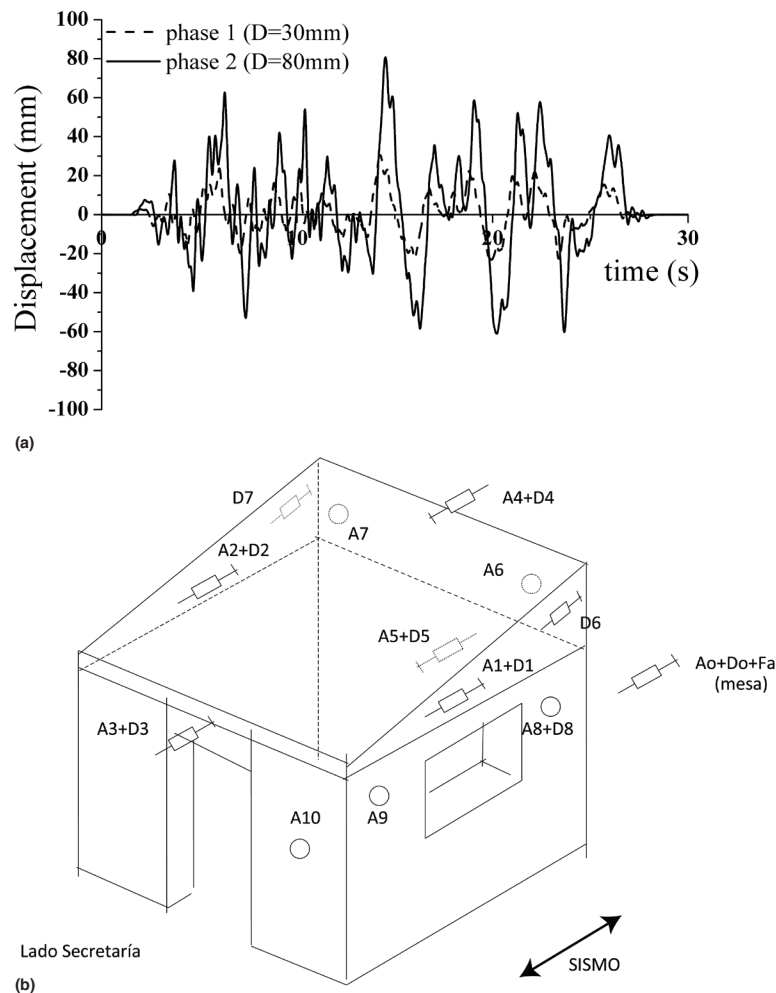
A wooden collar beam was placed on top of the specimens to integrate the walls and transmit the roof weight to the longitudinal walls. The roof consisted of wooden joists covered with tiles. Each specimen weighed around 140 kN. Both windows had wooden lintels. Masons with experience in building adobe houses were hired to produce the adobe blocks and construct the specimens (Blondet et al. 2006).

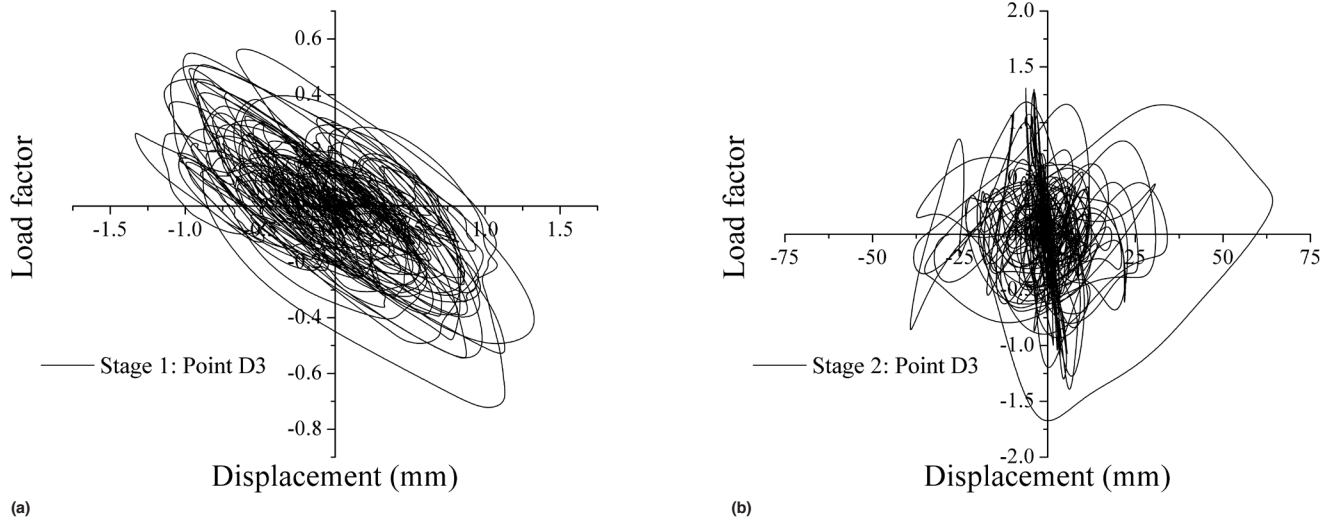
## Experimental Results for Calibration of Numerical Models

The displacement control signal introduced in the shaking table at PUCP was generated from an acceleration record obtained during the 1970 Huaraz earthquake in Peru. Each model was subjected to a sequence of table motions with increasing amplitude. The models were subjected to three successive motions (test phases), defined by their peak command displacements of  $D=30$ ,  $D=80$ , and  $D=130$  mm (fig. 6.2a). These motions represented earthquakes of low, medium, and severe magnitude, respectively. The displacement transducers were removed before the third and final severe test phase to prevent damage due to possible collapse of the models (Blondet et al. 2006). Therefore, recordings were made of only the first two phases regarding the displacement transducers and accelerometers (fig. 6.2b); however, a video and pictures taken after the third phase can be used to assess

FIGURES 6.2A, 6.2B.

(a) Results of table-motion testing of adobe models for phases 1 and 2; (b) model instrumentation (PUCP).





FIGURES 6.3A, 6.3B.

Force-displacement diagrams (at top, center, front wall) for (a) phase 1; (b) phase 2. Note the difference in scale from 1.5 to 75 mm displacement (Pereira and Lourenço 2016).

the failure modes. The data used for the numerical analysis consisted of displacements, accelerations, and force at the base during two of the tested phases ( $D=30$  and  $D=80$  mm). The video and photography report was also used for comparison of damage and failure modes.

With the relative displacement at different locations and the force at the base of the model, it is possible to plot capacity diagrams for each phase of loading. Figure 6.3a shows the force-displacement diagram (at top, center, front wall) for phase 1. As expected, for this first phase the behavior of the building remains mostly elastic. Figure 6.3b shows the force-displacement diagram (at top, center, front wall) for phase 2. At this stage, the building presents extensive nonlinear behavior. Besides the displacements and forces during the tested phases, a video of the final phase of testing was also supplied by PUCP. Figures 6.4a–d show the model at different stages during the final test phase. It is clear that the main damage to this model is concentrated in the longitudinal walls with diagonal cracking and in the transverse back wall with out-of-plane failure.

## Numerical Analysis

Numerical models were built to replicate the obtained experimental results. The finite element method (FEM) was chosen to perform the simulations using DIANA (Displacement method ANAlyser) 9.6 software.

### Definition of the Finite Element Model

A macro-modeling approach was used, assuming adobe masonry as a composite homogeneous material. The FEM model used 3D solid elements, and the created finite element mesh is composed of 36,787 isoparametric pyramid linear elements. The final finite element mesh can be seen in figure 6.5. The wooden collar beam on top of the building was replaced by wooden beams only on the longitudinal walls, the reason being that the interface between the wood elements and the adobe transverse wall seems very weak, as observed from the model in the previous phase (see figs. 6.4a–d). Besides these wooden beams, wooden lintels were modeled on top of every opening. For the wooden elements, reference values were used for the linear mechanical properties, assuming 10 GPa for Young's modulus ( $E$ ).



FIGURES 6.4A–D.

Photos of adobe model during the third and final test phase: (a) initial damage; (b) diagonal cracking on the longitudinal walls; (c) out-of-plane failure of the back wall; (d) model after testing was complete (Photos from video: PUCP).

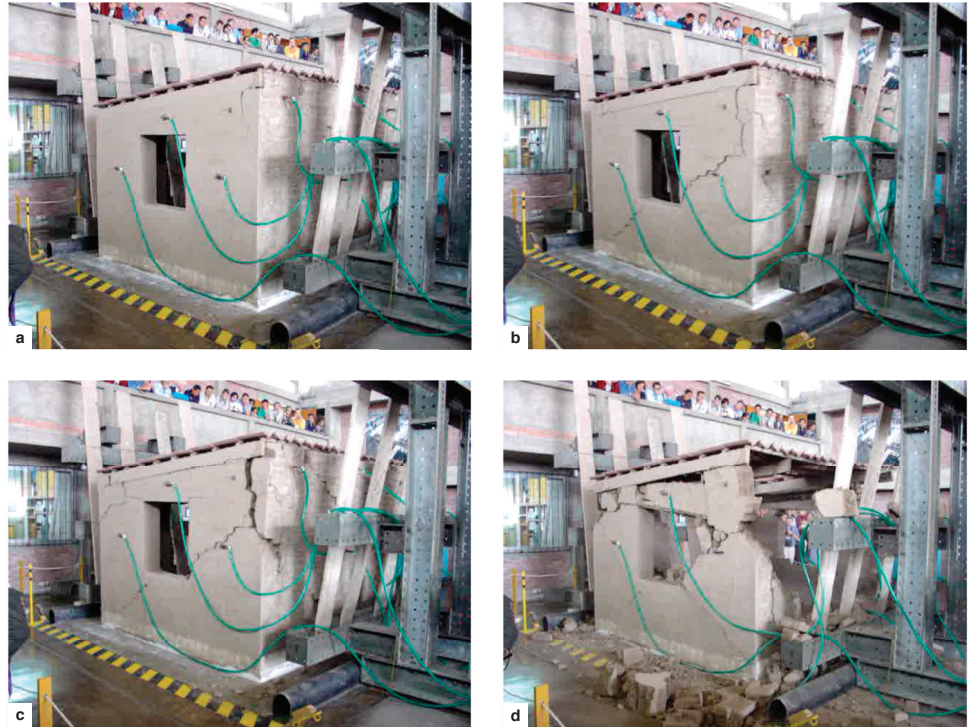
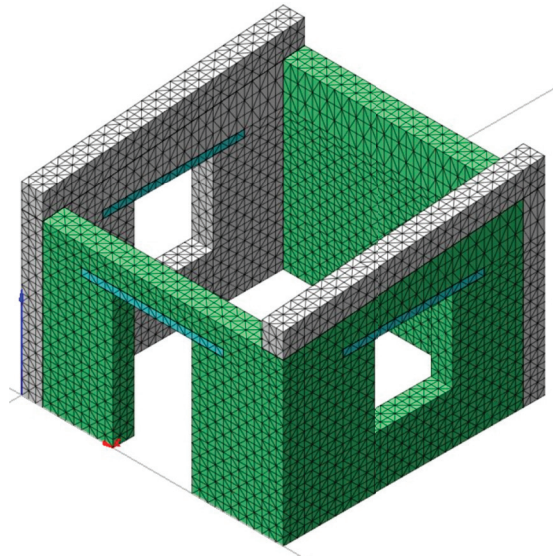


FIGURE 6.5.

Diagram of the final finite element mesh (Pereira and Lourenço 2016).



The TSC (total strain-based crack) model was selected (TNO DIANA 2009). Parabolic and exponential stress-strain relations were used to describe the tensile and compressive behaviors, respectively. The equilibrium solution of the equations in each step of the non-linear analysis is obtained using a regular Newton-Raphson iterative method, and a convergence criterion based on internal energy with a tolerance of  $10^{-3}$  has been used.

The calibrated mechanical properties obtained for this model are shown in table 6.1 and are similar to the values proposed for historic adobe masonry structures (see table 5.5, chap. 5). The obtained values are in excellent agreement with previous surveys developed by the University of Minho regarding historic adobe structures in Peru. Young's modu-

lus and the compressive mechanical properties are the same as those obtained in previous experimental campaigns (KaraniKoloudis, Lourenço, and Mendes 2015). The tensile mechanical properties are slightly higher than those obtained previously (KaraniKoloudis and Lourenço 2015; KaraniKoloudis, Lourenço, and Mendes 2015) and in table 5.5 but still fall in the range of expected values for this material (ASCE 41-06 2006). This also seems reasonable when comparing new buildings, such as the one constructed in the shaking table, with existing historical buildings.

TABLE 6.1.

Calibrated mechanical properties for the PUCP adobe model (Pereira and Lourenço 2016).

| Mechanical Property            | Calibrated Value |
|--------------------------------|------------------|
| $E$ (Young's modulus)          | 270 MPa          |
| $f_c$ (compressive strength)   | 0.45 MPa         |
| $G_c$ (fracture energy)        | 1.25 N/mm        |
| $f_t$ (tensile strength)       | 0.10 MPa         |
| $G_f$ (fracture energy mode-I) | 0.08 N/mm        |

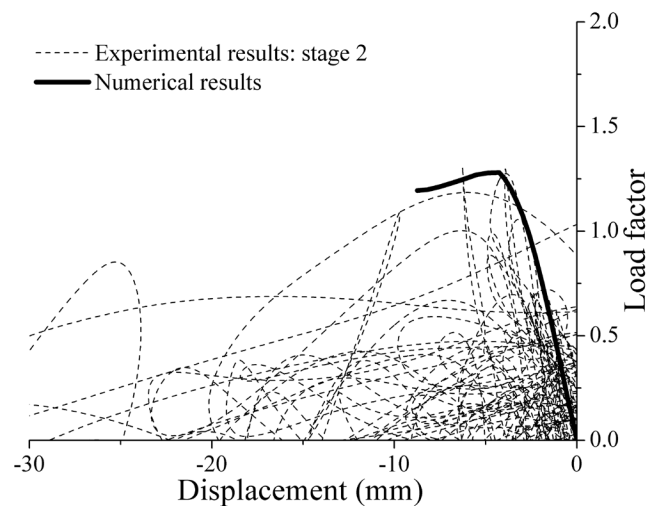
### Nonlinear Static Analysis

A nonlinear pushover analysis was chosen to analyze the building under the experimental conditions. First, the self-weight was applied. Subsequently, the model was subjected to a mass proportional pushover analysis in the longitudinal direction.

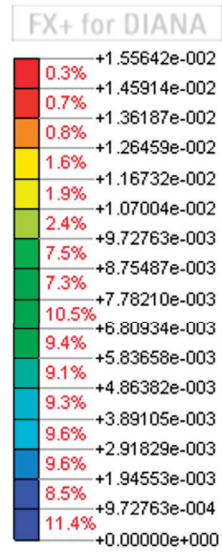
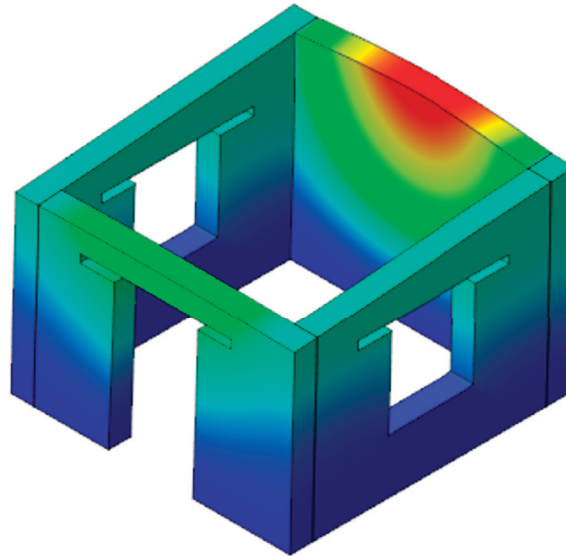
The obtained results can be seen in terms of a force-displacement diagram (fig. 6.6) and deformed shape (fig. 6.7). Here, the load factor is the relation between the lateral load and the vertical load. It is clear that the numerical model is able to properly capture the stiffness and the maximum capacity of the experimental model (see fig. 6.6). Besides maximum capacity and stiffness, damage was analyzed. Figures 6.8a–e show the obtained damage for the numerical model, which can be compared with the obtained damage for the experimental adobe model (see figs. 6.4a–d). Both the numerical and experimental models show concentrated damage on the longitudinal walls due to diagonal cracking and on the transverse walls due to out-of-plane bending, with cracks developing vertically at the edges and horizontally in the bottom of the transverse walls.

FIGURE 6.6.

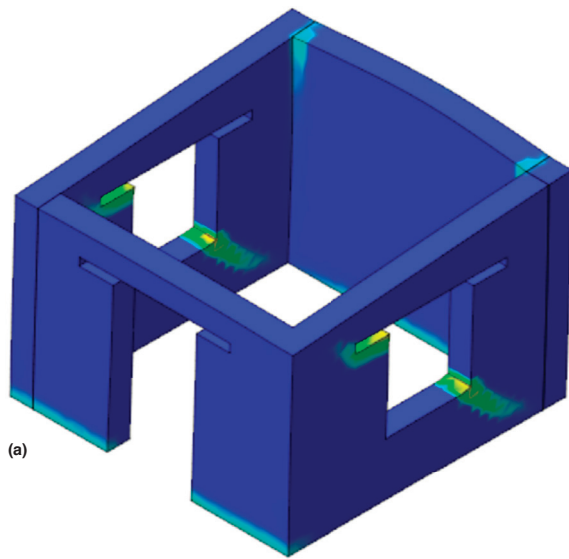
Force-displacement diagram comparing numerical and experimental results (Pereira and Lourenço 2016).



**FIGURE 6.7.** Diagram showing deformed shape for the numerical adobe model. Red indicates maximum value of displacement in the longitudinal direction; blue indicates minimum value (m) (Pereira and Lourenço 2016).



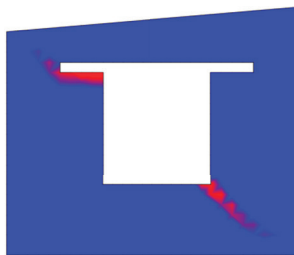
**FIGURES 6.8A–E.** Damage patterns for the numerical model: (a) 3D view; (b) front wall; (c) longitudinal wall; (d) transverse back wall. The legend in (e) shows the scale of strain. Principal strains are shown in red (maximum) and blue (minimum) (Pereira and Lourenço 2016).



(a)



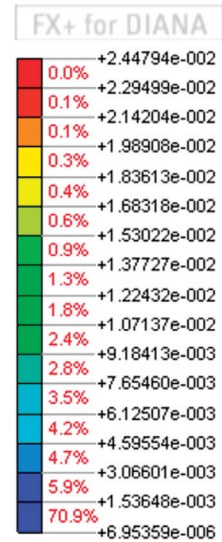
(b)



(c)



(d)



(e)

## Conclusions of the Comparison

This chapter used experimental tests on adobe models subjected to a shaking table test to validate the proposed modeling approach, including the constitutive model and the static pushover analysis method. It has been concluded that the numerical model is able to properly capture the stiffness, maximum capacity, and damage at collapse of the experimental model, and is therefore appropriate for engineering applications.



## Application Example: Kuñotambo, Peru

This chapter presents a summary of a numerical analysis on the structural performance and seismic assessment of the church of Santiago Apóstol de Kuñotambo, in Acomayo, Cusco, Peru. This numerical work was based on inspections and surveys provided by the Getty Conservation Institute and on in situ inspection and testing conducted by the University of Minho in May 2015 (Greco et al. 2015). It is aimed at reproducing the existing structural damage and assessing current safety status through nonlinear static analyses. The following pages focus on the ability of using numerical modeling for the seismic assessment of real adobe masonry structures. Additional information regarding the numerical modeling and the obtained results, together with other case studies, can be found in “Modeling of Prototype Buildings,” the second report in this series, part of the Seismic Retrofitting Project (SRP).

### General Description of the Building

The church of Kuñotambo is a religious structure of the seventeenth century, representative of churches built in the Andes during the period of the Spanish viceroyalty (fig. 7.1). Built in 1681, it consists of a single nave leading to an elevated presbytery and altar, with an adjacent

**FIGURE 7.1.**  
Aerial view of the church of Kuñotambo in Peru, taken from the southeast. Photo: Wilfredo Carazas.



sacristy and baptistery. The walls and buttresses are of thick adobe masonry, with a single-gable timber roof and clay tiles. The structure is built on a base course plinth of rubble stone masonry with earth mortar, over a sloping natural rock, with varying layers of compacted clay.

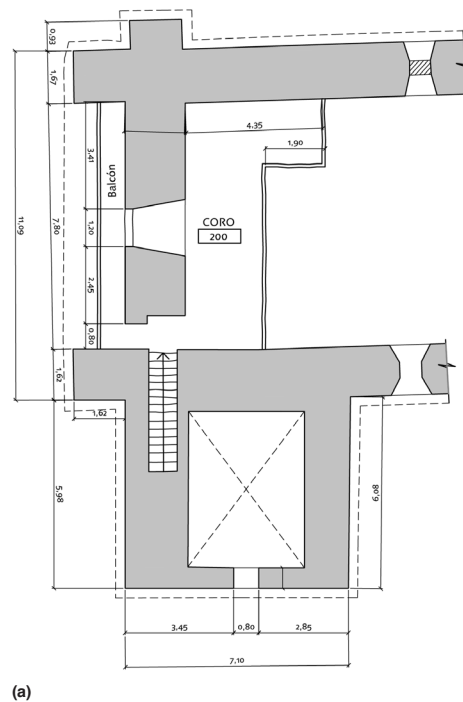
The church is characterized by a relatively simple geometry involving two longitudinal walls and two gable walls (facades) made of adobe resting over a rubble stone masonry foundation (figs. 7.2 a–d); dimensions are given in figures 7.2a and 7.2b. Due to the poor roof structural system, two different finite element models were prepared (one with and one without the presence of timber tie beams in the transversal direction of the main nave).

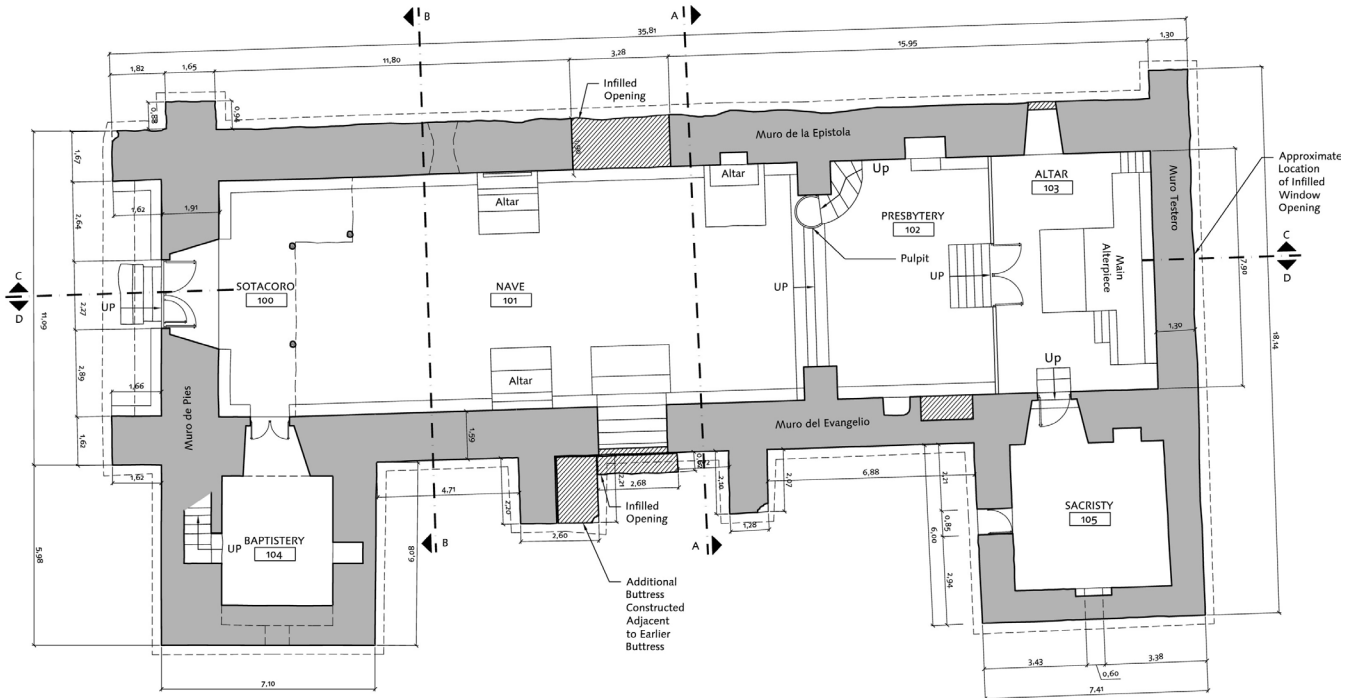
## Definition of the Finite Element Model

The finite element model was created using DIANA (Displacement method ANALyser) software (TNO DIANA 2009). The created finite element mesh was produced by setting maximum size of the elements at 30 cm, with the exception of the east arched opening, where there was a more refined mesh (with maximum element size at 15 cm). Several different types of elements were used: (a) isoparametric pyramid linear elements for the masonry; (b) two-node truss elements for the tie beams; and (c) two-node beam elements for the anchor beams. The resulting mesh was composed of around 320,000 elements and around 69,000 nodes (fig. 7.3). Details of the shape of the mesh are shown in figures 7.4a and 7.4b, namely those of the timber anchors and the openings. In the thickness of the structural elements, seven elements are present in the lateral walls of the nave, while four and six are present through the thicknesses in the west facade and east facade, respectively.

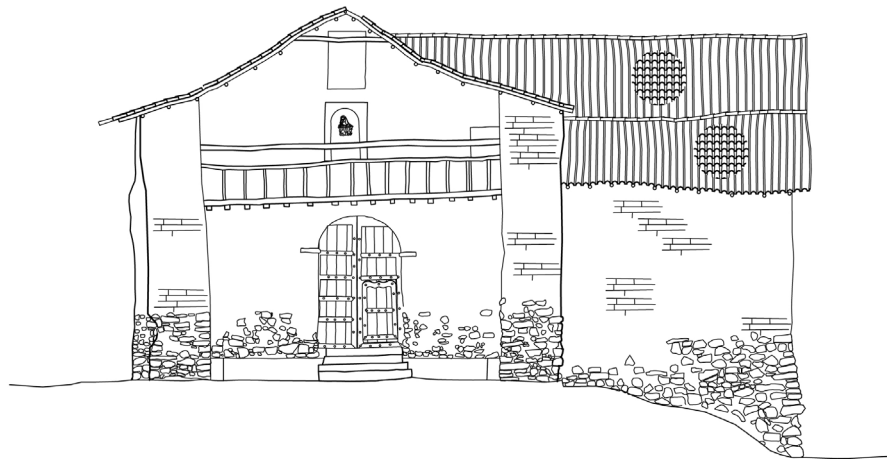
FIGURES 7.2A–D.

(a) Architectural plan view of the church coro at +4.00, (b) architectural plan view of the church at +2.50, (c) sectional drawing, and (d) elevation of the church of Kuñotambo (Cancino et al. 2012).

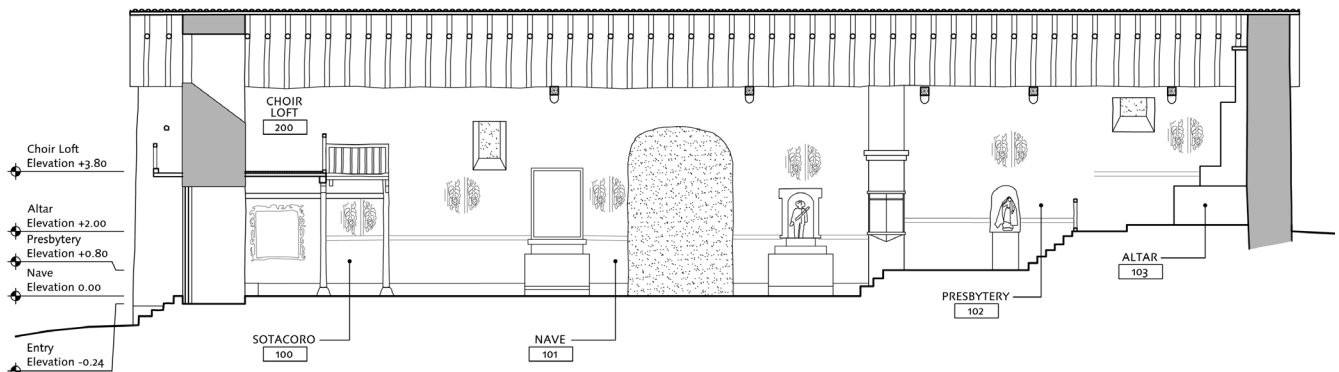




(b)



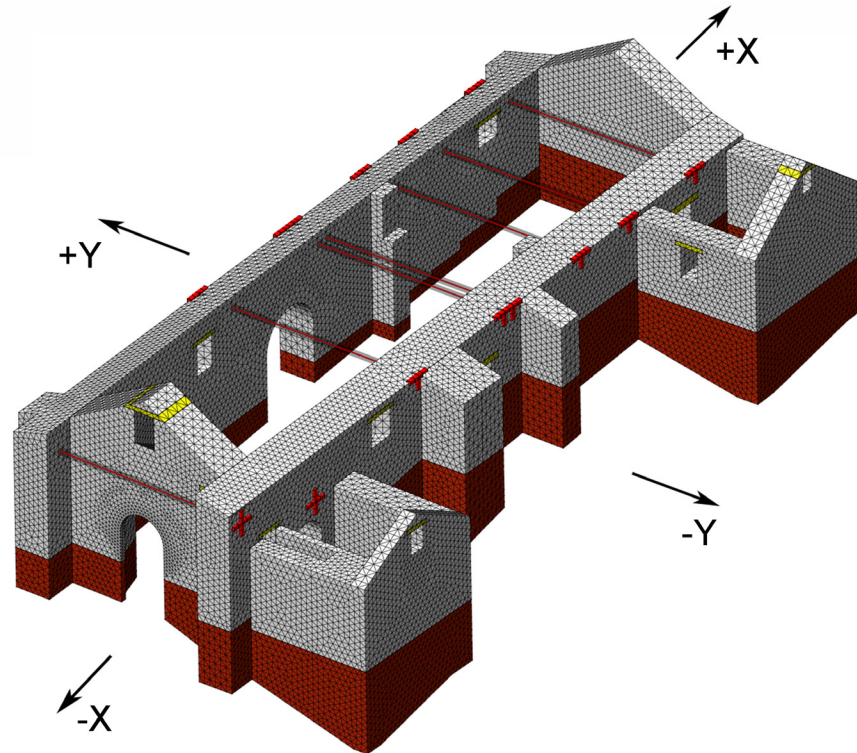
(c)



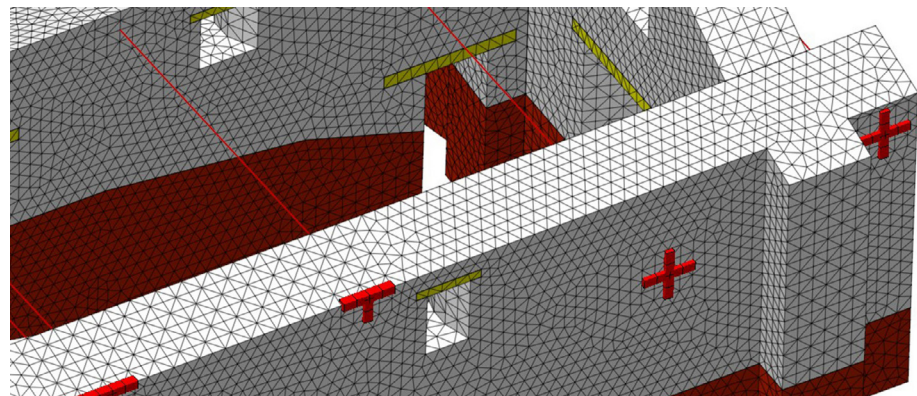
(d)



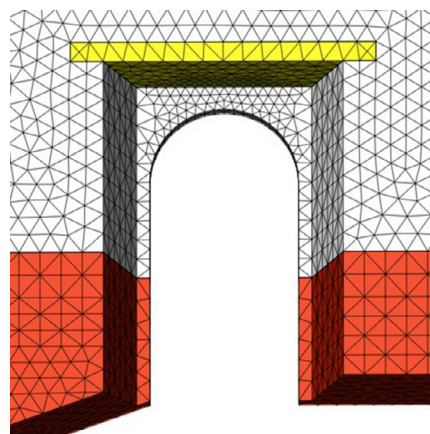
**FIGURE 7.3.**  
Drawing of finite element mesh,  
with base course founda-  
tion in brown and ties in red  
(KaraniKoloudis and Lourenço  
2015).



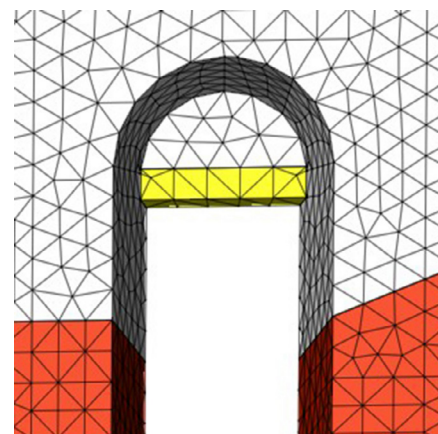
**FIGURES 7.4A–C.**  
Details of the shape of the  
finite element mesh: (a) timber  
anchors; (b) lintels above open-  
ings (KaraniKoloudis and Lourenço  
2015).



(a)



(b)



(c)

## Material Model and Mechanical Properties

The masonry was modeled following a macro-modeling approach using the total strain-based crack (TSC) available in DIANA. Exponential behavior in tension and parabolic behavior in compression were adopted.

The mechanical properties were determined from bibliographic resources and national technical building standards (FEMA 306 1998; NTC 2008; EC6 2005). Also taken into account were the results of experimental campaigns conducted for the SRP by the Pontificia Universidad Católica del Perú in 2011 and 2012 and the results of in situ sonic testing carried out by the University of Minho in May 2015 (Greco et al. 2015). Different materials were defined as part of the structural system of the model: (a) adobe masonry for the system of walls, gable ends, and buttresses; (b) rubble stone masonry for the base course; and (c) timber for tie beams, anchors, and lintels. Table 7.1 shows the mechanical properties adopted in the TSC model. Regarding the timber elements, there were two different types of timber in the model; both were kept in the elastic regime (Karanikoloudis and Lourenço 2015).

TABLE 7.1.

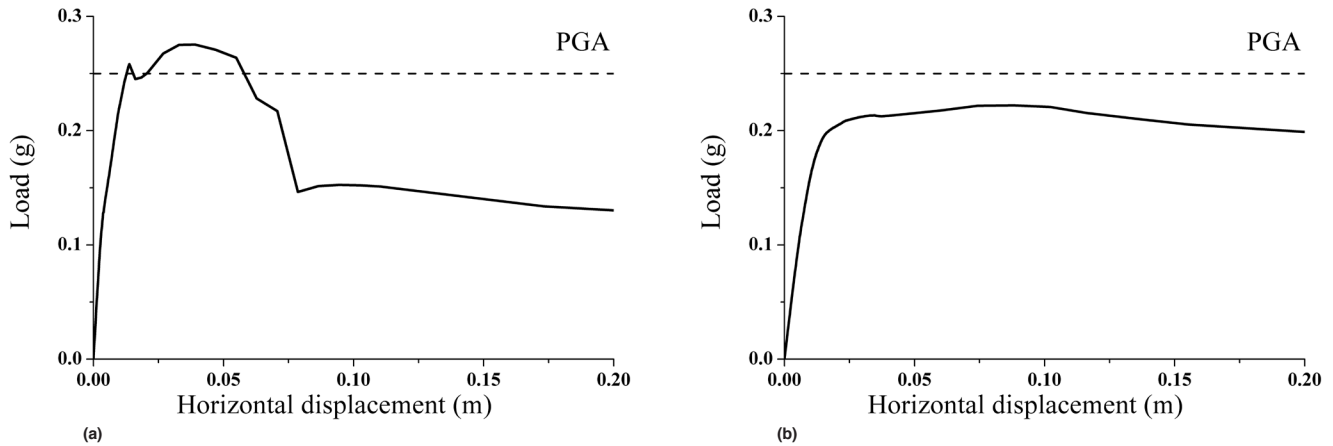
Mechanical properties adopted in the model for the church of Kuñotambo (Karanikoloudis and Lourenço 2015).

| Mechanical Property                   | Adobe Masonry          | Rubble Stone Masonry    |
|---------------------------------------|------------------------|-------------------------|
| $\rho$ (density) [kg/m <sup>3</sup> ] | 1900                   | 1900                    |
| $E$ (Young's modulus) [MPa]           | 100 / 270 <sup>1</sup> | 300 / 1570 <sup>1</sup> |
| $f_c$ (compressive strength) [MPa]    | 0.45                   | 0.60                    |
| $G_c$ (fracture energy) [N/mm]        | 1.0                    | 1.5                     |
| $f_t$ (tensile strength) [MPa]        | 0.05                   | 0.06                    |
| $G_f$ (fracture energy mode-I) [N/mm] | 0.01                   | 0.01                    |

<sup>1</sup> Range of values found in different sources of information.

## Numerical Results and Observed Conclusions

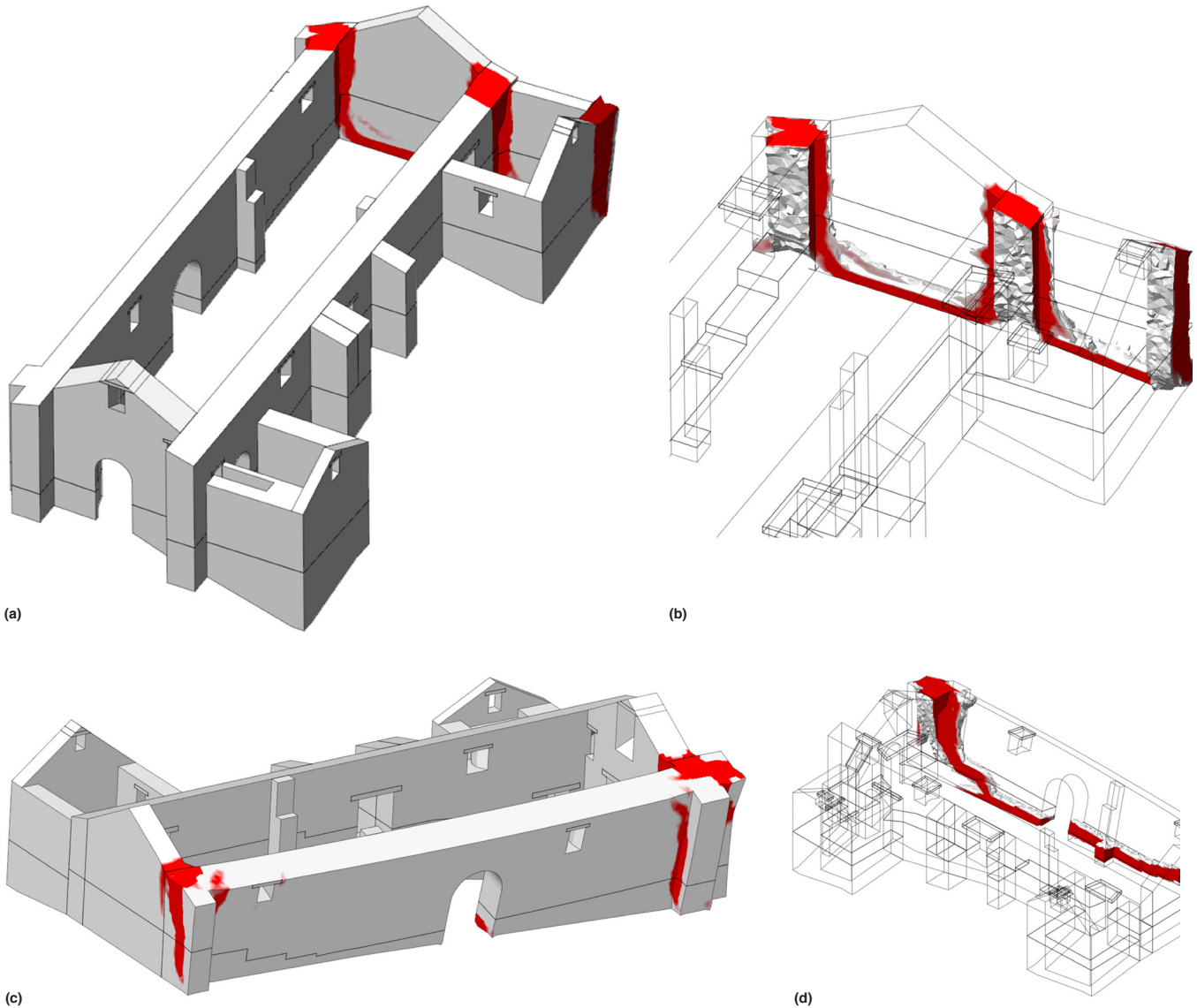
Several pushover analyses (mass proportional) were performed to assess the seismic behavior of the model of the church of Kuñotambo. Both orthogonal directions were studied (longitudinal, X, and transversal, Y) in the positive load application (direction of the altar and direction of the sacristy, respectively, for X and Y) and negative load application. These analyses allowed the assessment of the maximum load capacity of the model for all load application configurations. Figures 7.5a and 7.5b show the capacity curves of the model considering different mechanical properties (Karanikoloudis and Lourenço 2015). On the positive X axis, maximum capacity was 0.28 g, the failure mechanism being vertical separation cracks along the corners in the west part of the church. These cracks covered the entire elevation and thickness, with horizontal hinge lines at the bottom of the base course foundation, resulting in collapse of the west gable wall (fig. 7.6b). In the Y positive direction, the failure mechanism consisted of the separation and out-of-plane overturning of the south lateral wall. Large deformations were evident at the eaves of the south lateral wall (fig. 7.6c). The structure's lateral capacity reached 0.22 g with maximum outward displacements recorded at the middle top of the south lateral wall. Cracking started to appear at the south-east corner and continued in the southwest corner of the nave (fig. 7.6d).



**FIGURES 7.5A, 7.5B.**  
Examples of capacity curves obtained in numerical analyses: (a) capacity curve for X-direction positive; (b) capacity curve for Y-direction positive.

With the performed analyses, it was possible to assess the seismic behavior of the church of Kuñotambo in terms of maximum capacity to lateral loads and damage patterns. The numerical model can reproduce the damage condition (current) of the structure reasonably well. The present damage appears to be inflicted partly by earthquakes and settlements, amplified by erosion, improper drainage, lack of use and maintenance, and consequently abandonment. The system of existing timber ties along the span of the nave and altar, at eave level, and in between timber wall plates is discontinuous and the confinement rather poor, given the connections present. In the east facade, damage consists of vertical cracks at the corners and along the entire thickness and elevation. The south wall exhibits outward displacements, small cracks, and loss of material in exterior areas. The baptistery exhibits several vertical cracks located in the sidewalls and at the northeast corner.

The dispersion of material properties from literature, laboratory testing, and in situ sonic testing was accounted for by assigning lower and upper bound values. According to the pushover nonlinear analyses, under a mass proportional lateral load, strengthening is needed since the overall capacity does not reach the required peak ground acceleration (0.25 g). Additional models with proposed strengthening techniques were developed and analyzed, and, as indicated above, the full findings can be found in the report "Modeling of Prototype Buildings."



**FIGURES 7.6A–D.**  
 Examples of damage plots  
 obtained in numerical analyses (in  
 terms of crack patterns): (a) crack  
 pattern for positive X axis, west  
 wall; (b) crack pattern for positive  
 Y axis, west wall; (c) crack pattern  
 for positive Y axis, south wall;  
 (d) crack pattern for positive Y axis,  
 southwest corner (Karanikoloudis  
 and Lourenço 2015).



# Conclusions

This publication is part of a series within the Getty Conservation Institute's Seismic Retrofitting Project (SRP). It is intended to help engineering professionals who deal with assessment of historic earthen structures using advanced numerical modeling techniques.

Different structural analysis methods have been presented, both linear and nonlinear as well as static and dynamic. From the methods in this report, the nonlinear static analysis method, also termed *pushover analysis*, is highlighted. Although nonlinear time history analysis is taken as most representative in case of seismic assessment of structures, such time integration approaches are time consuming and unreasonable in engineering practice, being used only for a handful of high-impact structures and academic research. Pushover analysis seems to be, from the available methods, the most efficient type of analysis for advanced seismic assessment.

With the technological advancements made over the last few years, the computational capabilities and graphic environments in finite element method (FEM) allow the user to easily build up models with good representativeness of the real structures. Simplifications are required when building FEM models of complex structures in historic earthen sites. Different possibilities are available in terms of type of elements, type of integration, and so forth, which still require adequate knowledge on the part of the engineer. Some simple steps, such as linear elastic analysis and eigenvalue analysis, help ensure the model is properly replicated, dramatically increasing confidence in the later obtained results.

There are several modeling techniques to represent masonry materials. Because the objective of this report is to provide advice on the modeling of historic structures, only macro modeling was approached, as the alternatives are less reasonable for real-size structures and engineering applications. Two different commercial software tools were presented, including the available constitutive models able to reproduce the mechanical behavior of masonry. From the comparison of the commercial codes, it was observed that the results are similar, further demonstrating the reliability of these advanced numerical tools.

The mechanical properties of adobe masonry have a wide range of variation, depending mostly on soil characteristics and workmanship. Although there are some normative documents with reference values for mechanical properties of masonry, in most cases historic masonry and earthen masonry are less prescribed. Still, from the available information in the literature, it is possible to provide sound estimates of the mechanical properties to be adopted. Reasonable variations of these properties should provide limited changes in the structural response.

Application examples focused on showing the capability of reproducing the mechanical behavior of earthen structures in both laboratory environments and real structures. It was shown that nonlinear static analysis (pushover analysis) using the proposed constitutive models was able to reproduce the experimental results obtained in the laboratory using a shaking table. In the case of the church of Santiago Apóstol de Kuñotambo in Peru, it was

possible to reproduce in reasonable agreement the damage observed in the current condition of the structure.

The final outcome of this publication is to guide professionals in performing the complex task of using FEM for historic earthen structures. The different options and variables to consider have been highlighted, and the participants in the SRP, along with their partners, hope that this report will forward the analysis, understanding, and retrofitting of earthen historic buildings. The next two publications of the modeling phase of the SRP aim to provide specific examples of how the modeling was performed for all prototype buildings and to ensure that simple calculations, based on the research developed as part of the SRP modeling phase, can help to design retrofitting techniques for historic earthen buildings.

# References

- ABAQUS. 2010. ABAQUS User's Manual. Waltham, MA: Dassault Systemès.
- Angelillo, M., P. B. Lourenço, and G. Milani. 2014. "Masonry Behavior and Modeling." In *Mechanics of Masonry Structures*, vol. 551, edited by M. Angelillo, 1–26. Vienna: CISM International Centre for Mechanical Sciences.
- Anthoine, A. 1995. "Derivation of the In-plane Elastic Characteristics of Masonry through Homogenization Theory." *International Journal of Solids and Structures* 32 (2): 137–63.
- ASCE 41-06. 2006. *Seismic Rehabilitation of Existing Buildings*. American Society of Civil Engineers, Reston, VA.
- Atamturktur, H. S. 2006. "Structural Assessment of Gustavino Domes." MSc thesis, Pennsylvania State University, University Park.
- Aydinoğlu, M. N. 2003. "An Incremental Response Spectrum Analysis Procedure Based on Inelastic Spectral Displacements for Multi-mode Seismic Performance Evaluation." *Bulletin of Earthquake Engineering* 1 (1): 3–36.
- Babuska, I., and J. M. Melenk. 1997. "The Partition of Unity Method." *International Journal for Numerical Methods in Engineering* 40: 727–58.
- Belytschko, T., Y. Y. Lu, and L. Gu. 1994. "Element-free Galerkin Methods." *International Journal for Numerical Methods in Engineering* 37: 229–56.
- Beresnev, I. A., and G. M. Atkinson. 1998. "FINSIM I A FORTRAN Program for Simulating Stochastic Acceleration Time Histories from Finite Faults." *Seismological Research Letters* 69 (1): 27–32.
- Betti, M., and A. Vignoli. 2011. "Numerical Assessment of the Static and Seismic Behavior of the Basilica of Santa Maria all'Impruneta (Italy)." *Construction and Building Materials* 25 (12): 4308–24.
- Bjorkman, S., and J. M. Pottier. 2008. "Finite Element Mesh Considerations for Reduced Integration Elements." Paper presented at ASME Pressure Vessels and Piping Conference, Chicago, July 27–31, 2008.
- Blondet, M., D. Torrealva, J. Vargas, J. Velasquez, and N. Tarque. 2006. "Seismic Reinforcement of Adobe Houses Using External Polymer Mesh." Paper presented at First European Conference on Earthquake Engineering and Seismology, Geneva, Switzerland, September 3–8, 2006.
- Bommer, J. J., and A. B. Acevedo. 2004. "The Use of Real Earthquake Accelerograms as Input to Dynamic Analysis." *Journal of Earthquake Engineering* 1 (1): 43–91.
- Bommer, J. J., and C. Ruggieri. 2002. "The Specification of Acceleration Time-Histories in Seismic Design Codes." *European Earthquake Engineering* 16 (1): 3–17.
- Bommer, J. J., A. B. Acevedo, and J. Douglas. 2003. "The Selection and Scaling of Real Earthquake Accelerograms for Use in Seismic Design and Assessment." In *Proceedings of ACI International Conference on Seismic Bridge Design and Retrofit*. La Jolla, CA: American Concrete Institute.
- Bommer, J. J., S. G. Scott, and S. K. Sarma. 2000. "Hazard-Consistent Earthquake Scenarios." *Soil Dynamics and Earthquake Engineering* 19: 219–31.



- Boore, D. M. 2003. "Simulation of Ground Motion Using the Stochastic Method." *Pure and Applied Geophysics* 160: 635–76.
- Borst, R., J. J. C. Remmers, A. Needleman, and M. Abellan. 2004. "Discrete vs Smeared Crack Models for Concrete Fracture: Bridging the Gap." *International Journal for Numerical and Analytical Methods in Geomechanics* 28: 583–607.
- Cancino, C. 2011. *Damage Assessment of Historic Earthen Buildings after the August 15, 2007, Pisco Earthquake*. Los Angeles: Getty Conservation Institute.
- Cancino, C. and S. Lardinois. 2012. *Seismic Retrofitting Project: Assessment of Prototype Buildings*. Los Angeles: Getty Conservation Institute.
- Cervera, M., J. Oliver, and R. Faria. 1995. "Seismic Evaluation of Concrete Dams via Continuum Damage Models." *Earthquake Engineering and Structural Dynamics* 24: 1225–45.
- Chen, S. Y., F. L. Moon, and T. Yi. 2008. "A Macroelement for the Nonlinear Analysis of In-plane Unreinforced Masonry Piers." *Engineering Structures* 30 (8): 2242–52.
- Crisafulli, F. J. 1997. "Seismic Behavior of Reinforced Concrete Structures with Masonry Infills." PhD thesis, University of Canterbury, New Zealand.
- DNV GL. 2015. "Class Guideline—Finite Element Analysis." Part 3, chap. 7 in *Rules for Classification: Ships*. Report DNVGL-CG-0127. Høvik, Norway: DNV GL.
- Drucker, D. C. 1961. "On Structural Concrete and the Theorems of Limit Analysis." *Publications* 5 (21): 49–59. International Association for Bridge and Structural Engineering, Zurich.
- EC6 (EN 1996-1-1). 2005. *Eurocode 6: Design of Masonry Structures, Part 1-1: General Rules for Reinforced and Unreinforced Masonry Structures*. European Committee for Standardization.
- EC8 (EN 1998-1-1). 2004. *Eurocode 8: Design of Structures for Earthquake Resistance, Part 1: General Rules, Seismic Actions and Rules for Buildings*. European Committee for Standardization.
- Endo, Y., L. Pelà, and P. Roca. 2017. "Review of Different Pushover Analysis Methods Applied to Masonry Buildings and Comparison with Nonlinear Dynamic Analysis." *Journal of Earthquake Engineering* 21 (8): 1234–55.
- Endo, Y., L. Pelà, P. Roca, F. da Porto, and C. Modena. 2015. "Comparison of Seismic Analysis Methods Applied to a Historical Church Struck by 2009 L'Aquila Earthquake." *Bulletin of Earthquake Engineering* 13 (12): 3749–78.
- Fajfar, P. 2000. "A Nonlinear Analysis Method for Performance Based Seismic Design." *Earthquake Spectra* 16 (3): 573–92.
- FEMA 306. 1998. *Evaluation of Earthquake Damaged Concrete and Masonry Wall Buildings—Basic Procedures Manual*. Applied Technology Council (ATC-43 Project).
- FEMA 440. 2004. *Improvement of Nonlinear Static Seismic Analysis Procedures*. Federal Emergency Management Agency, Washington, DC.
- Galasco, A., S. Lagomarsino, and A. Penna. 2006. "On the Use of Pushover Analysis for Existing Masonry Buildings." In *Proceedings of First European Conference on Earthquake Engineering and Seismology (1st ECEES): Joint Event of the 13th ECEE and the 30th General Assembly of the ESC*, 5862–71. Zurich: Swiss Society for Earthquake Engineering (SGEB).
- Gilbert, M. 2007. "Limit Analysis Applied to Masonry Arch Bridges: State-of-the-Art and Recent Developments." In *Proceedings of the 5th International Conference on Arch Bridges*, edited by P. B. Lourenço, D. V. Oliveira, and A. Portela, 13–28. Funchal, Madeira, Portugal: University of Minho, Universidade da Madeira.
- Greco, F., G. Karanikoloudis, P. B. Lourenço, and N. Mendes. 2015. *Experimental In-situ Testing Campaign on Adobe Historic Structures in Peru, within the Getty SR Project*. Technical report 2015-DEC/E-30. University of Minho, Portugal.

- Gupta, A. K. 1992. *Response Spectrum Method in Seismic Analysis and Design of Structures*. Vol. 4. Boca Raton, FL: CRC Press.
- Hardy, M., C. Cancino, and G. Ostergren, eds. 2009. *Proceedings of the Getty Seismic Adobe Project 2006 Colloquium: Getty Center, Los Angeles, April 11–13, 2006*. Los Angeles: Getty Conservation Institute.
- Heyman, J. 1969. "The Safety of Masonry Arches." *International Journal of Mechanical Sciences* 11 (4): 363–85.
- Iervolino, I., G. Maddaloni, and E. Cosenza. 2008. "Eurocode 8 Compliant Real Record Sets for Seismic Analysis of Structures." *Journal of Earthquake Engineering* 12: 54–90.
- Ingraffea A. R., and V. Saouma. 1985. "Numerical Modeling of Discrete Crack Propagation in Reinforced and Plain Concrete." In *Fracture Mechanics of Concrete: Structural Application and Numerical Calculation, vol. 4 of Engineering Application of Fracture Mechanics*, edited by G. C. Sih and A. DiTommaso, 171–225. Dordrecht: Springer.
- Ivancic, S. R., C. Briceno, R. Marques, R. Aguilar, R. Perucchio, and J. Vargas. 2014. "Seismic Assessment of the St. Peter Apostle Church of Andahuayllillas in Cusco, Peru." In *Proceedings of SAHC2014, 9th International Conference on Structural Analysis of Historical Constructions*, 1–12. Mexico City: SAHC.
- Jankowiak, T., and T. Lodygowski. 2005. "Identification of Parameters of Concrete Damage Plasticity Constitutive Model." *Foundations of Civil and Environmental Engineering* 6 (1): 53–69.
- Jansen, D. C., and S. Shah. 1997. "Effect of Length on Compressive Strain Softening of Concrete." *Journal of Engineering Mechanics* 123 (1): 25–35.
- Johansen, K. W. 1930. *Styrekeforholden i Stobeskel i Beton* [The strength of joints in concrete]. *Bygningsstat. Medd.* 2: 67–68.
- Karaniouloudis, G., and P. B. Lourenço. 2015. *Seismic Assessment of Kuño Tambo Church (Current Condition), Peru*. Technical report 2015-DEC/E-41. University of Minho, Portugal.
- Karaniouloudis, G, P. B. Lourenço, and N. Mendes. 2015. *Experimental In-situ Testing Campaign on Adobe Historic Structures in Peru*. Technical report 2015-DEC/E-30. University of Minho, Portugal.
- Kmieciak, P., and M. Kaminski. 2011. "Modeling of Reinforced Concrete Structures and Composite Structures with Concrete Strength Degradation Taken into Consideration." *Archives of Civil and Mechanical Engineering* 11 (3): 623–36.
- Kooharian, A. 1952. "Limit Analysis of Voussoir (Segmental) and Concrete Arches." *Journal of the American Concrete Institute* 24: 317–28.
- Krawinkler, H. 1995. "New Trends in Seismic Design Methodology." In *Proceedings of 10th European Conference on Earthquake Engineering*, Vienna, 821–30. Rotterdam: A. A. Balkema.
- Lee, J., and G. L. Fenves. 1998. "Plastic-damage Model for Cyclic Loading of Concrete Structures." *Journal of Engineering Mechanics* 124 (8): 892–900.
- Liberatore, D., G. Spera, M. Mucciarelli, M. R. Gallipoli, D. Santarsiero, C. Tancredi, N. Masini et al. 2006. "Typological and Experimental Investigation on the Adobe Buildings of Aliano (Basilicata, Italy)." In *Proceedings 5th International Conference on Structural Analysis of Historical Constructions*, 851–58. New Delhi: Macmillan India.
- Lopez, J., S. Oller, and E. Onate. 1998. *Cálculo del comportamiento de la Mampostería Mediante Elementos Finitos*. Barcelona: International Centre for Numerical Methods in Engineering (CIMNE).
- Lourenço, P. B. 1996. "Computational Strategies for Masonry Structures." PhD diss., Delft University of Technology, the Netherlands.

- \_\_\_\_\_. 1998. "Experimental and Numerical Issues in the Modeling of the Mechanical Behavior of Masonry." In *Proceedings of Structural Analysis of Historical Constructions*, 57–91. Barcelona: CIMNE.
- \_\_\_\_\_. 2001. "Analysis of Historical Constructions: From Thrust-lines to Advanced Simulations." In *Historical Constructions 2001, Possibilities of Numerical and Experimental Techniques: Proceedings of the 3rd International Seminar*, edited by P. B. Lourenço and P. Roca, 91–116. Guimarães, Portugal: University of Minho.
- \_\_\_\_\_. 2002. "Computations on Historic Masonry Structures." *Progress in Structural Engineering and Materials* 4 (3): 301–19.
- \_\_\_\_\_. 2009a. "Recent Advances in Masonry Modeling: Micromodeling and Homogenization." In *Multiscale Modeling in Solid Mechanics*, 251–94. London: Imperial College Press.
- \_\_\_\_\_. 2009b. "Material Data to Use." Slideshow presentation, Advanced Masters in Structural Analysis of Monuments and Historical Constructions program, University of Minho.
- Lourenço, P. B., and S. Mourão. 2001. "Safety Assessment of Monastery of Jerónimos, Lisbon." In *Historical Constructions 2001, Possibilities of Numerical and Experimental Techniques: Proceedings of the 3rd International Seminar*, edited by P. B. Lourenço and P. Roca, 697–706. Guimarães, Portugal: University of Minho.
- Lourenço, P. B., N. Mendes, L. F. Ramos, and D. V. Oliveira. 2011. "On the Analysis of Masonry Structures without Box Behavior." *International Journal of Architectural Heritage* 5: 369–82.
- Lourenço, P. B., A. Trujillo, N. Mendes, and L. F. Ramos. 2012. "Seismic Performance of the St. George of the Latins Church: Lessons Learned from Studying Masonry Ruins." *Engineering Structures* 40: 501–18.
- Lubliner, J., J. Oliver, S. Oller, and E. Onate. 1989. "A Plastic-damage Model for Concrete." *International Journal of Solids and Structures* 25 (3): 299–329.
- Lumantarna, R., D. T. Biggs, and J. M. Ingham. 2014. "Uniaxial Compressive Strength and Stiffness of Field-Extracted and Laboratory-Constructed Masonry Prisms." *ASCE Journal of Materials* 26 (4): 567–75.
- MC2010. 2010. *Fib Model Code 2010, Final Draft, Vol. 1* (*fib* bulletin 65). Lausanne: International Federation for Structural Concrete (*fib*).
- Mendes, N., and P. B. Lourenço. 2010. "Seismic Assessment of Masonry 'Gaioleiro' Building in Lisbon, Portugal." *Journal of Earthquake Engineering* 14: 80–101.
- Milani, G., and P. B. Lourenço. 2009. "Blast Analysis of Enclosure Masonry Walls Using Homogenization Approaches." *International Journal for Multiscale Computational Engineering* 7 (2): 91–113.
- Ministerio de Transportes, Comunicaciones, Vivienda y Construcción. 2000. *ININVI: Adobe Construction. Technical Standard for Adobe Building. Special Disposition for Seismic-resistant Adobe Building*. NTE E-080. Lima: Ministerio de Transportes, Comunicaciones, Vivienda y Construcción.
- Moes, N., J. Dolbow, and T. Belytschko. 1999. "A Finite Element Method for Crack Growth without Remeshing." *International Journal for Numerical Methods in Engineering* 46: 131–50.
- Muttoni, A., J. Schwartz, and B. Thurlimann. 1997. *Design of Concrete Structures with Stress Fields*. Berlin: Birkhauser.
- Naeim, F., and J. M. Kelly. 1999. *Design of Seismic Isolated Structures: From Theory to Practice*. New York: John Wiley & Sons.
- Nielsen, M. P. 1998. *Limit Analysis and Concrete Plasticity* (2nd ed.). Boca Raton, FL: CRC Press.
- Ngo, D., and A. C. Scordelis. 1967. "Finite Element Analysis of Reinforced Concrete Beams." *Journal of the American Concrete Institute* 64: 152–63.

- NTC. 2008. *Norme tecniche per le costruzioni—Il Capo del Dipartimento della Protezione Civile*. With Circolare no. 617 (2009). Il Ministro Delle Infrastrutture, Italy (in Italian).
- NZSEE. 2006. *Assessment and Improvement of the Structural Performance of Buildings in Earthquakes*. New Zealand Society for Earthquake Engineering.
- Orduña, A., and P. B. Lourenço. 2001. "Limit Analysis as a Tool for the Simplified Assessment of Ancient Masonry Structures." In *Historical Constructions 2001, Possibilities of Numerical and Experimental Techniques: Proceedings of the 3rd International Seminar*, edited by P. B. Lourenço and P. Roca, 511–20. Guimarães, Portugal: University of Minho.
- Ottazzi, G. P., J. F. L. Yep, S. M. Blondet, M. G. Villa-Garcia, and C. J. F. Ginocchio. 1989. *Ensayos de simulación sísmica de viviendas de adobe*. Technical report. Pontificia Universidad Católica del Perú, Departamento de Ingeniería, Peru.
- Page, A. W. 1978. "Finite Element Model for Masonry." *Journal of the Structural Division—ASCE* 104: 1267–85.
- \_\_\_\_\_. 1981. "The Biaxial Compressive Strength of Brick Masonry." *Proceedings of the Institution of Civil Engineers* 71 (3): 893–906.
- \_\_\_\_\_. 1983. "The Strength of Brick Masonry under Biaxial Compression–Tension." *International Journal of Masonry Construction* 3 (1): 26–31.
- Page, A. W., W. Kleeman, and M. Dhanasekar. 1985. "In-plane Finite Element Model for Brick Masonry." In *Proceedings of New Analysis Techniques for Structural Masonry—ASCE*. New York: American Society of Civil Engineers.
- Papanikolaou, V. K., and A. S. Elnashai. 2005. "Evaluation of Conventional and Adaptive Pushover Analysis I: Methodology." *Journal of Earthquake Engineering* 9 (6): 923–41.
- Park, J., K. El-Deib, C. Butenweg, and C. Gellert. 2011. "A Novel Microelement Approach for Masonry Walls." In *Proceedings of the 8th International Conference on Structural Dynamics Eurodyn*. Leuven, Belgium: Katholieke Universiteit Leuven.
- Paulay, T., and M. J. N. Priestley. 1992. *Seismic Design of Reinforced Concrete and Masonry Buildings*. New York: John Wiley & Sons.
- Pelà, L., A. Aprile, and A. Benedetti. 2013. "Comparison of Seismic Assessment Procedures for Masonry Arch Bridges." *Construction and Building Materials* 38: 381–94.
- Pereira, J. M., and P. B. Lourenço. 2016. *Numerical Analysis of the SismoAdobe Conference Models from PUCP, Peru*. Technical report 2016-DEC/E-19. University of Minho, Portugal.
- Pietruszczak, S., and X. Niu. 1992. "A Mathematical Description of Macroscopic Behavior of Brick Masonry." *International Journal of Solids and Structures* 29 (5): 531–46.
- Quagliarini, E., S. Lenci, and M. Iorio. 2010. "Mechanical Properties of Adobe Walls in a Roman Republican Domus at Suasa." *Journal of Cultural Heritage* 11 (2): 320–25.
- Rajadurai, S., M. G. Prasad, R. Kaven, and M. Sandaravadivelu. 2014. "FEA Best Practices Approach." *International Journal of Recent Development in Engineering and Technology* 2 (3): 58–66.
- Rashid, Y. R. 1968. "Analysis of Reinforced Concrete Pressure Vessels." *Nuclear Engineering and Design* 7: 334–44.
- Reiter, L. 1990. *Earthquake Hazard Analysis: Issues and Insights*. New York: Columbia University Press.
- Roca, P., M. Cervera, and G. Gariup. 2010. "Structural Analysis of Masonry Historical Constructions. Classical and Advanced Approaches." *Archives of Computational Methods in Engineering* 17: 299–325.
- Roca, P., M. Cervera, L. Pelà, R. Clemente, and M. Chiumenti. 2013. "Continuum FE Models for the Analysis of Mallorca Cathedral." *Engineering Structures* 46: 653–70.

- Rots, J. G. 1988. "Computational Modeling of Concrete Fracture." PhD thesis, Delft University of Technology, Netherlands.
- \_\_\_\_\_. 1991. "Numerical Simulation of Cracking in Structural Masonry." *Heron Journal* 36 (2): 49–63.
- Saloustros, S., L. Pelà, P. Roca, and J. Portal. 2015. "Numerical Analysis of Structural Damage in the Church of the Poblet Monastery." *Engineering Failure Analysis* 48: 41–61.
- Sayed-Ahmed, E. Y., and N. G. Shrive. 1996. "Nonlinear Finite-Element Model of Hollow Masonry." *Journal of Structural Engineering* 122 (6): 683–90.
- Simões, A., R. Bento, S. Cattari, and S. Lagomarsino. 2014. "Seismic Performance Based Assessment of 'Gaioleiro' Buildings." *Engineering Structures* 80: 486–500.
- Tarque, N. 2008. "Seismic Risk Assessment of Adobe Dwellings." Master's thesis, University of Pavia, Italy.
- TNO DIANA. 2009. DIANA, Displacement method ANALyser, release 9.4, User's Manual. Delft: TNO DIANA.
- Tolles, E. L., F. A. Webster, A. Crosby, and E. E. Kimbro. 1996. *Survey of Damage to Historic Adobe Buildings after the January 1994 Northridge Earthquake*. Los Angeles: Getty Conservation Institute.
- Tolles, E. L., E. E. Kimbro, and W. S. Ginell. 2002. *Planning and Engineering Guidelines for the Seismic Retrofitting of Historic Adobe Structures*. Los Angeles: Getty Conservation Institute. Also in Spanish.
- Tomazevic, M. 1999. *Earthquake-resistant Design of Masonry Buildings*. London: Imperial College Press.
- Torrevalva, D. 2012. "Seismic Design Criteria for Adobe Buildings Reinforced with Geogrids." In *Proceedings of the 15th World Conference on Earthquake Engineering*. Lisbon: Sociedade Portuguesa de Engenharia Sismica.
- Vargas, J., J. Bariola, M. Blondet, and P. K. Mehta. 1986. "Seismic Strength of Adobe Masonry." *Materials and Structures* 19 (4): 253–58.
- Varum, H., A. Costa, H. Pereira, and J. Almeida. 2006. "Comportamento estrutural de elementos resistentes em alvenaria de adobe." Paper presented at TerraBrasil 2006: I Seminário Arquitetura e Construção com Terra no Brasil / IV Seminário Arquitetura de Terra em Portugal, Ouro Preto, Minas Gerais, Brazil, November 2006.
- Varum, H., N. Tarque, D. Silveira, G. Camata, B. Lobo, M. Blondet, A. Figueiredo, M. M. Rafi, C. Oliveira, and A. Costa. 2014. *Structural Rehabilitation of Old Buildings, Building Pathology and Rehabilitation 2*. Berlin: Springer-Verlag.
- Vecchio, F. J., and M. P. Collins. 1986. "The Modified Compression-Field Theory for Reinforced Concrete Elements Subjected to Shear." *ACI Structural Journal* 83 (2): 219–31.
- Yamin, L. E., C. Phillips, J. C. Reyes, and D. M. Ruiz. 2004. "Seismic Behavior and Rehabilitation Alternatives for Adobe and Rammed Earth Buildings." In *Proceedings of the 13th World Conference on Earthquake Engineering, Vancouver, BC*. Bogotá: CITEC, Universidad de Los Andes.
- Zeng, Y., J. G. Anderson, and G. Yu. 1994. "A Composite Source Model for Computing Realistic Synthetic Strong Ground Motions." *Geophysical Research Letters* 21 (8): 725–28.
- Zhuge, Y., D. Thambiratnam, and J. Corderoy. 1998. "Nonlinear Dynamic Analysis of Unreinforced Masonry." *Journal of Structural Engineering* 124 (3): 270–77.
- Zucchini, A., and P. B. Lourenço. 2002. "A Micro-mechanical Model for the Homogenization of Masonry." *International Journal of Solids and Structures* 39 (12): 3233–55.



The Getty Conservation Institute